Higher Order Electrokinetic Effects for Applied Biological Analytics

by

Claire Victoria Crowther

A Dissertation Presented in Partial Fulfillment
of the Requirements for the Degree
Doctor of Philosophy

Approved November 2018 by the
Graduate Supervisory Committee:

Mark Hayes, Chair
Gillian Gile
Alexandra Ros
Pierre Herckes

ARIZONA STATE UNIVERSITY

December 2018

ABSTRACT

Microfluidic systems have gained popularity in the last two decades for their potential applications in manipulating micro- and nano- particulates of interest. Several different microfluidics devices have been built capable of rapidly probing, sorting, and trapping analytes of interest. Microfluidics can be combined with separation science to address challenges of obtaining a concentrated and pure distinct analyte from mixtures of increasingly similar entities. Many of these techniques have been developed to assess biological analytes of interest; one of which is dielectrophoresis (DEP), a force which acts on polarizable analytes in the presence of a non-uniform electric fields. This method can achieve high resolution separations with the unique attribute of concentrating, rather than diluting, analytes upon separation. Studies utilizing DEP have manipulated a wide range of analytes including various cell types, proteins, DNA, and viruses. These analytes range from approximately 50 nm to 1 μm in size. Many of the currently-utilized techniques for assessing these analytes are time intensive, cost prohibitive, and require specialized equipment and technical skills.

The work presented in this dissertation focuses on developing and utilizing insulator-based dielectrophoresis (iDEP) to probe a wide range of analytes; where the intrinsic properties of an analyte will determine its behavior in a microchannel. This is based on the analyte's interactions with the electrokinetic and dielectrophoretic forces present. Novel applications of this technique to probe the biophysical difference(s) between serovars of the foodborne pathogen, *Listeria monocytogenes*, and surface modified *Escherichia coli*, are investigated. Both of these applications demonstrate the capabilities of iDEP to achieve high resolution separations and probe slight changes in

the biophysical properties of an analyte of interest. To improve upon existing iDEP strategies a novel insulator design which streamlines analytes in an iDEP device while still achieving the desirable forces for separation is developed, fabricated, and tested. Finally, pioneering work to develop an iDEP device capable of manipulating larger analytes, which range in size 10-250 μm, is presented.

To my family, whose love and support made this possible.

"You're braver than you believe and stronger and smarter than you think."

– Christopher Robin, Winnie the Pooh

ACKNOWLEDGMENTS

To my advisor, Dr. Mark A. Hayes, I owe my sincerest gratitude for all his encouragement, guidance, and support throughout my graduate career. His passion and gift for science is truly inspiring. Thank you for challenging me with many scientific pursuits outside of my comfort zone. To Dr. Gillian Gile, thank you for sharing your excitement for science and allowing me to broaden my scientific scope. To the rest of supervisory committee members, Dr. Alexandra Ros and Dr. Pierre Herckes, I appreciate all of your guidance and support. This dissertation would not have been possible without your valuable input and guidance.

Of course, none of this would have been possible without the help of my 'village'. To my fellow members of the Hayes Lab, I cannot image a better group of people to work with. To Dr. Paul Jones thank you for helping me get my graduate career rolling. Dr. Michael Keebaugh, your assistance with COMSOL was invaluable. Dr. Jie Ding thank you for the thought-provoking scientific discussions and wandering conversations about culture. Shannon Huey Hilton thank you for always being ready to have a stimulating conversation (especially at 4 pm on a Friday), being my 'twin', and being a genuine friend. To Fanyi Zhu and Yameng Liu you light up the lab with your keen intellect and passion. I am lucky to call you colleagues and friends. Ryan Yanashima, thank you for your help learning the ropes. To the wonderful Katalina Freeman, your unending positivity and ingenuity made working with termites fun. To Paige Davis, Sam Hayes, Jared Nettles, Alex Ramirez, Max Duvall, and Jared Smithers thank you for the amusing conversations, assistance with experiments, and willingness to learn on the fly. LaKeta Kemp, thank you for your insight on all 'things' bacteria. Bobby Abdallah and

Austin Echelmeier, your scientific intuition and friendships made this work possible.

To all my new-found friends that have come into my life during graduate school I will never be able to adequately express my gratitude for your friendship and assistance in helping keep me sane. To all the ‘Chemistry Peeps’ (you know who you are), thank you for all the adventures. To Amanda and Andrew Young-Gonzales, you are some of the most generous people I know; thank you for homemade dinners, coffee dates, random craft adventure, etc. Chris and Amanda Rock, thank you for all the laughter, Canadian thanksgivings, and days reserved for railing at the sun. To Alyssa Sherry, thank you for always being up for an adventure (no matter how big or small). To Tim Baxter and Tara MacCulloch, words cannot explain how much I appreciate you two. Your willingness to grab a drink, hang by the pool, play with the puppies, and tolerating me while I wrote this document speaks volumes to the wonderful people you are. To Sam Hernandez and Sravani Vadlamani, I will forever be grateful that GPSA brought you into my life; your sass, quick wit, and willingness to take on anything will always inspire me.

To my boyfriend Jesse, your unending support has been invaluable. Your willingness to pick me up during the lows and celebrate the successes made this possible. Your companionship on our many adventures makes every day better.

To my family, your support through this journey has been nothing but phenomenal. Thank you for always picking up the phone, coming to visit, and just being awesome. Bridget, you are the best sister a girl could ask for. Thank you for constantly reminding me that I could do this and telling me not to give up. To my parents, thank you for supporting and nurturing my love of science. I would not be here without your unending love and faith in me. I love you guys!

TABLE OF CONTENTS

Page

CHAPTER Page

CHAPTER Page

LIST OF TABLES

LIST OF FIGURES

Figure Page

CHAPTER 1

INTRODUCTION

1.1 Biological Analytes

The human understanding of the world around us is rapidly growing as new techniques are introduced and implemented to tackle bigger and more complicated challenges. Many of these scientific pursuits have centered around the study of biological material, including such analytes as cells, proteins, DNA, viruses, etc. (Figure 1.1). Each of these analytes represents fascinating systems, which scientists want to better understand and mimic. However, each of these analytes presents their own unique challenges to study. Scientists continue to develop new technologies and methodologies to further their ever-growing understanding of the world around us, enabling disease prevention, rapid identification of pathogenic material, improved understanding of evolution, and so much more.

The advancement of the human understanding of biological analytes has grown through time with massive knowledge gains within the past century. The first cell was identified in 1665 by Robert Hooke [1] and since then the functions of the cell itself and its individual smaller components have been the focus of an ever increasing number of scientific inquires. Delving into cells alone, they represent a wide swath of biologically relevant analytes including animal, plant, and bacterial cells; which are all associated with their own interesting scientific pursuits. For example, in the 1670s Antonie van Leeunwenhoke discovered bacteria.[1] Then, in 1928, the discovery of the first antibiotic, penicillin, resulted in a method capable of treating a bacterial infection.[2] Since then the evolution of antibiotic resistant bacteria has resulted in a race to develop new effective

antibiotics.[3] The many components of a cell pose a wide array of scientifically interesting questions about things like their structure and function. In the case of DNA, its structure was discovered 65 years ago by Watson, Crick, and Franklin [4] and now DNA can be manipulated to create biomimetic structures.[5] These examples only skim the surface of the knowledge gain which have been made with respect to biological analytes.

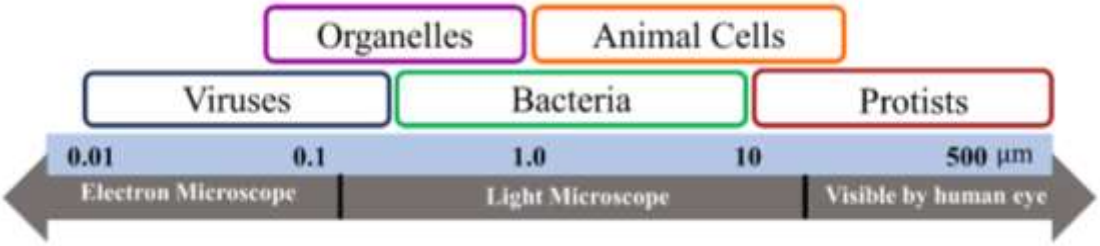

Figure 1.1. Size comparison of various biological analytes of interest and the typical method of visualization based on the size distribution.

One of the greatest challenges with studying biological analytes is the inherently complex nature of both the bioanalyte itself and the real-world sample in which it is present.[6-8] Many of the commonly-used microbiological methods are limited as they are time consuming, lack specificity, and need extensive sample preparation.[9] For some biological assessments culturing is used for detection; however this can take several days and generally only result in a positive or negative result. Culture methods are also further limited by the level of specificity which they can achieve.[10, 11] Other methods for biological assessment such as mass-spectrometry, polymerase chain reactions (PCR), flow cytometry, and genetic sequencing can provide a lot of insight. However, these methods can be time intensive, cost prohibitive, require specialized equipment and cold chain reagents, and necessitate technical skill to perform.[12-16] The desire to be able to isolate, concentrate, and probe an analyte from a real-world sample in a rapid and cost-effective manner has driven the field of separation science.

1.2 Separation Science

One of the fundamental fields in analytical chemistry is separation science; which focuses on the ability to rapidly, accurately, and precisely isolate an analyte of interest from a mixture. This is especially important for biological samples, which are complex by nature, and the isolation of specific components of a given sample is highly desirable.

Several different techniques are used to achieve separations including centrifugation, filtration, chromatography, flow cytometry, and electric field-based techniques. Various forces are employed in each of these techniques to differentiate and isolate a given analyte of interest based on their intrinsic properties. Some of the commonly utilized properties that are interrogated include size, charge, surface properties, and density. In some cases, labeling is used to identify analytes of interest to achieve isolation.

Improvements to separation techniques are constantly being developed to achieve higher resolution separations of increasingly similar analytes, but several challenges remain. In the case of centrifugation, the gravitational force that drives the separation is generally insufficient to achieve high resolution separations. For example, centrifugation cannot achieve the isolation of viral particles present in a blood sample.

For separation methods that are dependent on labeling techniques, they are reliant upon the availability of sensitive and specific labels which only interact with the analyte of interest. To achieve this a significant amount of prior knowledge of the analyte is

required. Furthermore, this can be challenging if the label utilized interacts with more than the analyte of interest, or impossible in the case that no label exists.

1.3 Microfluidics

The field of microfluidics has exploded in the last two decades, helping to revolutionize the way that science can be performed. Microfluidic systems, as the name suggests, are designed to manipulate volumes on the order of 10^{-6} to 10^{-18} liters.[17-19] This can be extremely beneficial for working with biological analytes, when a limited amount of sample is available. A wide array of microfluidic devices have been developed for numerous different applications, which is are further developed in Chapter 2.[17-23] For cells alone several microfluidic platforms have been developed.[20-22] Some examples of microfluidic devices include those for cell sorting [24, 25], cell culture and analysis [26, 27], and analysis of secreted molecules [28, 29].

Advantages to microfluidic systems include their inexpensive nature, when compared with traditional methodologies, and their ability to achieve rapid analysis, high resolution and sensitive separations, and to be multiplexed in order to achieve several functions.[21, 30] Furthermore, microfluidic systems can be incorporated into lab-on-a-chip (LOC) devices, which combine all the necessary functions for an experiment onto a single chip which is in the size range of milli- to centi- meters squared. The ability to contain an entire experiment in a small and portable device has many applications in several fields including the food and health care industries.

1.4 Manipulation of Biological Analytes using Dielectrophoresis

The work presented in this dissertation focuses on probing analytes in a microfluidic channel using dielectrophoresis (DEP). An in-depth description of the forces

in the microchannel and some of the applications are presented in Chapter 2 of this dissertation.

Analysis of particles using electric field-based techniques allows for a unique insight into a given analyte. Electrophoretic (EP) techniques are based on manipulating charged analytes in a uniform electric field of a microchannel. In the case that a direct current potential is applied, the movement of buffer is driven by electroosmosis (EO). When a non-uniform electric field is utilized the DEP force is introduced, which can influence any polarizable particle. Two main systems have been developed for DEP applications: one where electrodes are distributed throughout the microchannel to influence the electric field, known as eDEP, and one where insulating features are used to shape the electric field between two distal electrodes, known as iDEP.

Dielectrophoresis is a unique method which can be used for separation, interrogation, and manipulation of analytes based on their intrinsic properties. These properties include, but are not limited to, surface charge, zeta potential, conductivity, permittivity, and deformability. As DEP is dependent on such a wide range of properties, highly accurate and precise manipulations of analytes is possible in theory. [31] Examples of various bioanalytes which have been studied using DEP include bacterial cells [32-38], mammalian cells[39, 40], cell organelles[41], blood cells[7, 42, 43], viruses[44, 45], DNA[46-49], and proteins[24, 50, 51]. Further discussions of previous work using DEP is presented in Chapter 2. The work presented in this dissertation builds on these efforts and focuses on utilizing, developing, and improving iDEP for applications in detection, separation, and interrogation of intrinsic particle properties.

1.5 Dissertation Overview

This dissertation focuses on work done to both develop and utilize iDEP to probe various analytes of interest. The fundamental physics behind iDEP are detailed in Chapter 2, along with an overview of the field and current common methods of fabrication. The development of iDEP as a method to both rapidly identify and gain epidemiological insight into pathogenic bacteria is presented in Chapter 3. To probe the capabilities of iDEP, bacteria with various surface modifications were interrogated using iDEP in Chapter 4; giving insight into the effect that surface modifications have on the internal and external biophysical properties of a cell. The development of a novel insulator shape is presented in Chapter 5, which is capable of streamlining analytes to achieve higher resolution separations. Chapter 6 seeks to develop a microfluidic DEP system for a new realm of biological analytes, specifically protists. As the analytes are larger than most currently assessed analytes, ranging up to hundreds of microns in size, different fabrication schemes are implemented. Finally, Chapter 7 focuses on the conclusions which can be drawn from this work and lays out potential future work.

1.6 References

[1] Raven, P., Johnson, G., Mason, K., Losos, J., Singer, S., *Biology*, McGraw Hill Education 2017.

[2] Fleming, A., *British journal of experimental pathology* 1929, *10*, 226-236.

[3] Willyard, C., *Nature* 2017, *543*, 15.

[4] Watson, J. D., Crick, F. H. C., *Nature* 1953, *171*, 737-738.

[5] Liu, X., Zhang, F., Jing, X., Pan, M., Liu, P., Li, W., Zhu, B., Li, J., Chen, H., Wang, L., Lin, J., Liu, Y., Zhao, D., Yan, H., Fan, C., *Nature* 2018, *559*, 593-598.

[6] Yager, P., Edwards, T., Fu, E., Helton, K., Nelson, K., Tam, M. R., Weigl, B. H., *Nature* 2006, *442*, 412.

[7] Toner, M., Irimia, D., *Annual Review of Biomedical Engineering* 2005, *7*, 77-103.

[8] Ho, C. M. B., Ng, S. H., Li, K. H. H., Yoon, Y.-J., *Lab on a Chip* 2015, *15*, 3627-3637.

[9] *Difco & BBL Manual: Manual of Microbiological Culture Media*, BD Diagnostics, Sparks, MD 2009.

[10] Palumbo, J. D., Borucki, M. K., Mandrell, R. E., Gorski, L., *Journal of Clinical Microbiology* 2003, *41*, 564-571.

[11] Doumith, M., Buchrieser, C., Glaser, P., Jacquet, C., Martin, P., *Journal of Clinical Microbiology* 2004, *42*, 3819-3822.

[12] Ng, P. C., Kirkness, E. F., in: Barnes, M. R., Breen, G. (Eds.), *Genetic Variation: Methods and Protocols*, Humana Press, Totowa, NJ 2010, pp. 215-226.

[13] Barbuddhe, S. B., Maier, T., Schwarz, G., Kostrzewa, M., Hof, H., Domann, E., Chakraborty, T., Hain, T., *Applied and Environmental Microbiology* 2008, *74*, 5402.

[14] Jadhav, S., Sevior, D., Bhave, M., Palombo, E. A., *Journal of Proteomics* 2014, *97*, 100-106.

[15] Heck, A. J. R., *Nature Methods* 2008, *5*, 927.

[16] Belgrader, P., Benett, W., Hadley, D., Richards, J., Stratton, P., Mariella, R., Milanovich, F., *Science* 1999, *284*, 449.

[17] Whitesides, G. M., *Nature* 2006, *442*, 368.

[18] Squires, T. M., Quake, S. R., *Reviews of Modern Physics* 2005, *77*, 977-1026.

[19] Sackmann, E. K., Fulton, A. L., Beebe, D. J., *Nature* 2014, *507*, 181.

[20] Bhagat, A. A. S., Bow, H., Hou, H. W., Tan, S. J., Han, J., Lim, C. T., *Medical & Biological Engineering & Computing* 2010, *48*, 999-1014.

[21] Sibbitts, J., Sellens, K. A., Jia, S., Klasner, S. A., Culbertson, C. T., *Analytical Chemistry* 2018, *90*, 65-85.

[22] Roper, M. G., *Analytical Chemistry* 2016, *88*, 381-394.

[23] Dittrich, P. S., Manz, A., *Nature Reviews Drug Discovery* 2006, *5*, 210.

[24] Abdallah, B. G., Chao, T.-C., Kupitz, C., Fromme, P., Ros, A., *ACS Nano* 2013, *7*, 9129-9137.

[25] Srivastava, S. K., Baylon-Cardiel, J. L., Lapizco-Encinas, B. H., Minerick, A. R., *Journal of Chromatography A* 2011, *1218*, 1780-1789.

[26] Subramanian, S., Tolstaya, E. I., Winkler, T. E., Bentley, W. E., Ghodssi, R., *ACS Applied Materials & Interfaces* 2017, *9*, 31362-31371.

[27] Martin, W. E., Ge, N., Srijanto, B. R., Furnish, E., Collier, C. P., Trinkle, C. A., Richards, C. I., *ACS Omega* 2017, *2*, 3858-3867.

[28] Li, L., Zhang, Y., Zhang, L., Ge, S., Liu, H., Ren, N., Yan, M., Yu, J., *Analytical Chemistry* 2016, *88*, 5369-5377.

[29] Son, K. J., Rahimian, A., Shin, D.-S., Siltanen, C., Patel, T., Revzin, A., *Analyst* 2016, *141*, 679-688.

[30] Stone, H. A., Kim, S., *AIChE Journal* 2004, *47*, 1250-1254.

[31] Jones, P. V., Hayes, M. A., *Electrophoresis* 2015, *36*, 1098-1106.

[32] Jones, P. V., DeMichele, A. F., Kemp, L., Hayes, M. A., *Analytical and Bioanalytical Chemistry* 2014, *406*, 183-192.

[33] Jones, P. V., Hilton, S. H., Davis, P. E., Yanashima, R., McLemore, R., McLaren, A., Hayes, M. A., *Analyst* 2015, *140*, 5152-5161.

[34] Johari, J., Hübner, Y., Hull, J. C., Dale, J. W., Hughes, M. P., *Physics in Medicine and Biology* 2003, *48*, N193.

[35] Labeed, F. H., Coley, H. M., Thomas, H., Hughes, M. P., *Biophysical Journal* 2003, *85*, 2028-2034.

[36] Braff, W. A., Willner, D., Hugenholtz, P., Rabaey, K., Buie, C. R., *PloS one* 2013, *8*, e76751.

[37] Lapizco-Encinas, B. H., Simmons, B. A., Cummings, E. B., Fintschenko, Y., *Analytical Chemistry* 2004, *76*, 1571-1579.

[38] LaLonde, A., Romero-Creel, M. F., Lapizco-Encinas, B. H., *Electrophoresis* 2015, *36*, 1479-1484.

[39] Wang, M. M., Tu, E., Raymond, D. E., Yang, J. M., Zhang, H. C., Hagen, N., Dees, B., Mercer, E. M., Forster, A. H., Kariv, I., Marchand, P. J., Butler, W. F., *Nature Biotechnology* 2005, *23*, 83-87.

[40] Bhattacharya, S., Chao, T.-C., Ariyasinghe, N., Ruiz, Y., Lake, D., Ros, R., Ros, A., *Analytical and Bioanalytical Chemistry* 2014, *406*, 1855-1865.

[41] Luo, J., Abdallah, B. G., Wolken, G. G., Arriaga, E. A., Ros, A., *Biomicrofluidics* 2014, *8*, 021801.

[42] Ding, J., Woolley, C., Hayes, M. A., *Analytical and Bioanalytical Chemistry* 2017, *409*, 6405-6414.

[43] Srivastava, S. K., Artemiou, A., Minerick, A. R., *Electrophoresis* 2011, *32*, 2530-2540.

[44] Hughes, M. P., Morgan, H., Rixon, F. J., Burt, J. P. H., Pethig, R., *Biochimica et Biophysica Acta (BBA) - General Subjects* 1998, *1425*, 119-126.

[45] Ding, J., Lawrence, R. M., Jones, P. V., Hogue, B. G., Hayes, M. A., *Analyst* 2016, *141*, 1997-2008.

[46] Gallo-Villanueva, R. C., Rodríguez-López, C. E., Díaz-de-la-Garza, R. I., Reyes-Betanzo, C., Lapizco-Encinas, B. H., *Electrophoresis* 2009, *30*, 4195-4205.

[47] Martinez-Duarte, R., Camacho-Alanis, F., Renaud, P., Ros, A., *Electrophoresis* 2013, *34*, 1113-1122.

[48] Swami, N., Chou, C.-F., Ramamurthy, V., Chaurey, V., *Lab on a Chip* 2009, *9*, 3212-3220.

[49] Gan, L., Chao, T.-C., Camacho-Alanis, F., Ros, A., *Analytical Chemistry* 2013, *85*, 11427-11434.

[50] Nakano, A., Camacho-Alanis, F., Ros, A., *Analyst* 2015, *140*, 860-868.

[51] Lapizco-Encinas, B. H., Ozuna-Chacón, S., Rito-Palomares, M., *Journal of Chromatography A* 2008, *1206*, 45-51.

CHAPTER 2

OVERVIEW OF DIELECTROPHORESIS

2.1 Basic Principles of Electrokinetic Effects

All matter in the universe is made up of a conglomeration of electrostatically-interacting atoms held together by Coulombic forces. Atoms are composed of electrons, neutrons, and protons, and can therefore carry various charges resulting in an overall net-positive, -negative, or -neutral charge. This results in a distribution of charges present in all particles that can be uniquely correlated to their intrinsic physical properties. As a result, many possibilities for particle manipulation open up. Utilizing electric fields (Equation 1 & 2), the electro-physical properties of an analyte can be probed and manipulated, based on their net charge, charge distribution, or polarizability. In the implementation of the work described here, these forces can be used to stream, deflect, trap, concentrate, separate, and isolate particles.

Particles can be influenced by forces induced by uniform and non-uniform electric fields. In a uniform electric field, the force ($\vec{F}$) on a given particle is described as the effect of an electric field, $\vec{E}$, on the net charge of the particle (q).[1]

$$\vec{F} = q\vec{E} \tag{1}$$

The most basic electric force acts on the permanent or induced dipole ($\vec{p}$) in a spatially non-uniform electric field, where the gradient operator is denoted by the dell operator (∇).[2]

$$\vec{F} = (\vec{p} \cdot \nabla)\vec{E} \tag{2}$$

2.2 Electrokinetic Transport: Driven by Electroosmosis and Electrophoresis

Electroosmosis (EO) is the bulk movement of a fluid in a channel in response to an applied electric field, occurring when the immobile surfaces, typically the walls of the channel, carry a charge. The charged walls interacting with the buffer result in a double layer of counter ions. The counter ions closest to the walls create a boundary in the channel that is assumed to be stationary and thin compared to the overall width of the channel, which is known as the Stern layer.[3] The other layer is more diffuse, meaning that the charges are free to be manipulated and flow through the solution. With an applied electric field, the diffuse layer responds and drags the bulk solution, resulting in the motion of the fluid. A plug like flow of the liquid is observed as the velocity of the diffuse layer is uniform, and then drops off rapidly so that the velocity at the channel walls is zero (Figure 2.1.).

The effect of EO for the applications found in this dissertation can be further understood by looking at a device, which was made by using oxygen plasma to bond a glass slide with a polydimethylsiloxane (PDMS) cast of the microchannel. The plasma generates silanol groups (Si-OH) on the surface of the PDMS, which in an aqueous solution are ionizable.[4] This leads to a negative charge on the surface of the PDMS, which attracts counterions from the solution. Some of which are immobile, making up the Stern layer in this case (Figure 2.1.). The counterions in the Stern layer cannot directly attach to the solid surface due to their hydrated radius, which in turn affects the thickness of the Stern layer. The diffuse layer is close to the Stern layer and contains several cations, which can move freely with electrostatic attraction and thermal diffusion. The plane between the Stern and diffuse layers is known as the shear plane and denotes the

zeta potential (ζ). Together the Stern and diffuse layers are termed the electric double layer (EDL). The electric potential (Ψ) at the interface of the solid surface and liquid, Ψ_{wall}, is dependent on the surface charge density. The Debye length (λ_D) is the thickness of the EDL and can be expressed mathematically as:

$$\lambda_D = \left(\frac{\varepsilon_m RT}{2F^2 cz^2}\right)^{1/2} \tag{3}$$

where *R* is the gas constant, *T* is the temperature, *F* is the Faraday constant, *c* is the electrolyte concentration, z is the electrolyte valence, and ε_m is the medium permittivity. [5]

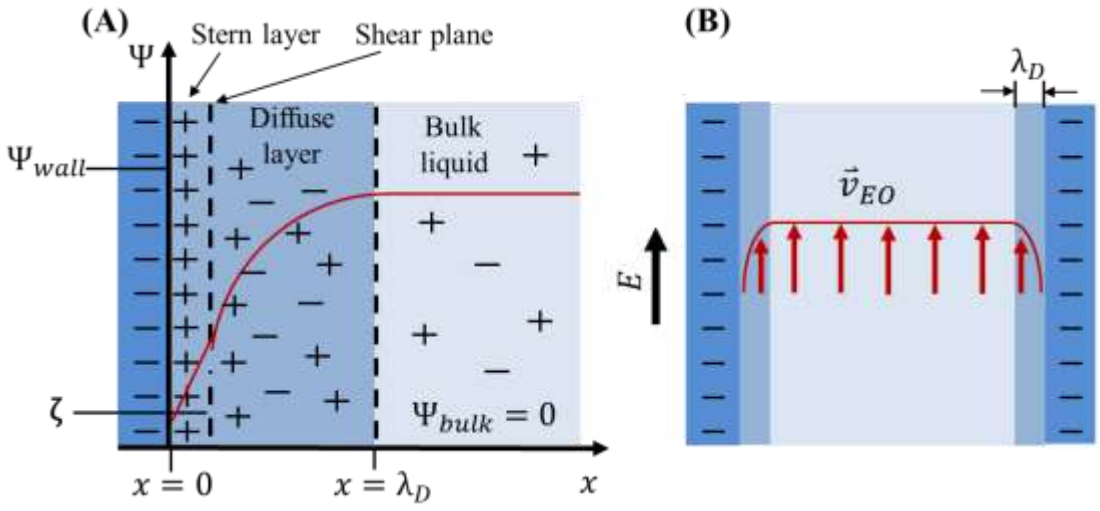

Figure 2.1. (A)Schematic representation of the electric double layer (EDL) and the flow profile of electroosmosis. The solid surface is negatively charged and this results in the buildup of immobile counterions known as the Stern layer. The diffuse layer has loosely associated charges that can diffuse freely. The electric potential decreases linearly across the Stern layer, then exponentially across the diffuse layer. The EDL is composed of the Stern and diffuse layers. The zeta potential is the potential between the Stern and diffuse layers, known as the shear plane. (B) The electroosmotic flow profile in a microfluidic device. The flow profile is uniform in the bulk fluid, and rapidly drops in the electric double layer down to zero at the microchannel walls.

The electroosmotic mobility (μ_{EO}) is an intrinsic property of the buffer/surface system in terms of ε_m, ζ , and the viscosity of the buffer (η). The electroosmotic mobility

can be combined with the effect of the electric field to describe the electroosmotic velocity ($\vec{v}_{EO}$) , according to the Smoluchowski equation [6, 7].

$$\vec{v}_{EO} = -\frac{\varepsilon_m \zeta}{\eta}\vec{E} = \mu_{EO}\vec{E} \quad (4)$$

Electrophoresis (EP) is the movement of a charged particle in a uniform field along the electric field lines. The constant velocity of a particle that occurs with an applied homogenous electric field is a balance of the electrical force and viscous drag. The electrophoretic force is similar to that which is described in Equation 1, such that the force on the particle is altered by the charge of the particle and the applied electric field (Figure 2).

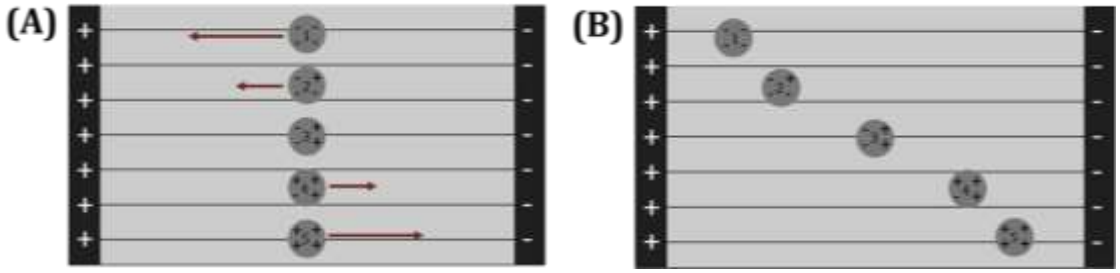

Figure 2.2. Representation of the effect of the electrophoretic force on differently charged particles. (A) Depicts the charges of the particles and the arrows depict the direction and relative magnitude of the force that each particle experiences. (B) Illustrates the particles placement after a potential has been applied to the system. Particle 3 is net neutral so with the application of a homogenous electric it experiences no net force. However, Particles 1, 2, 4, and 5 all carry a net charge. Particles 1 and 2 are net negative, and thus attracted to the positively charged end of the device; whereas particles 4 and 5 are net positive and are therefore attracted to the negatively charged end of the device. Particle 1 and 5 will experience a greater net force because of their stronger net charge, meaning that in the same amount of time they will travel further than their similarly charged counterparts.

Defining the friction coefficient as $f = 6\pi r\eta$, where r is the radius of the particle, and η is the viscosity of the suspending medium, the electrophoretic velocity can be described as [6]:

$$\vec{v}_{EP} = \frac{q\cdot\vec{E}}{f} = \frac{\vec{F}_{EP}}{f} \quad (5)$$

The electrophoretic mobility of a particle (μ_{EP}) is an intrinsic property of the particle in a specified medium that combines the forces previously described:[8]

$$\mu_{EP} = \frac{q}{6\pi r\eta} \tag{6}$$

By combining the effect of the electric field and $\mu_{EP,}$ the electrophoretic velocity can be described by the following equation [6]:

$$\vec{v}_{EP} = \mu_{EP}\vec{E} \tag{7}$$

The effects of electroosmosis and electrophoresis can be combined to determine the net electrokinetic velocity that the particles experience in a microchannel. This can also be described using the electrokinetic mobility (μ_{EK}), which combines the electrophoretic and electroosmotic mobilities.

$$\vec{v}_{EK} = \vec{v}_{EP} + \vec{v}_{EOF} = \mu_{EK}\vec{E} \tag{8}$$

2.3 Dielectrophoresis

2.3.1 Theory

H. A. Pohl was the first to explore and formalize the idea of dielectrophoresis (DEP), which is the effect of an inhomogeneous electric field on a particle with a permanent or induced dipole.[2, 9] An inhomogeneous electric field acting on a particle leads to the different ends of a particle interacting with the electric field such that they experience different magnitudes of force. The particle's interaction with the medium and

the inhomogeneous electric field causes the particle to either be repelled or attracted to the areas with stronger electric fields.

The most basic form to depict the dielectrophoretic force is reflected by Equation 2, where $\vec{F}_{DEP} = (\vec{p} \cdot \nabla)\vec{E}$. The equation was further developed to describe the DEP force which is exerted on a polarizable spherical particle present in a non-uniform electric field [2, 8].

$$\vec{F}_{DEP} = 2\pi\varepsilon_m r^3 f_{CM} \nabla \left| \vec{E} \right|^2 \tag{9}$$

where $\vec{F}_{DEP}$ is the DEP force and f_{CM} is the Clausius-Mossotti factor.

The Clausius-Mossotti factor relates to the effective polarizability of the particle, and is determined using the absolute permittivity of the particle (ε_p) and surrounding medium (ε_m):

$$f_{CM} = \frac{\varepsilon_p - \varepsilon_m}{\varepsilon_p + 2\varepsilon_m} \tag{10}$$

The real part of the Clausius-Mossotti factor, which describes a particle that is subject to conduction losses, is described using the complex permittivity (ε^*), where $i = \sqrt{-1}$ and ω is the angular frequency. Therefore, the complex permittivity of the particle can be denoted as:

$$\varepsilon_p^* = \varepsilon_p - \frac{i\sigma_p}{\omega} \tag{11}$$

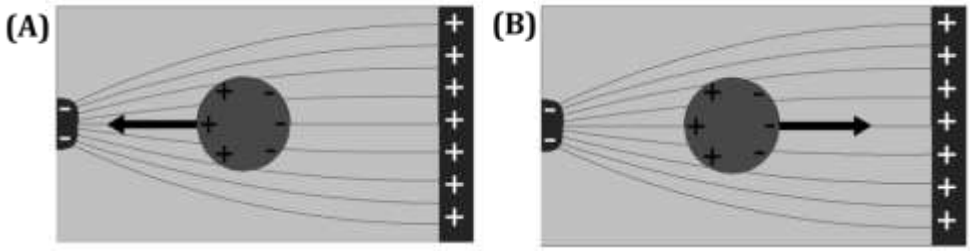

Figure 2.3. The effect of the dielectrophoretic force on a polarizable particle. The non-uniform electric field results in the particle being (A) attracted to or (B) repelled from areas of high electric field. The direction of the DEP is determined using the permittivity or conductivity of the particle and medium. (A) Represents positive DEP, when the particle is more polarizable than the medium. (B) Depicts when the medium is more polarizable than the particle, representing negative DEP.

For the systems presented in this dissertation, DC fields are used, denoting that the angular frequency is zero. Consequently, the Clausius-Mossotti factor can be approximated in terms of the real conductivity of the particle and the medium.

$$f_{CM} = \frac{\sigma_p - \sigma_m}{\sigma_p + 2\sigma_m} \tag{12}$$

The magnitudes of the conductivities of the particle and medium are then used to determine the influence of dielectrophoresis on the particle's direction of travel; where the particles are either attracted or repelled from areas of greatest electric field (Figure 3). When the conductivity of the particle is greater than that of the media, the particle will be attracted to areas of high electric field (positive DEP). Alternatively, if the conductivity of the medium is greater than that of the particle, the particle will be repelled from the high electric fields (negative DEP).

In the case of an ellipsoidal particle, the DEP force equation can be modified to account for the dimensions of the analyte of interest:[8, 10]

$$\vec{F}_{DEP} = \frac{4}{3}\pi abc\varepsilon_m \left(\frac{\sigma_p - \sigma_m}{Z\sigma_p + (1-Z)\sigma_m}\right) \nabla \left| \vec{E} \right|^2 \tag{13}$$

In this case Z represents the depolarization factor, and the semi-principal axes of the ellipsoid are represented by a, b, and c (a>b=c). This equation is taken into consideration when working with rod-shaped bacteria; specifically, *Listeria monocytogenes* and *Escherichia coli*, are the two considered in this dissertation.

The DEP velocity, $\vec{v}_{DEP}$, can be represented in terms of dielectrophoretic mobility (μ_{DEP}) and the gradient of the electric field squared.[2, 8, 11]

$$\vec{v}_{DEP} = \mu_{DEP} \nabla \left| \vec{E} \right|^2 \tag{14}$$

The dielectrophoretic force has several unique aspects, as compared to other analyte manipulation techniques. First, the size of the particle affects the force, such that larger particles will experience a greater force. Additionally, the ability for dielectrophoretic forces to manipulate particles is largely dependent on the gradient of the electric field. Furthermore, unlike electrophoresis, dielectrophoresis can be used with both DC and AC fields and will influence both neutral and charged particles. These characteristics are what enable manipulation of unique particles by several methods including streaming, deflecting, and trapping analytes.[12-22]

2.3.2 Particle Pathlines and Trapping Conditions

In a microchannel, the flow of a particle is controlled by advection, diffusion, and electrokinetic effects.[21] Advection can be minimized by eliminating pressure driven flow, and for large particles (>1 μm) in microchannel diffusion can be disregarded. The flow of a particle, $\vec{J}$, can be described by [12, 13, 21, 23, 24]:

$$\vec{J} = D\nabla \mathrm{C} + C(\vec{v}_{Bulk} + \vec{v}_{EK} + \vec{v}_{DEP}) \approx C(\vec{v}_{EK} + \vec{v}_{DEP}) \tag{15}$$

where *D* is the diffusion coefficient, *C* is the particle concentration, and $\vec{v}_{Bulk}$ is the motion of the fluid due to pressure driven flow. Therefore, particle flow is only affected by the concentration of the analyte, EK, and DEP.[24]

The highest gradients in the electric field occur at the constrictions in a microchannel and thus result in the strongest dielectrophoretic forces. Therefore, particle motion is attributed to the EK, when not strongly influenced by DEP (Equation 15). As EK is influenced by the electric field and the particle's mobility (Equation 8), the particle pathlines in a microchannel can be approximated by the electric field lines.[24]

For trapping DEP to occur, the particle velocity along the electric field line has to be zero such that $\vec{j} \cdot \vec{E} = 0$.[21, 25] This trap can be described as a point when the co-linear part of the dielectrophoretic force dominates over electrokinetic force, and therefore the dielectrophoretic velocity dominates over the electrokinetic velocity. This results in a steady-state trapping zone that acts as a kinetic barrier to particles in the microchannel, which can be described using the electrokinetic and dielectrophoretic mobilities:

$$\left(\mu_{EK}\vec{E} + \mu_{DEP}\nabla\left|\vec{E}\right|^2\right) \cdot \vec{E} > 0 \tag{16}$$

Equation 16 can be rearranged such that dielectrophoretic trapping is described as [19]:

$$\frac{\nabla\left|\vec{E}\right|^2}{E^2} \cdot \vec{E} \geq \frac{\mu_{EK}}{\mu_{DEP}} \tag{17}$$

This equation denotes particle trapping such that the left side depicts the field characteristics and the right side represents the electrokinetic and dielectrophoretic mobilities which are intrinsic properties of a particle. When the above inequality is not

met the particles can still be influenced by DEP which is the case for streaming and deflection DEP techniques (Equation 15).

2.3.3 Applications and Development of DEP

All matter is dielectric and can be manipulated by the application of an electric field. The interaction of a particle with that electric field is unique and based upon the particle's make-up. The manipulation of the electric field is achievable in a myriad of ways, which can be engineered for a specific application. A common technique to alter the electric field is the application of conductive electrodes that deliver charge to the system, and thus alter the field, known as electrode-based DEP (eDEP). Different materials can be introduced based on their ability to conduct and propagate charge. Aqueous media is advantageous as it is influenced by the electric field and can be used to suspend analytes of interest. The ability to suspend non-aqueous analytes allows for their intrinsic electro-physical properties to be probed.

Pohl conducted the initial experiments using DEP to manipulate analytes of interest. His first experiment focused on separating living and dead cells using DEP where the electrodes were asymmetrically arranged.[26] He continued his work manipulating and separating particles based on if they experienced positive or negative DEP utilizing closely spaced electrodes to achieve high field gradients.[27, 28]

The use of electrodes to generate inhomogeneous electric fields has remained a common method. Over time there have been improvements in the ability to manipulate both the electrode geometries and positioning. This is achieved by photolithography and other microfabrication techniques. The electrodes are either supplied with a voltage or can float in the presence of an AC field.[27-30] To improve the applicability of the

technique, the systems were down-sized and improved methods for electrode placement have been utilized; thus achieving the desired effects with a lower applied voltage. Numerous electrode geometries have been used for particle manipulations [31-38].

Dielectrophoretic research as a field has grown rapidly over the last 65 years, for its ability to manipulate small particles. Several small analytes have been studied including latex spheres[39], bacterial cells[40], viruses[41], and cells [42]. However, limitations to eDEP systems have been identified as the strong electric fields are local only to the electrodes, can be easily fouled, and generate bubbles in the aqueous media.[43-45] Furthermore, as the complexity and precision of the systems continue to grow, the cost swells along with the difficulty of fabrication.[46, 47] Platinum electrodes, which are common to many systems, can be problematic in that they undergo a process of dissolution and redeposition which leads to chloride and oxide formation on the electrode.[47] An alternative to eDEP involves introducing insulating features between two distal electrodes to influence the electric field. This development resulted in the field of insulator-based dielectrophoresis (iDEP). The insulators constrict the electric field to achieve the high gradients necessary for influential dielectrophoretic force (Figure 4). Using distal electrodes is advantageous as it helps to avoid the issue of electro-chemical interactions between the aqueous media and the electrode. To allow for easy optical analysis, iDEP microdevices are often fabricated with transparent materials. Furthermore, in most cases the fabrication complexity and cost associated with iDEP is greatly improved from eDEP systems.

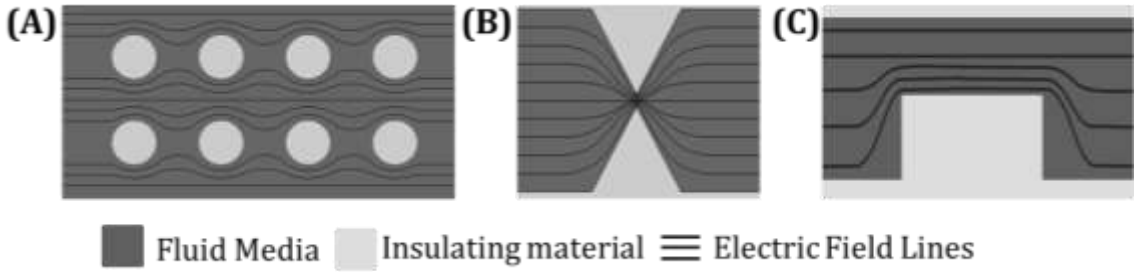

Figure 2.4. Representation of the electric field lines in the fluid media around various insulating features. Note that the electrodes used to generate the fields are not included but are assumed to be in distal reservoirs and that the field lines that penetrate the insulators are not represented. These three shapes, (A) circles (B) triangles (C) rectangles, represent three of the most common insulator designs. (A) represents an array method while (B) and (C) represent a single insulating feature. The highest electric field for all the designs is present at the points of constriction, which is where the DEP force is the strongest.

The first use of iDEP was performed by Masuda et al. for the manipulation of cells in 1989.[48] This work does not specifically focus on the application of DEP, but rather focuses on the ability for contactless trapping and the creation of pearl-chained cells. A little over ten years later the next use of iDEP was presented by Chou et al. where the capture of double and single-stranded DNA was achieved using an array of insulating microstructures under the application of an AC field.[43] In 2003 Cummings and Singh used insulating posts and low frequency or DC electric fields to alter the electrokinetic and dielectrophoretic forces in a microchannel. They were able to alter the pathlines of the particles (streaming DEP) and induce trapping of the particles with the application of higher electric fields.[12] This work is unique in that it was the first to utilize the electrokinetic force to manipulate the flow of the analytes, meaning that the sample of interest is moved to areas influenced by the DEP force. This results in more of the sample reaching a point where it can be analyzed and manipulated in shorter amount of time. Lapizco-Encinas et al. advanced the field of iDEP by employing the strategy on bacteria,

such that the separation of live and dead bacteria, and the selective trapping of various bacteria were achieved.[14, 25] This work was done using a uniform array of posts in a straight microchannel.

Over the past decade iDEP has been used for many different applications and using a wide range of insulator shapes. A myriad of analytes have been studied including polystyrene spheres [21, 49] animal cells [15], organelles[50], proteins[51-53], DNA[43, 54], and bacterial cells [14, 22, 42, 55]. This work has been achieved using various microchannels and insulators including: serpentine channels [56], oil droplet insulators [57, 58], single insulators [20, 59, 60], arrays [25, 54, 61], and multiple insulators [49, 62, 63]. Three main behaviors are observed using iDEP: streaming, trapping, and deflection. The DEP force constricting the analyte of interest to a specific pathline is considered streaming DEP [12, 13]. Deflection uses streaming DEP to alter the pathline of various analytes based on their unique intrinsic electro-physical properties [16, 18, 20, 59, 60]. Trapping occurs when the bulk transport is opposed collinearly by the separatory effects, where particles will reach a steady state stopping point in the microchannel based on their inherent electro-physical properties (Equations 15–17).[15, 16, 19, 21, 22, 50, 52, 55, 64, 65] Most current methods result in the trapping of only one analyte from another component or mixture, or a bipurification. To determine an analyte's trapping behavior the ratio of electrokinetic and dielectrophoretic mobilities is considered such that if the ratio is above a certain threshold the analyte will continue in the microchannel, while if it is equal to or below the threshold a steady state trap will occur (Equation 17).

Gradient insulator-based dielectrophoresis (g-iDEP) builds upon the prior work of iDEP, designed to create more refined separation than the bipurifications previously

achieved. This is unique in that the constrictions in the microchannel decrease in size as the particles progress electrokinetically down the microchannel. Altering the constriction size in turn alters the dielectrophoretic force, as smaller constrictions result in a stronger local electric field, thus creating a unique trap at every constriction in the microchannel. Having several unique traps in the microchannel allows for analytes with different electrokinetic and dielectrophoretic mobilities to be trapped at different locations. This allows for the isolation and concentration of more than one analyte based on many factors including their size, charge, polarizability, and shape. Fine tuning of the insulator shapes, constriction size, and channel dimensions will result in higher resolution separations for a wide range of analytes from tens of nanometers to micrometers in diameter.[66] Currently, this technique has been used on wide range of particles including polystyrene spheres [67], red blood cells[15], amyloid fibrils[53], viruses[68], and various bacteria [22, 55, 62]. Trapping of multiple analytes in one channel at different unique trapping locations has also been achieved.[22, 62] Further developments will seek to improve separation resolution and trap more than two analytes.

2.4 Fabrication of Microfluidic Devices

2.4.1 Device Design

Depending on the necessary experimental requirements for microfluidic devices various aspects must be considered when designing a microdevice. Several factors will all affect the overall design of a microfluidic device. The desired resolution and aspect ratio will come into play when determining the dimension of potential micro- and nano-structures, as well as the overall desired depth of the channel. Different methods of fabrication will have various advantages depending on the desired application of the

microdevice and the need to be able to easily change components of the design. Furthermore, the overall cost of fabrication must be considered. While many different techniques have been developed for manufacturing microfluidic devices, several are associated with exorbitant costs, which is prohibitive for developing and prototyping devices.[69, 70] Furthermore, the accessibility to the equipment for various fabrication methods must be taken into account.

2.4.2 Cleanrooms

Highly controlled environments, known as cleanrooms, are often necessary to produce microfluidic devices. These environments limit possible contamination and potential degradation from various sources such as airborne and dust particles as well as chemical vapors.[70] Specifically, cleanrooms ensure a highly controlled environment by limiting the number of particles in the air and precisely controlling the temperature, humidity, and pressure. Cleanrooms are classified based on the allowable number of particles per volume of air. The International Organization for Standards (ISO) has a logarithmic scale based on the allowable number of particles, which are ≥ 0.1 μm in diameter, in a cubic meter that goes from ISO 1 to ISO 9. For example, there are approximately one billion (10^9) $\geq 0.1\ \mu m$ diameter particles in a cubic meter in ambient air from an urban environment. This corresponds to an ISO 9 cleanroom. An ISO 4 cleanroom denotes that there at most 10,000 particles/m^3. Due to the photosensitivity of photoresists, cleanrooms where photolithography is performed use yellow light to prevent unwanted development of the photoresists.[70] The cleanroom classification needed will depend upon the desired precision and the processes carried out for fabrication.

2.4.3 Substrates

A wide array of materials have been used to make microfluidic devices. Many of the early devices were fabricated from silicon and glass by using and altering techniques used in the manufacturing of micromechanical systems (MEMS) and semiconductors. An in-depth understanding of the structure, properties, and applications of silicon resulted from the rapid growth of the semiconductor industry. Silicon is a semiconducting material so it acts as an insulator at low temperatures, whereas at higher temperature it acts as a conductor.[70] The applications of it for microfluidic application is limited due to its high cost, fragile nature, and optical opacity. Glass on the other hand is optically transparent, but has significant expenses associated with fabrication, meaning that its implementation has been limited. Furthermore, bonding glass to other substrates can require high temperature or applied potentials.[69, 70]

Currently, one of the most commonly used substrates for microfluidic devices are polymers because they are inexpensive, disposable, can be optically transparent, and are applicable to a wide array of applications. Some of the most commonly used polymeric materials include polydimethylsiloxane (PDMS), polymethylmethacrylate (PMMA), polycarbonate (PC), and polystyrene (PS). [69] Even with several materials available, PDMS is one of the most prevalently-used compounds as it is optically transparent, easy to use for prototyping, biocompatible, inert, nontoxic, nonflammable, and relatively inexpensive.[69-73] Furthermore, PDMS can bond with several materials, including itself and glass, with the assistance of oxygen or air plasma treatment.[74] Though there are many advantages to using PDMS, there are some drawbacks that must be considered as PDMS readily swells in the presence of non-polar organic solvents, can be difficult to use

for multilayer fabrication, has a size limit for possible features, and small molecules can be absorbed into the PDMS.[75] PDMS is traditionally molded to a master template, made via photolithography and then bonded with another material to complete a microdevice. This process is known as soft lithography. Several materials are used to make the master templates including but not limited to, silicon, glass, SU-8, and various plastics.[69, 70, 76]

2.4.4 Fabrication Strategies

There are many methods to develop microfluidic devices. Some of the most common methods utilize dry and wet etching, mask-based photolithography, or thin film deposition.[70] In the past few decades devices that utilize soft lithography and PDMS have been used for a wide variety of applications.[71] Recently, other approaches of fabricating microdevices such as inkjet- or 3D-printing[73] and laser etching[77] have come to the forefront. More information on these techniques is detailed in Chapter 6 of this dissertation.

Photolithography is a common technique used to pattern desired designs onto various substrates. Generally, a photoresist, which is UV- sensitive, is employed to transfer the desired geometry from a photomask onto a substrate. Figure 2.5. depicts the basic steps of photolithography.

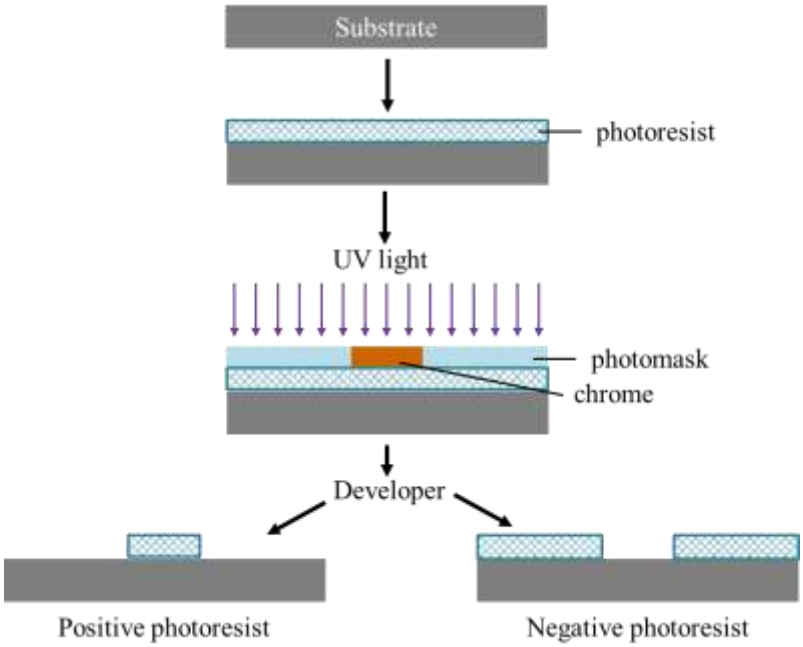

Figure 2.5. Schematic representation of photolithography. The developer will either remove the photoresist that was exposed (positive photoresist) or not exposed (negative photoresist) to the UV light.

For photolithography, a chromium mask can be created on polyester film, glass, or quartz; where quartz has the highest possible resolution and lowest probability of defects.[78] A laser or electron beam is used to etch the chromium mask based on the desired design, where the resolution of the final mask is dependent on the accuracy of the beam. When designing the mask, consideration for whether the desired features or surrounding area of the photomask need to keep the chrome coating must be accounted for, as this decide whether a positive or negative photoresist is need for fabrication.

To pattern a substrate, commonly to a silicon wafer, the first step is to spin a thin layer of photoresist onto the wafer. Known parameters are used for different spinners to reach a specific depth of photoresist, which can be verified using profilometry. Care must be taken when selecting a photoresist as each resist has a characteristic thickness and minimum feature sizes that it can support.[72, 79, 80] Using an aligner, UV light is used

to expose the photomask onto the photoresist. This can be done using three methods: (1) contact printing where the photomask is in direct contact with the photoresist (2) proximity printing where the mask is a set small distance from the photoresist and (3) projection printing where an optical system is used to expose the photoresist.[70] After exposure, a developer is used to remove the photoresist that was either exposed, for a positive photoresist, or not exposed for a negative photoresist.

Following photolithography there is the option to further establish the features by deposition or etching (Figure 2.6). Physical vapor deposition (PVD) can be used to deposit thin metal layers. Common metals for deposition include gold, aluminum, nickel, titanium, and platinum. One of the most commonly used PVD techniques is thermal evaporation, however sputtering is also utilized. A lift off procedure is then used to remove any unwanted deposited material. In contrast, wet and dry etching techniques are used to remove substrate that is not protected by the photoresist. In the case of wet etching techniques, liquids, which are generally strong acids, including HF, HCl, H_2SO_4, and H_3PO_4, are used to remove the substrate not protected by the photoresist. Wet etching techniques usually result in an isotropic etch meaning the etch rate is equal in all directions and results in an undercut of the mask lowering resolution and rounding the features, however it is normally insignificant and can be ignored.[70] In the case of a dry etch, plasma is used to etch away the substrate. Common gases used for plasma etches include SF_6, C_4F_8, and CHF_3 where O_2, H_2, and He can be used to improve and stabilize the process.[70, 81] Dry etching techniques generally result in an anisotropic etch, where the etch rate is direction-dependent, resulting in sloped walls with increasing depth.

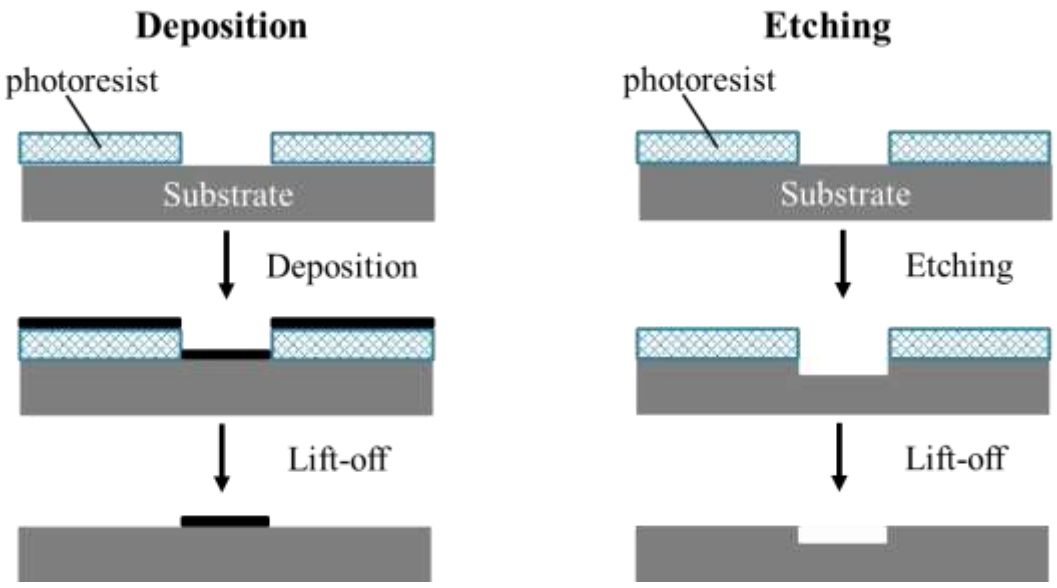

Figure 2.6. Depiction of deposition versus etching.

Soft lithography can then be employed, where a mold of the master micro- and/or nano-fabricated structure is used to create the microfluidic device. Commonly, PDMS is used to make a mold of the master and is then bonded to other substrates, such as a glass slide, to make the microfluidic device (Figure 2.7.)

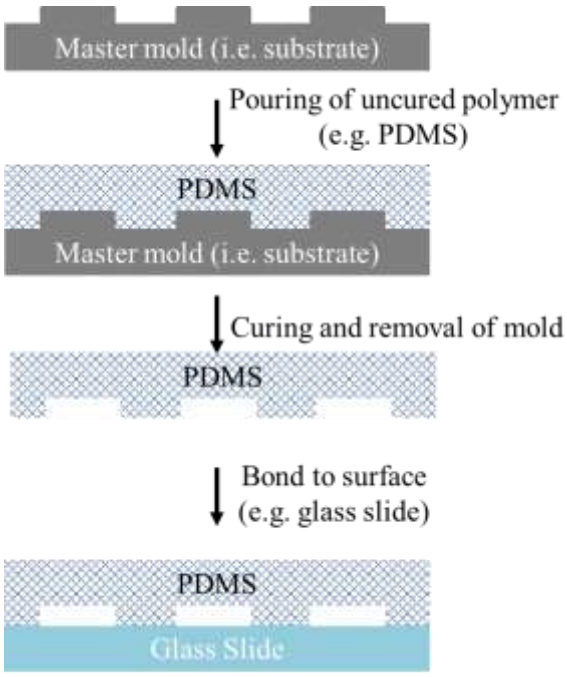

Figure 2.7. Soft lithography technique for creating microdevices.

Microdevice fabrication for the work done in this dissertation was performed using common soft-lithography techniques.[80] A template mold was made using photolithography. Device patterns were designed in-house on AutoCAD (Autodesk, Inc., San Rafael, CA) and a chrome photomask was produced by JD Photo Data (United Kingdom).[78] In a cleanroom, silicon wafers were coated with AZ 4330 photoresist (AZ Electronic Materials, Branchburg, NJ) and patterned with the photomask via contact printing on either an EVG 620 Contact Aligner (EV Group, Austria) or an OAI 808 Contact Aligner (OAI, San Jose, CA). The photoresist was then developed and an anisotropic etch was achieved using reactive ion etching (ICP etcher, SPTS, San Jose, CA).[81] All devices were characterized using optical profilometry (Zygo Zegage, Middlefield, CT) to determine depth and feature size.

Microdevices were made from the template silicon wafers by pouring polydimethylsiloxane (PDMS) (Sylgard 184, Dow/Corning, Midland, MI) on the wafers and curing the PDMS for one hour at 70°C. Once cured, the PDMS casts were removed from the wafer, trimmed, and access holes ($d = 3$ mm) were punched in the terminal reservoirs. PDMS casts were kept in airtight plastic bags in the freezer. All casts were utilized within two weeks of fabrication.

Before use, the PDMS microchannel casts were washed using isopropyl alcohol and 18 MΩ·cm water. The PDMS casts were then sonicated in 18 MΩ·cm water and dried with air. Glass slides were washed using the same procedure, except they received an acetone wash prior to the isopropyl alcohol wash. The PDMS casts were bonded to glass slides using oxygen plasma in a plasma cleaner (PDC-32G, Harrick Plasma, Ithaca, NY). Oxygen plasma was applied for 60 seconds at 18W with an approximate chamber pressure of 530 mTorr. The PDMS cast and the glass slide were bonded on contact to create the microchannels. All microchannels were cleaned and bonded on the day of use.

2.5 References

[1] Ohanian, H. C., Markert, J. T., *Physics for Engineers and Scientists*, W. W. Norton & Company, New York 2007.

[2] Pohl, H. A., *Dielectrophoresis : the behavior of neutral matter in nonuniform electric fields*, Cambridge University Press, Cambridge; New York 1978.

[3] Kirby, B. J., *Micro-and nanoscale fluid mechanics: transport in microfluidic devices*, Cambridge University Press 2010.

[4] Ren, X., Bachman, M., Sims, C., Li, G. P., Allbritton, N., *J. Chromatogr. B* 2001, *762*, 117-125.

[5] Kleinstreuer, C., *Microfluidics and nanofluidics : theory and selected applications*, Hoboken, New Jersey : Wiley 2014.

[6] Probstein, R. F., *Physicochemical Hydrodynamics: An Introduction*, John Wiley & Sons, Inc. 1994, pp. 1-8.

[7] von Smoluchowski, M., *Elektrische endosmose und stromungsstrome. In Handbuch der Elektrizitat und des Magnetimus*, Leipzig 1914.

[8] Jones, T. B., *Electromechanics of Particles*, Cambridge University Press 1995.

[9] Pohl, H. A., *Journal of Applied Physics* 1951, *22*, 869-871.

[10] Clarke, R. W., Piper, J. D., Ying, L., Klenerman, D., *Physical Review Letters* 2007, *98*, 198102.

[11] Pethig, R., *Biomicrofluidics* 2010, *4*, 022811.

[12] Cummings, E. B., Singh, A. K., *Analytical Chemistry* 2003, *75*, 4724-4731.

[13] Cummings, E. B., *Engineering in Medicine and Biology Magazine, IEEE* 2003, *22*, 75-84.

[14] Lapizco-Encinas, B. H., Simmons, B. A., Cummings, E. B., Fintschenko, Y., *Analytical Chemistry* 2004, *76*, 1571-1579.

[15] Jones, P. V., Staton, S. J. R., Hayes, M. A., *Analytical and Bioanalytical Chemistry* 2011, *401*, 2103-2111.

[16] Abdallah, B. G., Chao, T.-C., Kupitz, C., Fromme, P., Ros, A., *ACS Nano* 2013, *7*, 9129-9137.

[17] Saucedo-Espinosa, M. A., Lapizco-Encinas, B. H., *Electrophoresis* 2015, *36*, 1086-1097.

[18] Abdallah, B. G., Roy-Chowdhury, S., Coe, J., Fromme, P., Ros, A., *Analytical Chemistry* 2015, *87*, 4159-4167.

[19] Baylon-Cardiel, J. L., Lapizco-Encinas, B. H., Reyes-Betanzo, C., Chavez-Santoscoy, A. V., Martinez-Chapa, S. O., *Lab on a Chip* 2009, *9*, 2896-2901.

[20] Srivastava, S. K., Baylon-Cardiel, J. L., Lapizco-Encinas, B. H., Minerick, A. R., *Journal of Chromatography A* 2011, *1218*, 1780-1789.

[21] LaLonde, A., Gencoglu, A., Romero-Creel, M. F., Koppula, K. S., Lapizco-Encinas, B. H., *Journal of Chromatography A* 2014, *1344*, 99-108.

[22] Jones, P. V., Hilton, S. H., Davis, P. E., Yanashima, R., McLemore, R., McLaren, A., Hayes, M. A., *Analyst* 2015, *140*, 5152-5161.

[23] Kwon, J.-S., Maeng, J.-S., Chun, M.-S., Song, S., *Microfluidics and Nanofluidics* 2008, *5*, 23-31.

[24] Crowther, C. V., Hayes, M. A., *Analyst* 2017, *142*, 1608-1618.

[25] Lapizco-Encinas, B. H., Simmons, B. A., Cummings, E. B., Fintschenko, Y., *Electrophoresis* 2004, *25*, 1695-1704.

[26] Pohi, H. A., Hawk, I., *Science* 1966, *152*, 647-649.

[27] Crane, J. S., Pohl, H. A., *Journal of The Electrochemical Society* 1968, *115*, 584-586.

[28] Pohl, H. A., Crane, J. S., *Biophysical Journal* 1971, *11*, 711-727.

[29] Golan, S., Elata, D., Orenstein, M., Dinnar, U., *Electrophoresis* 2006, *27*, 4919-4926.

[30] Chaurey, V., Polanco, C., Chou, C.-F., Swami, N. S., *Biomicrofluidics* 2012, *6*, 012806.

[31] Price, J. A. R., Burt, J. P. H., Pethig, R., *Biochimica et Biophysica Acta (BBA) - General Subjects* 1988, *964*, 221-230.

[32] Huang, Y., Pethig, R., *Measurement Science and Technology* 1991, *2*, 1142.

[33] Pethig, R., Huang, Y., Wang, X.-b., Burt, J. P. H., *Journal of Physics D: Applied Physics* 1992, *25*, 881.

[34] Washizu, M., Kurosawa, O., *Industry Applications, IEEE Transactions on* 1990, *26*, 1165-1172.

[35] Washizu, M., Nanba, T., Masuda, S., *Industry Applications, IEEE Transactions on* 1990, *26*, 352-358.

[36] Hoettges, K. F., Hughes, M. P., Cotton, A., Hopkins, N. A. E., McDonnell, M. B., *Engineering in Medicine and Biology Magazine, IEEE* 2003, *22*, 68-74.

[37] Gonzalez, C. F., Remcho, V. T., *Journal of Chromatography A* 2009, *1216*, 9063-9070.

[38] Martinez-Duarte, R., Camacho-Alanis, F., Renaud, P., Ros, A., *Electrophoresis* 2013, *34*, 1113-1122.

[39] Hughes, M. P., Morgan, H., *Analytical Chemistry* 1999, *71*, 3441-3445.

[40] Labeed, F. H., Coley, H. M., Thomas, H., Hughes, M. P., *Biophysical Journal* 2003, *85*, 2028-2034.

[41] Hughes, M. P., Morgan, H., Rixon, F. J., Burt, J. P. H., Pethig, R., *Biochimica et Biophysica Acta (BBA) - General Subjects* 1998, *1425*, 119-126.

[42] Johari, J., Hübner, Y., Hull, J. C., Dale, J. W., Hughes, M. P., *Physics in Medicine and Biology* 2003, *48*, N193.

[43] Chou, C.-F., Tegenfeldt, J. O., Bakajin, O., Chan, S. S., Cox, E. C., Darnton, N., Duke, T., Austin, R. H., *Biophysical Journal* 2002, *83*, 2170-2179.

[44] Srivastava, S., Gencoglu, A., Minerick, A., *Analytical and Bioanalytical Chemistry* 2011, *399*, 301-321.

[45] Hsiao, F.-B., Jen, C.-P., Chen, H.-Y., Hsu, H.-L., Lee, Y.-C., Chuang, C.-H., Wang, C.-H., IEEE 2008, pp. 951-954.

[46] Chen, K. P., Pacheco, J. R., Hayes, M. A., Staton, S. J. R., *Electrophoresis* 2009, *30*, 1441-1448.

[47] Gencoglu, A., Minerick, A., *Lab on a Chip* 2009, *9*, 1866-1873.

[48] Masuda, S., Washizu, M., Nanba, T., *Industry Applications, IEEE Transactions on* 1989, *25*, 732-737.

[49] Staton, S. J. R., Chen, K. P., Taylor, J. P., Pacheco, J. R., Hayes, M. A., *Electrophoresis* **2010**, *31*, 3634-3641.

[50] Luo, J., Abdallah, B. G., Wolken, G. G., Arriaga, E. A., Ros, A., *Biomicrofluidics* 2014, *8*, 021801.

[51] Nakano, A., Ros, A., *Electrophoresis* 2013, *34*, 1085-1096.

[52] Nakano, A., Camacho-Alanis, F., Ros, A., *Analyst* 2015, *140*, 860-868.

[53] Staton, S. J. R., Jones, P. V., Ku, G., Gilman, S. D., Kheterpal, I., Hayes, M. A., *Analyst* 2012, *137*, 3227-3229.

[54] Regtmeier, J., Duong, T. T., Eichhorn, R., Anselmetti, D., Ros, A., *Analytical Chemistry* 2007, *79*, 3925-3932.

[55] Jones, P. V., DeMichele, A. F., Kemp, L., Hayes, M. A., *Analytical and Bioanalytical Chemistry* 2014, *406*, 183-192.

[56] Zhu, J., Tzeng, T.-R., Hu, G., Xuan, X., *Microfluidics and Nanofluidics* 2009, *7*, 751-756.

[57] Barbulovic-Nad, I., Xuan, X., Lee, J. S. H., Li, D., *Lab on a Chip* 2006, *6*, 274-279.

[58] Thwar, P. K., Linderman, J. J., Burns, M. A., *Electrophoresis* 2007, *28*, 4572-4581.

[59] Kang, K. H., Kang, Y., Xuan, X., Li, D., *Electrophoresis* 2006, *27*, 694-702.

[60] Kang, Y., Li, D., Kalams, S., Eid, J., *Biomedical Microdevices* 2008, *10*, 243-249.

[61] Ozuna-Chacón, S., Lapizco-Encinas, B. H., Rito-Palomares, M., Martínez-Chapa, S. O., Reyes-Betanzo, C., *Electrophoresis* 2008, *29*, 3115-3122.

[62] Pysher, M. D., Hayes, M. A., *Analytical Chemistry* 2007, *79*, 4552-4557.

[63] Jones, P., Staton, S. R., Hayes, M., *Analytical and Bioanalytical Chemistry* 2011, *401*, 2103-2111.

[64] Perez-Gonzalez, V. H., Gallo-Villanueva, R. C., Cardenas-Benitez, B., Martinez-Chapa, S. O., Lapizco-Encinas, B. H., *Analytical Chemistry* 2018, *90*, 4310-4315.

[65] Braff, W. A., Willner, D., Hugenholtz, P., Rabaey, K., Buie, C. R., *PloS one* 2013, *8*, e76751.

[66] Jones, P. V., Hayes, M. A., *Electrophoresis* 2015, *36*, 1098-1106.

[67] Staton, S. J. R., Chen, K. P., Taylor, T. J., Pacheco, J. R., Hayes, M. A., *Electrophoresis* 2010, *31*, 3634-3641.

[68] Ding, J., Woolley, C., Hayes, M. A., *Analytical and Bioanalytical Chemistry* 2017, *409*, 6405-6414.

[69] Becker, H., Locascio, L. E., *Talanta* 2002, *56*, 267-287.

[70] Leester-Schadel, M., Lorenz, T., Jurgens, F., Richter, C., in: Dietzel, A. (Ed.), *Microsystems for Pharmatechnology*, Springer 2016, pp. 23-57.

[71] McDonald, J. C., Duffy, D. C., Anderson, J. R., Chiu, D. T., Wu, H., Schueller, O. J. A., Whitesides, G. M., *Electrophoresis* 1999, *21*, 27-40.

[72] Xia, Y., Whitesides, G. M., *Annual Review of Materials Science* 1998, *28*, 153-184.

[73] Sochol, R. D., Sweet, E., Glick, C. C., Wu, S.-Y., Yang, C., Restaino, M., Lin, L., *Microelectronic Engineering* 2018, *189*, 52-68.

[74] Lucas, N., Demming, S., Jordan, A., Sichler, P., S., B., *Journal of Micromechanics and Microengineering* 2008, *18*, 075037.

[75] Toepke, M. W., Beebe, D. J., *Lab on a Chip* 2006, *6*, 1484-1486.

[76] Lorenz, H., Despont, M., Fahrni, N., LaBianca, N., Renaud, P., Vettiger, P., *Journal of Micromechanics and Microengineering* 1997, *7*, 121.

[77] da Costa, E. T., Santos, M. F. S., Jiao, H., do Lago, C. L., Gutz, I. G. R., Garcia, C. D., *Electrophoreis* 2016, *37*, 1691-1695.

[78] Dingley, J., in: Photo-Tools, J. (Ed.), JD Photo-Tools 2014, pp. 1-89.

[79] AZ Electronic Materials: AZ® 3300 Series Crossover Photoresists 2005.

[80] Mack, C., *Fundamental principles of optical lithography: the science of microfabrication*, John Wiley & Sons 2008.

[81] Bhardwaj, J., Ashraf, H., McQuarrie, A., *Proc. Symp. Microstructures and Microfabricated Systems, ECS* 1997.

CHAPTER 3

ISOLATION AND IDENTIFICATION OF *LISTERIA MONOCYTOGENES* UTILIZING DC INSULATOR-BASED DIELECTROPHORESIS

3.1 Introduction

3.1.1 *Listeria monocytogenes*

Listeriosis is an infection caused by *Listeria monocytogenes*, and while rare, is one of the deadliest foodborne illnesses. In the United States alone each year, 48 million new cases of illness can be associated with foodborne origins. They result in around 128,000 hospitalizations and 3,000 deaths, of which 19% of the deaths are caused by *L. monocytogenes*.[1, 2] *Listeria monocytogenes* is unique and hard to contain as it is able to grow and thrive in refrigeration and can also survive heating and drying remarkably well.[3] Furthermore, outbreaks of *L. monocytogenes* are notoriously difficult to detect as the organism has a long incubation time[4] and obtaining complete food histories can be challenging to impossible as patients are often extremely ill or deceased.[5]

Listeria monocytogenes is a rod-shaped gram-positive bacterium and is approximately 0.4-0.5 × 0.5-2.0 μm in size. There are thirteen serovars (serotypes), although 95% of outbreaks can be linked to three serovars, 1/2a, 1/2b, and 4b, where 4b causes more than half of these outbreaks.[6-8] A unique combination of expression of O-somatic and H-flagellar antigens defines the designation of each serovar.[9-11] The variable gene content in *L. monocytogenes* is described by three lineages I, II, and III, where serovars 1/2a is a part of lineage I and 1/2b and 4b are part of lineage II.[12, 13] These serovars represent broadly distinct phylogenetic groups.[8] There are several methods to detect *L. monocytogenes* and they can be categorized as culture-based

techniques, immuno-based techniques, molecular methods for identification and confirmation, and 'other'.[14] Beyond identification and confirmation, subtyping is performed using a variety of techniques including serotyping, phage typing; amplification-based, restriction digest-based, electrophoretic, and sequencing-based methods; along with single nucleotide polymorphism-based analysis.[15] Methods which utilize phenotypic subtyping are generally less sensitive, and therefore have a lower differentiation ability, and are hard to reproduce, while genotypic approaches are more reliable and sensitive.[14]

Many of the current techniques used for identification, confirmation, and subtyping of *L. monocytogenes* face limitations based on their lengthy time for assessment, issues of reproducibility between analysts; need of cold chain reagents, highly specific antisera, or restriction enzymes; and technical expertise.[5, 16] The most commonly used technique for confirmation and speciation of *L. monocytogenes* is Pulsed Field Gel Electrophoresis (PFGE); a national network of the laboratories performing PFGE to detect outbreaks is known as PulseNet.[5, 13, 17-20] In Europe and the US there has been a push to use PFGE in combination with whole-genome sequencing (WGS), which has greatly improved the ability for accurate speciation of *L. monocytogenes* and helped minimize the size of outbreaks.[5, 13] The complete process for running PFGE takes 1-4 days, while WGS takes 4-5 days.[17] However, it takes several weeks from confirmation of the presence of *L. monocytogenes* in a patient sample to the completion of PFGE and WGS, increasing the chances for outbreaks to spread.[17] There is a well-recognized need for a faster, high resolution, reproducible method of identifying and subtyping *L. monocytogenes*.[5, 10]

Serotyping can be performed as a preliminary method to subtype *L. monocytogenes* as it allows for comparison of results from different studies and offers context for phylogenetic or phenetic relationships.[10, 12, 21] Furthermore, serotyping gives insight into the epidemiology of *L. monocytogenes* serovars. However, there is some cross over in that *L. monocytogenes* and *L. seeligeri* share some serotypes so the incorrect species identification can occur.[22] Therefore, serotyping alone is not able, in the case of a listeriosis outbreak, to identify a positive correlation between foodborne and clinical isolates or identify the causal organism behind an outbreak. However, there is potential to demonstrate a negative correlation between a foodborne and a clinical isolate.

To accomplish serotyping, the traditional method of agglutination is costly and expertise-limited; and is dependent on high-quality sera, which is in turn dependent on standardized strains and antigen prep methods.[12, 23, 24] Alternatively, PCR methods can be more accessible, but they still require sequence-specific primers, and can have difficulties distinguishing some serovars.[10, 12, 25-27] Multi-locus sequence typing (MLST) and multi-locus virulence gene sequencing typing (MLVST) are also used to gain insight into various *L. monocytogenes* samples, but are time consuming and require technical reproducibility.[8] Recently, MALDI-TOF has been developed for the confirmation of various bacteria, including *Listeria*, down to the species level.[28-30] For *L. monocytogenes* lineage level detection has been established, however speciation of the specific serovars has not yet been achieved. Furthermore, the culture conditions will affect the accuracy of MALDI-TOF.[14, 28, 29]

3.1.2 Cell Manipulation Using Dielectrophoresis in Microfluidic Devices

This work proposes a new method of serotyping, which is not dependent on antisera or primers and can eventually be done in a in a cost-effective manner, by minimally trained personnel in a matter of minutes to a few hours based on biophysical properties of cells using microfluidics (Figure 3.1.).

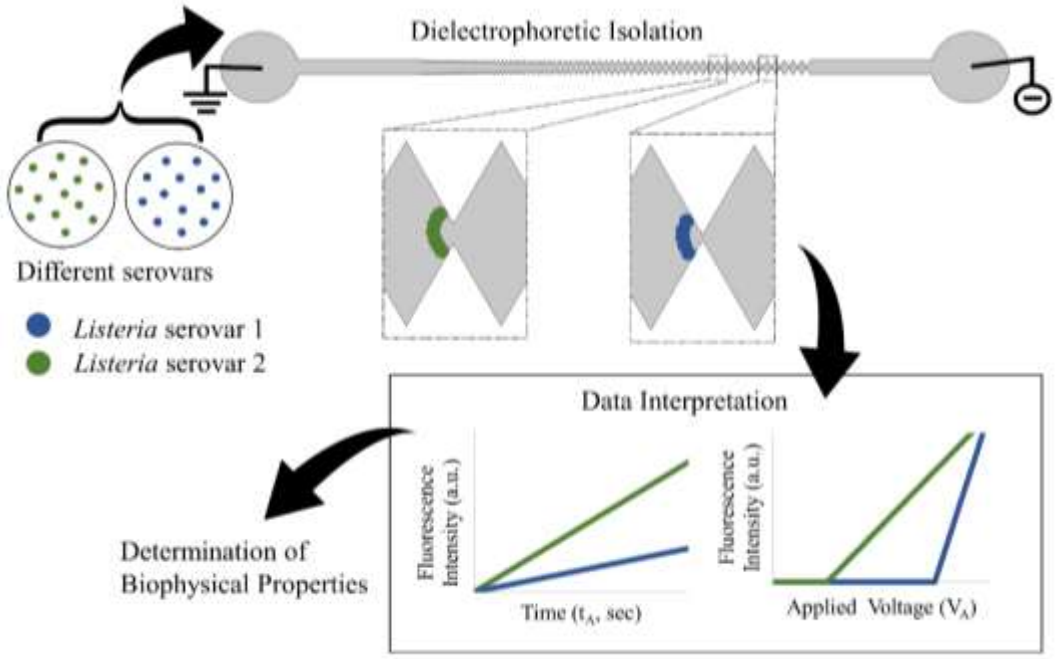

Figure 3.1. Representation of dielectrophoretic trapping in a gradient-iDEP microdevice for determination of biophysical properties of serovars. (Top) Two *Listeria* serovars analyzed using DEP in a microdevice. The microdevice has a sawtooth geometry, where the distance between the triangular insulator tips decreases from left to right. The hybrid device made of PDMS, fabricated with soft lithography, and glass are sealed together using an oxygen plasma treatment. The electrokinetic and dielectrophoretic properties for specific analytes interact uniquely with the microdevice which directly reflects their biophysical properties. The specific location of trapping for an analyte in the microdevice is based on differences in their biophysical properties; the point when the electrokinetic force is balanced by the dielectrophoretic force. (Bottom) The trapping behavior of an analyte can be interrogated and modeled using two methods: 1) based on the time potential has been applied or 2) varying the voltage applied to the system and monitoring signal at given time point.

The explosion of the microfluidics field in recent years is driven by the need for a low sample consumption, easy to use, inexpensive, rapid, precise, and accurate method

capable of probing biological samples.[31-40] Microfluidic techniques have been applied to a wide range of analytes, but as a relatively young field there are still many applications to investigate, improvements to be made, and potentially novel methods to explore.

One prominent set of techniques utilizes electrokinetic (EK) forces to interrogate analytes based on their response to an electric field. These techniques are comparatively simple to use and are applied to a wide variety of applications. One prominent EK technique is dielectrophoresis (DEP), which utilizes a non-uniform electric field to manipulate particles in response to their polarizability and can influence both charged and neutral particles.

Dielectrophoresis was first performed in 1951 using a two-electrode system.[41] The field initially developed as electrode-based dielectrophoresis (eDEP) using low voltages, where the size, shape, and positioning of the electrodes defines the distribution of the electric field. This strategy has been used to influence several analytes including, but not limited to: viruses[42, 43], bacteria[44], yeast[45], and mammalian cells[36, 46]. Some limitations to eDEP are that the electrodes are prone to fouling, channels cannot normally be reused, electrolysis (and other electron transfer reactions) can occur at the electrodes creating bubbles and potentially altering the buffers present, and fabrication can be expensive. Additionally, the forces are only effective in the volume near the electrodes where the high gradients are achieved.

An alternative to eDEP is insulator-based dielectrophoresis (iDEP), established in the early 2000s [37-40, 47-54], where electrodes are placed in distal reservoirs and insulating features are used to manipulate the distribution of the electric field. Alternating

Current (AC) and Direct Current (DC) fields can be used, where DC fields drive the movement of the analytes with EK transport, while AC fields can be used to refine separations. Properties of the particle, including size, structure, permittivity, surface charge, etc., will affect its behavior in a microchannel. At the constrictions in the microchannel the DEP force is the highest, and this is where the analytes will either be streamed or trapped in response to their individual properties. A significant application of the technique focuses on manipulation of bacterial cells to allow faster identification, isolate them from complex mixtures, and create a better understanding of their biophysical properties.[35, 47, 48, 51, 55]

This work uses iDEP to interrogate three serovars of *L. monocytogenes* by studying their trapping behavior in a microchannel. The trapping behavior of the serovars is quantified using a physical model of trapping which enables the explicit determination of both the electrophoretic and dielectrophoretic mobilities (Figure 3.1.). This system introduces a new technique for serotyping of *L. monocytogenes*, which is rapid, simple to use, and cost effective.

3.2 Theory

The manipulation of analytes using iDEP is possible because of the effects induced by the electrokinetic and dielectrophoretic forces. Further development of the effect of these forces is detailed in Chapter 2 and can be found in previous works.[51, 52, 56-59] For clarity a brief review is included here.

Using DC potentials, the electrophoretic (EP) and electroosmotic (EOF) velocities can be combined to define the electrokinetic velocity ($\vec{v}_{EK}$).

$$\vec{v}_{EK} = \mu_{EK}\vec{E} = (\mu_{EOF} + \mu_{EP})\vec{E} \quad (1)$$

Where μ_{EK}, μ_{EOF}, and μ_{EP} are the electrokinetic, electroosmotic, and electrophoretic mobilities, respectively, and $\vec{E}$ is the electric field. The dielectrophoretic velocity can be similarly described using the dielectrophoretic mobility (μ_{DEP}) and the gradient of the electric field squared $\left(\nabla \left| \vec{E} \right|^2\right)$.

$$\vec{v}_{DEP} = -\mu_{DEP} \nabla \left| \vec{E} \right|^2 \quad (2)$$

The effect of a non-uniform electric field acting on a polarizable particle is known as the dielectrophoretic force, $\vec{F}_{DEP}$. For a spherical particle with a single dipole, the force is described as:

$$\vec{F}_{DEP} = 2\pi\varepsilon_m r^3 f_{CM} \nabla \left| \vec{E} \right|^2 \quad (3)$$

where ε_m is the permittivity of the medium, r is the radius of the particle, and f_{CM} is the Clausius-Mossotti factor. The Clausius-Mossotti factor is dependent on the conductivity of the particle and medium in DC fields, and the resulting sign will result in either positive or negative DEP. Positive DEP occurs when the conductivity of the particle is greater than the conductivity of the media. This results in the particle being attracted to areas with high electric field strength. Conversely, negative DEP occurs when the conductivity of the media is larger than the conductivity of particle, which effectively repels the particle from areas with high electric field strength.

In the case of *L. monocytogenes*, which are rod shaped, when the DEP force is modelled the equation for an ellipsoid particle must be considered, which is described by:[60, 61]

$$\vec{F}_{DEP} = \frac{4}{3}\pi abc\varepsilon_m \left(\frac{\sigma_p - \sigma_m}{Z\sigma_p + (1-Z)\sigma_m}\right) \nabla \left| \vec{E} \right|^2 \quad (4)$$

where the semi-principal axes of the ellipsoid are represented by *a*, *b* and *c* (*a* > *b* = *c*) and *Z* is the depolarization factor.

Diffusion, advection, and electrokinetic effects control the movement of particles in a microfluidic channel. Advection ($\vec{v}_{Bulk}$) can be ignored since pressure driven flow is absent, and as *L. monocytogenes* is larger than 1 μm the effects of diffusion can also be disregarded. Particle flow can therefore be described by:[62, 63]

$$\vec{j} = D\nabla \mathrm{C} + C(\vec{v}_{Bulk} + \vec{v}_{EK} + \vec{v}_{DEP}) \approx C(\vec{v}_{EK} + \vec{v}_{DEP}) \quad (4)$$

where *D* is the diffusion coefficient and *C* is the concentration of particles. The movement of particles is therefore only affected by EK and DEP. The DEP velocity will only have an effect with high gradients of the electric field, which occur at the constriction points in the microchannel. Therefore, particle motion is mostly due to the EK, and the electric field lines approximate the particle movement in the microchannel.

Analytes are trapped in the microchannel when the particle velocity along the field line is zero: $\vec{j} \cdot \vec{E} = 0$. This trapping occurs such that $\vec{v}_{DEP}$ is equal to $\vec{v}_{EK}$. Using the EK and DEP mobilities the trapping of analytes can be described by:[56, 63]

$$\left(\mu_{EK}\vec{E} - \mu_{DEP}\nabla\left|\vec{E}\right|^2\right) \cdot \vec{E} \leq 0 \quad (5)$$

$$\frac{\nabla\left|\vec{E}\right|^2}{E^2} \cdot \vec{E} \geq \frac{\mu_{EK}}{\mu_{DEP}} \quad (6)$$

Trapping of particles in the microchannels provides absolute values for both the electrokinetic and dielectrophoretic mobilities which can in turn provide insight into the biophysical properties.

3.3 Materials and Methods

3.3.1 Microdevice Fabrication

A sawtooth microchannel was used for the manipulation of the three serovars of *L. monocytogenes*, which has been described in detail elsewhere.[32, 48, 64-67] Briefly, the microchannel walls consist of equilateral triangular shaped insulators that are adjoined. Gates in the microchannel occur at the constriction points in the microchannel when the two triangles from the channel walls are closest together in the microchannel. The size of the triangles increases from inlet to outlet, and as a result the gate sizes decrease. A given gate size repeats six times in the microchannel prior to the gate size decreasing. The characteristics of the microchannel are such that the length, width, and depth are 4.2 cm, 1000 μm, and 16.9 ± 1 μm (average between templates), respectively. The gates in the microchannel range in size from the initial 945 μm gate to the final 27 μm gate. All microchannels were cleaned and bonded on the day of use.

3.3.2 Cell Culture and Labeling

Three serovars of *L. monocytogenes*, specifically 1/2a (ATCC 51772), 1/2b (ATCC 51780), and 4b (ATCC 13932) were obtained. Seed stocks of each serovar were stored in Listeria enrichment broth (LEB) and 16.7% glycerol at -80°C. To grow the serovars, 10 mL of sterile LEB was aliquoted into a culture tube, inoculated, and placed in a shaker/incubator over night at 250 rpm (37°C). When cultures reach the late log phase, the approximate concentration of cells is 10^9 CFU mL^{-1}. The cultures were stored at 4°C.

Cells were labelled using NHS-rhodamine (excitation/emission wavelength: 552/575 nm). A 1:10 dilution of cultured cells in 2 mM phosphate buffer (PB), pH 7.4

was prepared. The NHS-rhodamine solution (10 mg/mL) was prepared fresh daily in DMSO. A 20 µL aliquot of the dye solution was added to the diluted cell suspension and vortexed and incubated in a water bath (37°C) for 20 minutes. To remove excess dye a wash procedure was repeated thrice with 2 mM PB. The first centrifugation was performed for 10 minutes at 2000 g, while all subsequent centrifugations were done for only 5 minutes. The final suspension of the labeled cell pellet was in 1 mL of 2 mM PB with 4 mg/mL of bovine serum albumin (BSA).

3.3.3 Experimental

A microdevice was filled with 2 mM PB, pipetting 15 µL into the inlet and outlet reservoirs. The solution was then removed from both inlet and outlet reservoirs and 15 µL of 2 mM PB with 4 mg/mL of BSA was introduced into the inlet reservoir for 10 minutes, providing a static coating of BSA on the channel walls prior to introduction of bacteria to the channel. Platinum electrodes (diameter 0.404 mm; Alfa Aesar, Ward Hill, MA) were inserted into the inlet and outlet reservoirs. The BSA solution was then removed and 15 µL of the labelled bacteria was added to the inlet reservoir and allowed to fill the channel without electrical manipulation for 10 minutes. The outlet reservoir was then filled with 15 µL of 2 mM PB with 4 mg/mL of BSA to eliminate hydrodynamic flow with a resulting conductivity of 3×10^2 µS/cm.

The microchannel was imaged using an Olympus IX70 inverted microscope with a 4× objective. The device was placed on the microscope stage and the platinum electrodes were connected to a HVS448 3000D high voltage sequencer (Labsmith, Inc., Livermore, CA). Illumination was provided by a mercury short arc lamp (H30 102 w/2, OSRAM). Fluorescence microscopy was enabled by an Olympus DAPI, FITC, Texas

Read triple band pass filter cube (Olympus, Center Valley, PA). DC potentials across the device ranged from 0-500 V in 50 V increments.

Images were digitally captured with a monochrome QICAM cooled CCD camera (QImaging, Inc., Surrey, BC) using Streampix V image capture software (Norpix, Inc., Montreal, QC). To assess, manipulate, quantify images, generate data, and convert files, Image J (NIH freeware) was used. For the velocity determination, individual bacteria were traced frame to frame at various applied voltages until the that specific particle could not be unequivocally identified in the subsequent frame. This was performed at or near the centerline of the microchannel just prior to the 27 μm gate. For each serovar, the path of ten bacterial cells were traced, determining their starting and ending locations and the time between location measurements. Analysis of particle velocity was performed for three trials of each serovar.

3.3.4 Safety Considerations

Organisms used in this experiment were Biosafety Level (BSL) II. Experiments were performed in an approved BSL II laboratory within accordance to the current version of the CDC/NIH BMBL publication.

3.4 Physical Modeling

3.4.1 Multiphysics

The distribution of the electric potential within the microchannel utilized in experiments was modelled using a finite element, multi-physics software (COMSOL, Inc., Burlington, MA). A detailed description of the modeling methods have been published elsewhere.[56] Briefly, an accurately-scaled 2D representation of the channel was built in AutoCAD and imported to COMSOL. A 2D model was used as it simplifies

the calculation and decreases computational time, and the electric potential will vary minimally across the relatively small depth. It is noted that the surface charge of glass and PDMS likely differ, which may affect the accuracy of the computations.

3.4.2 Model of the Data

A region of interest (ROI) is defined as an 80 × 50 pixel box at the first of the 27 μm gates (see data figures) was used to quantify the collection of bacteria in response to the trapping forces. The changing fluorescence intensity (*FI*) within this region was assessed with respect to time with a single voltage applied and with respect to the applied voltage at a set time of collection. To further understand the parameters effecting trapping, a model of the data, which correlates these factors was utilized.[68]

Briefly, the model determines the total number of particles that will arrive and can therefore be trapped at gate of interest. For these methods of data assessment, the distance (*d*) that a given particle may travel under the experimental conditions must be established.[68] Throughout most of the channel DEP forces are minimal (the exception being at the smaller gates) and the velocity is defined by EK effects.[56, 62, 63] Therefore, the distance a given particle travels to its trapping location can be described by combining $\vec{v}_{EK}$ (Eq. 1) and the basic equation for velocity:

$$d = \left(\mu_{EK}\vec{E}_{ave}\right)t \tag{7}$$

where *t* is time and $\vec{E}_{ave}$ is the average applied electric field. The total number of particles (*N*) in a given volume that can reach their trapping location can be described as:

$$N = ndwh = n\mu_{Ek}\vec{E}_{ave}wht \tag{8}$$

where and *n* is the concentration of particles, *w* is the width, and *h* is the height of channel. Each particle has an average fluorescence intensity (γ) which will contribute to

the total fluorescence intensity (*FI*). However, the trapped particles cannot all be simultaneously visualized since the depth of the focal plane is smaller than the depth of the channel and particles will overlap with one another. Therefore, to account for the depth of the microchannel, a stacking factor, *s*, is included, based on the number of particles that can be stacked in the depth of the channel:

$$FI = \frac{\gamma n \mu_{Ek} \vec{E}_{ave} wht}{s} \tag{9}$$

The time for which the potential is applied or the magnitude of the applied potential may be held constant. Holding the $\vec{E}_{ave}$ constant gives a time-dependent model. For the microchannel in this study, $\vec{E}_{ave}$ (V/m) is the applied potential (V_A) divided by the length of the microchannel:

$$\vec{E}_{ave} = 24V_A \tag{10}$$

For the microchannel used in this chapter, the time-based model is:

$$FI = \frac{24V_A \gamma n \mu_{Ek} wh}{s} t \tag{11}$$

The collection rate is directly proportional to the electrokinetic mobility (Figure 3.2.).

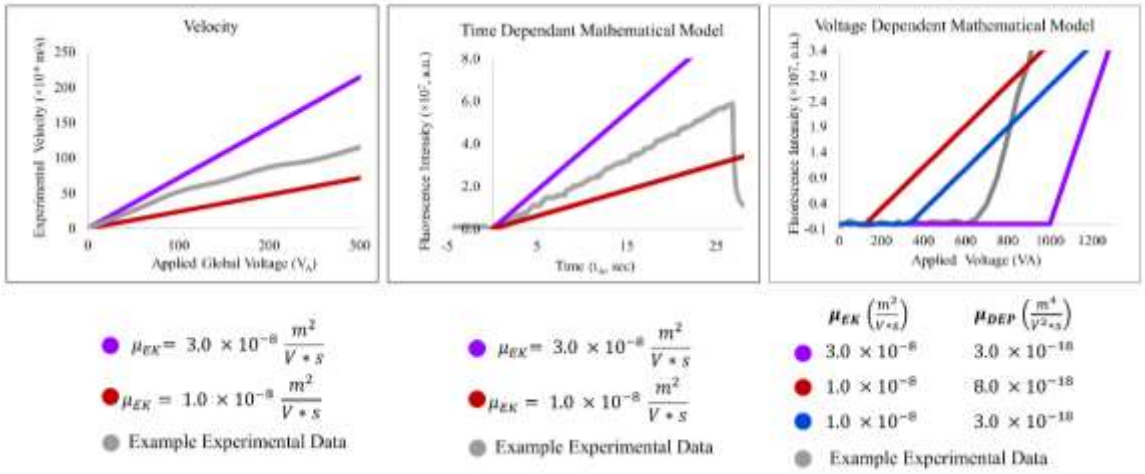

Figure 3.2. Illustration showing general structure of model and data. The behavior of analytes is monitored for velocity (left), time-dependent collection (middle) and voltage-dependent collection (right). Purple, red, and blue lines are representative values of biophysical properties and the grey lines are typical experimental behaviors. Velocity is monitored in the open portions of the channel and is reflective of the electrokinetic properties only (left). Time-dependent data (middle) is a function of the relative fluorescence intensity and the electrokinetic mobility of the particles. For the voltage dependent data (right), both the electrokinetic and dielectrophoretic mobility affect the onset voltage for trapping (correlating to the *x*-intercept of the line describing the sloped data, the discontinuity in the data structure). The slope is indicative of the amount of bacteria that have been collected given the application of voltage for a set amount of time at each voltage. A detailed description of the models for each data type can be found in the text. For both models the following values are used: $\gamma n = 5 \times 10^5 (a.u.m^{-3})$, $w = 0.3\ mm$, $h = 17\ \mu m$, $s = 15$. For time dependent model, the applied potential is 300 V and for the voltage-dependent model $t = 10\ s$ was used.

For a voltage-dependent data assessment of *FI* Equation 9 is rearranged such that, *t* is held constant at specific time after the initiation of applied potential, while V_A is varied, and a factor, *c*, relative to the onset of voltage is introduced:

$$FI(V_A) = \frac{\gamma n \mu_{Ek} wht}{s} \vec{E}_{ave}(V_A) + c \tag{12}$$

The onset of trapping can be correlated to the ratio of mobilities (Eq. 6) for a given analyte of interest.

$$\frac{\nabla |\vec{E}|^2}{E^2} \cdot \vec{E}(c) \geq \frac{\mu_{EK}}{\mu_{DEP}} \tag{13}$$

Values for the electric field and gradient were determined with finite element multi-physics modeling using the centerline and the maximum ratio achieved (Vm^{-2}) at the first 27 µm gate. Using the specific properties of the channel used in this chapter results in the following relationship:

$$\left[\frac{\nabla\left|\vec{E}\right|^2{}_{max}}{E^2{}_{max}} \cdot \vec{E}_{max}(c)\right] = 1.0 \times 10^7 * c = \frac{\mu_{EK}}{\mu_{DEP}} \tag{14}$$

$$c = \frac{1}{1.0\times10^7}\left(\frac{\mu_{EK}}{\mu_{DEP}}\right) \tag{15}$$

The signal from the voltage-dependent data is well-described by a piecewise function, with the discontinuity at *c*:

$$FI(V_A) = \begin{cases} 0, \ if\ V_A < \frac{1}{1.0\times10^7}\left(\frac{\mu_{EK}}{\mu_{DEP}}\right) \\ 24\frac{\gamma n \mu_{Ek} wht}{s}\left[V_A - \frac{1}{1.0\times10^7}\left(\frac{\mu_{EK}}{\mu_{DEP}}\right)\right], \ if\ V_A \geq \frac{1}{1.0\times10^7}\left(\frac{\mu_{EK}}{\mu_{DEP}}\right) \end{cases} \tag{16}$$

When no trapping occurs in the microchannel, the contribution to *FI* from the trapped analyte is absent.

3.5 Results

The three most common serovars of *L. monocytogenes* were interrogated using iDEP. Each of the serovars was studied in the V1 microchannel, which has been described in detail.[48, 64] For this work, the behavior of the bacteria was assessed at a consistent gate position in each microchannel.

3.5.1 Determining the Velocity and Electrokinetic Mobilities of the *Listeria monocytogenes* Serovars

The velocity for all three serovars were determined in the more open portion of the channel, prior to the gate of interest, where no evidence of trapping behavior was observed (Figure 3.3.). The velocity was linear with respect to V_A allowing for an accurate estimate of μ_{EK} from a range of voltages and velocities. The characteristic value for the serovars of *L. monocytogenes* (Eq. 1), and their 95% CI, were determined as 19 ± 0.7, 17 ± 0.7, and $9.2 \pm 0.3 \times 10^{-9}$ $\frac{m^2}{Vs}$ for serovars1/2a, 1/2b, and 4b, respectively.

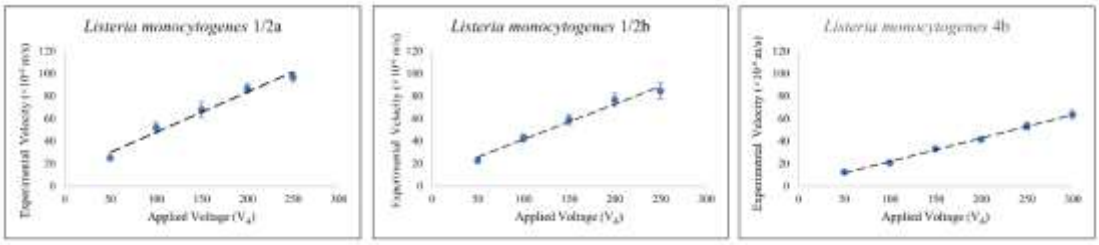

Figure 3.3. Plots of the velocity of three serovars at various applied potentials (V_A). All data collected near the first 27 µm gate in the V1 microchannel. Dotted lines are linear fits to the data and error bars are at the 95 % confidence interval. The linear fit is used to determine the electrokinetic mobility for each serovars using $\vec{v}_{Ek} = \mu_{EK}\vec{E}$.

3.5.2 Trapping Experiments

The behavior of the three serovars of *L. monocytogenes* were studied in an iDEP microchannel where the magnitude of V_A or its duration of application (t_A) were varied. The structure of the data for all three of the serovars was consistent with previous work that used similar methods in a microdevice with comparable geometry. The movement of the analyte toward the outlet with applied potential supports EOF-dominated transport.[47, 48, 54] Trapping behavior of *L. monocytogenes* was assessed at the first 27 µm gate, where no trapping of the analyte was observed at the 90 µm or larger gates.

Characteristically, the fluorescently-labelled bacteria collected in a crescent shape a few microns prior to the first 27 µm gate on the inlet side of the gate (Figures 3.1. and 3.4.).

The amount of trapped analyte was determined by measuring the *FI* in a given ROI centered near the point of typical trapping (Figure 3.4., left, blue box). There are several factors which affect the trapping of material in the microchannel, including the biophysical properties of the analyte of interest, the channel geometry, and the experimental conditions (voltage, buffer properties).

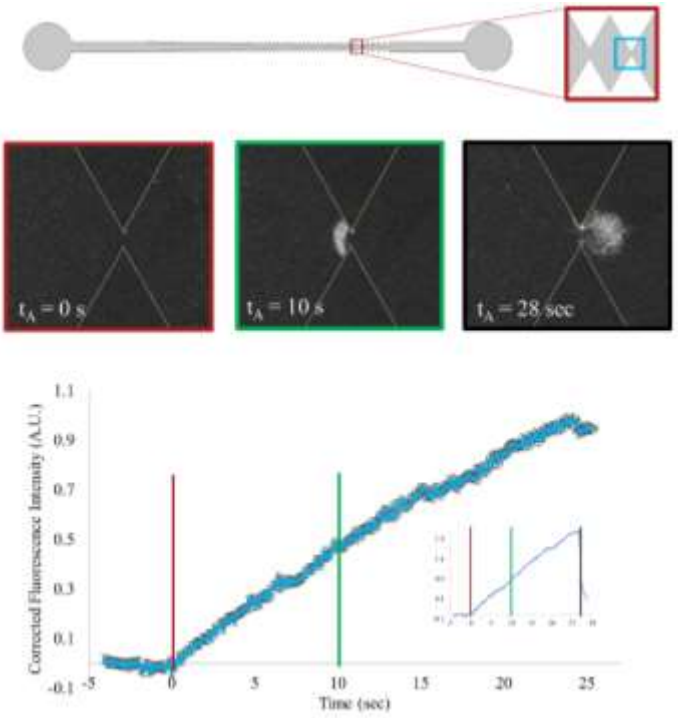

Figure 3.4. Typical trapping behavior and data in a V1 microchannel at the 27 µm gate (top illustration, the light blue box represents the area in the images). The data depicted is of *Listeria monocytogenes* 1/2a with an applied potential of 350 V (85 V/cm). Negative dielectrophoresis results in the collection of the material in a crescent-shaped band on the inlet side of the gate (middle micrograph). Trapping occurs at applied potentials above a threshold value specific to the serovar. The bacteria are continuously collected when potential is applied. Three time points are shown as images, color coded corresponding to lines on *FI* vs *t* plot demonstrating the channel before, during, and after trapping (red = 0 s, green = 10 s, black = 28 s; *n* = 12, ROI described in the text). The grey region around each data point in plot is the 95% confidence interval. Inset is typical data for a single trial. The reversible nature of capture of the bacteria is demonstrated in the last image, at 28 s, immediately after the voltage is removed.

There is a threshold electric potential (c) which meets the trapping ratio that results in bacteria being collected instead of continuing to move past the gate (Eq. 5, 6, &16). The rate at which the bacteria collects is characteristic of the particle transport rate, which is dependent on the $\vec{v}_{EK}$. The material continues accumulating in a linear fashion as long as the potential is applied (Figure 3.4., bottom).

The trapping behavior of all three serovars were assessed at a consistent time point (t_A = 10 s, Figure 3.4., green line) at voltages from 50-500 V in increments of 50 V. The *FI* was then normalized for concentration, and the *FI* in the ROI prior to the application of voltage. The *FI* with no applied voltage was measured prior to the application of voltage, specifically 2 seconds after recording was started for the 50 V trials. The threshold value of trapping (when V_A=c) was determined by first determining baseline behavior at low applied potentials where no trapping occurred. The baseline for serovars 1/2b and 4b was determined using the data from 0-150 V applied, while for 1/2a was determined using the data for 0-250V. The background signal limit is denoted by two standard deviations above the average baseline. Statistically significant trapping was considered to be occurring when the *FI* of the trapped material exceed the background limit. In the case of serovars 1/2a and 1/2b, their respective data points of 300 and 250 V were determined to be significantly different at the 95% CI than the background limit using a 2-tailed *t*-test. Whereas for serovar 4b, the 250 V data point is not significantly different from the background limit, however if the data point is included in the determination of c, it does not result in a significant difference. Increasing the applied

potential resulted in more material being trapped in the 10 second timeframe for applied potential (Figure 3.4.).

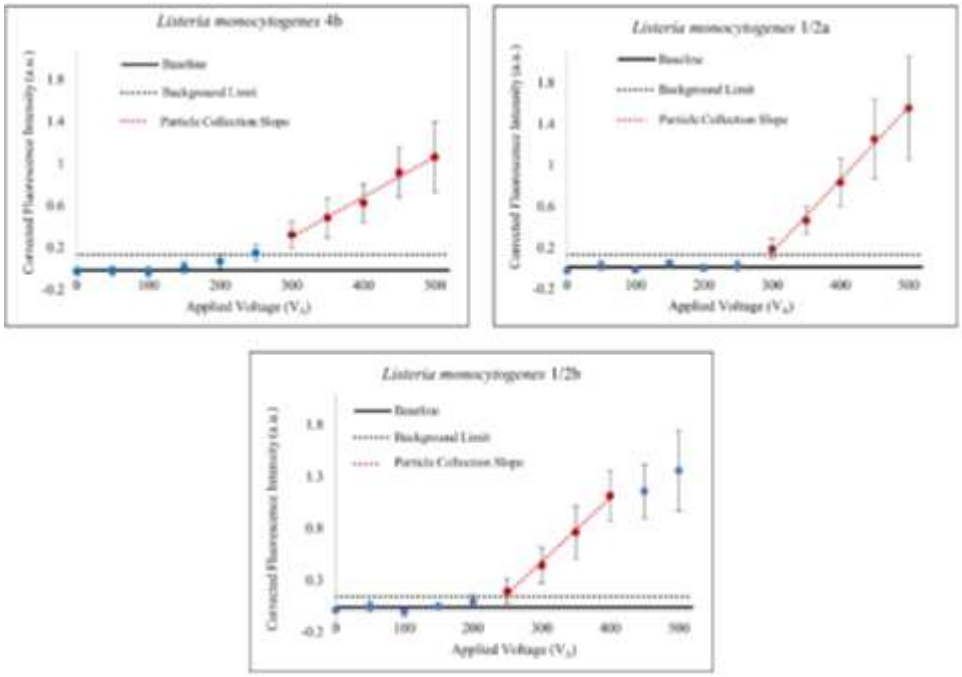

Figure 3.5. Trapping behavior for three serovars (identification noted above each plot) at various applied potentials (V_A). All data was collected at a 27 μm gate in the V1 microchannel after the potential was applied for 10 seconds (t_A). Slope was assessed using signals exceeding the background limit (twice the standard deviation of the baseline data points). Dotted red lines are fitted from the linear part of the data (see text) above the baseline and background limit. The initial trapping voltage is determined by the *x*-intercept of the linear fit line. The error bars are the 95% confidence interval. Using the linear fits, both the electrokinetic and dielectrophoretic mobilities can be determined using the voltage based physical model (see text).

All three serovars resulted in a predominantly linear, positive slope at applied potentials greater than their respective values of *c*. For all three serovars the red data points were utilized to determine *c* and to calculate the trapping ratio of mobilities (Figure 3.5.). The values of *c* were determined to be 280 ± 18, 220 ± 15, and 220 ± 31 V for the *L. monocytogenes* serovars 1/2a, 1/2b, and 4b, respectively. The ratio of mobilities necessary for trapping was then determined, using COMSOL models, to be

$2.8 \pm 0.2 \times 10^9$, $2.2 \pm 0.2 \times 10^9$, and $2.2 \pm 0.3 \times 10^9$ $\frac{V}{m^2}$ for the *L. monocytogenes* serovars 1/2a, 1/2b, and 4b, respectively.

3.5.3 Modeling of the Data

To verify the efficacy of the data modeling, μ_{EK} for all three serovars was determined using the voltage-dependent data (Eq. 16). Only data beyond the value of V_A where statistically significant trapping occurred were used for the determination of μ_{EK} (Figure 3.5.). The *FI* for all the trials were taken after 10 seconds of applied potential, the channel height in all cases was 17 μm, and $\vec{E}_{ave}$ was determined from Eq. 10. The determination has bracketed variables of the *FI* observed for trial and the number of trapped particles that can reasonable fit in the trapping zone. The microchannel width, in this study, is between 27 to 1000 μm, however given that the majority of the channel has insulating features a realistic range for the average channel width that the bacteria may be trapped in is 0.25 ± 0.05 mm. As the channel height is 17 μm a maximum of 34 stacked *L. monocytogenes* cells can be stacked with 1 being the obvious minimum. The actual number of stacked bacteria when trapped is dependent on the size and interactions of individual bacterium. Within this range, the calculated value of μ_{EK} easily falls within the independently measured values (Figure 3.3. and narrative). Serovars 1/2a and 1/2b fall within the 95% CI interval ($19 \pm 3.4 \times 10^{-9}$ and $17 \pm 3.3 \times 10^{-9}$ $\frac{m^2}{Vs}$, respectively) of the μ_{EK} as determined from velocity measurements if 20 bacterial cells are assumed to be stacked and the average channel width is 0.22 μm. For serovar 4b, the data fits within the 95% CI ($9.2 \pm 1.3 \times 10^{-9} \frac{m^2}{Vs}$) if 12 bacterial particles are stacked with the same average channel width. I recognize that the observed *FI* provides for a rather generous

multiplicative range for stacked bacteria (1-34), but the fact that reasonable values are observed (~12 and ~20), I find this to be supportive of an appropriate treatment and interpretation of these data. This is in spite of some obvious sources of variance which can be attributed to necessarily low number of replicates ($n \leq 11$) for a proof-of-principle study, occasional aggregate formation (changing the trapping location and/or altering the electric field across the device), and small variations in the prototype microdevices. In the case of the serovar 1/2b the data plateaus for the voltage dependent assessment (Figure 3.5.). This is potentially caused by several factors, including reaching the maximum amount of material collected in the ROI after 10 seconds, surpassing the detection limit of the CCD camera, or bacteria starting to collect at the 60 μm gate.

3.6 Discussion

Subtyping, specifically serotyping, in a rapid and reproducible manner is desirable to obtain epidemiological information about *L. monocytogenes*. However, serotyping faces several challenges, including ambiguity, difficulties in inter-laboratory reproducibility, availability and excessive cost of cold chain reagents, and lack of correlation between strains from different listeriosis infections.[24, 69, 70] This study serves as a proof-of-principle study for a technique that uses microfluidics and electrokinetic forces to rapidly identify, isolate, and serotype *L. monocytogenes*. The three most common serovars have been demonstrated to have distinct behavior in the microchannel, which is indicative of their electrokinetic and dielectrophoretic properties (Figures 3.3.-3.6.).

The *L. monocytogenes* serovars tested in this study each behave uniquely according to their biophysical properties (Figure 3.3.). One sub-component which can be

independently determined is their $\vec{v}_{EK}$, how fast they move in the microchannel when not influenced by DEP, and by extension their μ_{EK}. The electrokinetic mobility determination allows insight into the biophysical properties of the cell centered on the concentration and distribution of charge on the surface. Linear electrophoretic approaches have been used to measure μ_{EK} with some success [71-73], consistent with these results. These linear assessments, as practiced, were time consuming, gave broad uneven distributions of μ_{EK}, and required pure, well characterized samples. Dielectrophoretic trapping probes the same biophysical properties of the cell as electrokinetic measurements but addresses them in a significantly different format because of the focusing, gradient nature of the technique. Mixed populations may be assessed and the 'distributions' can be closely examined, quantified, and parsed for biological significance. Of course, in the DEP experiments, their respective μ_{DEP} is also captured and can be related to several biophysical cell properties including (but not limited to) to the size and ability for charge to pass through the cell.

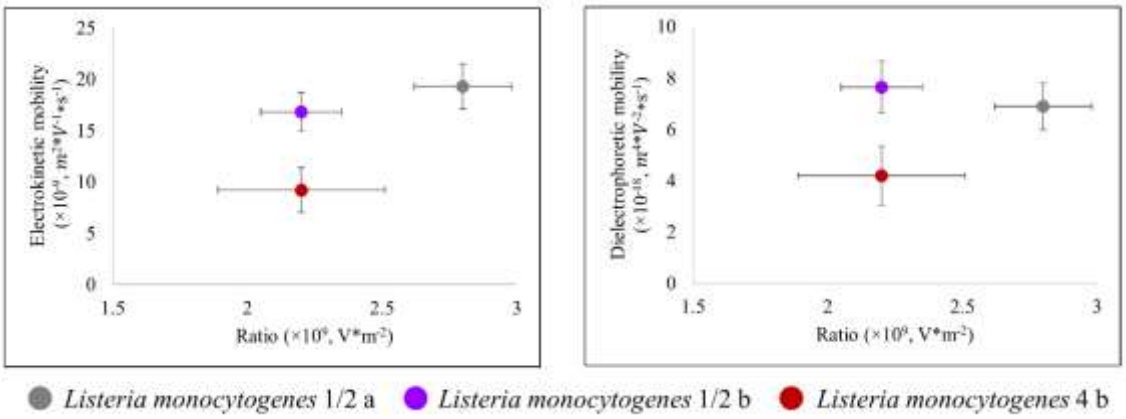

Figure 3.6. Comparison of the mobilities and their ratio for the three serovars of *L. monocytogenes* (note vertical axis for each plot). Each serovar possesses a unique set of biophysical properties that can be probed by iDEP. Some serovars pairs have significant statistical overlap in μ_{EK} and μ_{DEP}. Including both mobilities, however, allows for differentiation. These differences can be displayed with regard to either the electrokinetic or dielectrophoretic properties without preference in this case. For other serovar or strain comparisons, one plot or the other may allow for the unique differentiation.

The different biophysical properties of the three *L. monocytogenes* serovars can be displayed in different configurations (Figures 3.5. and 3.6.). The variations in the slope correlate to the rate of collection, and thus μ_{EK}; whereas the variations in *c* are a result from differences in both μ_{EK} and μ_{DEP} (Figure 3.5.). The necessary trapping conditions can be represented for each of the *L. monocytogenes* serovars based on the parameters defined in this work and either the μ_{EK} or μ_{DEP}. The three serovars of *L. monocytogenes* studied in this chapter can be differentiated using their μ_{EK} and μ_{DEP}, even though there is statistical overlap in their trapping ratios. This is indicative of the fact that all the serovars have unique biophysical properties.

Some of the differences between the serovars' behavior can be attributed to changes on the surface of the cell. For the *L. monocytogenes* serovars this is with respect to the O-somatic and H-flagellar antigens.[74] Genetic differences between serovars have been defined using the large amount of genetic information collected by PFGE, WGS,

MLST, and MLVST. Correlation between various genetic elements and phenotype have been identified, however a direct connection is not always apparent.[8, 13, 75]

The use of DEP and microfluidics allows for a new method of rapidly subtyping, specifically serotyping, *L. monocytogenes*. Unlike current diagnostic methods this strategy can be performed with minimal sample preparation, in a less than a few hours, and can be automated allowing for reproducibility between analysts without the need for specialized techniques. Dielectrophoretic trapping could be used as a method to determine positive or negative correlation of a clinical isolate to a known isolate, helping to rapidly determine which serovar is present. Beyond the proof-of-concept presented here, this method will need to be fully characterized for its ability to reliably serotype all strains of *L. monocytogenes* and identify *L. monocytogenes* versus other strains of *Listeria*. Further testing would also need to be performed to confirm that this method can overcome the challenges which PCR faces.[10, 12] Current isolation methods for clinical samples requires growth on selective solid media and the fastidious nature of *Listeria* means it may take from one to three days for growth with additional testing required for identification.[17] These methods cannot determine specific serovars of *L. monocytogenes*, and is what results in the need for further testing by PFGE and WGS to identify outbreaks. This dielectrophoretic method would allow rapid, straightforward isolation, identification, and subtyping from a single sample.

Beyond applications of identifying strains of *Listeria*, the combination of finite element multi-physics calculations and the model of the data enables a new understanding of how biophysical differences of analytes result in differing trapping behaviors. Specifically, using the ratio of mobilities and *c*, unique values for both μ_{EK}

and μ_{DEP} can be determined. To verify the accuracy of this model a comparison of the $\mu_{EK}$was determined based on the velocity of the bacterial particles and using the model. For the model of the data, a change in the number of stacked particles can significantly shift the determination of μ_{EK}. This is seen for the *L. monocytogenes* serovars as when all the parameters except the stacking factor are held constant, the respective serovars fall within the 95% CI of the velocity determined measurements for *L. monocytogenes* 1/2a and 1/2b with 20 stacked particles and for *L. monocytogenes* 4b with 12 stacked particles. It should be noted that *L. monocytogenes* 4b has the largest error in *c*, which will result in less accuracy in the of μ_{EK} determined by the model. To further refine the values determined by the model more trials may be necessary. With more data points that fall in the linear range of the voltage dependent data (Figure 3.5.) an estimate with lower variance for the mobilities should be possible. Furthermore, the assumptions made for the width and stacking factor are bounded independent variables. The width of the channel when trapping occurs will vary slightly with the applied voltage.

3.7 Conclusion

This work demonstrates the ability for iDEP to differentiate the three most common serovars of *L. monocytogenes*, establishing a foundation for a subtyping/serotyping method and a new investigative tool for basic scientific studies of *Listeria*. The serovars behavior in the microchannel allows for their differentiation, and their electrokinetic and dielectrophoretic mobilities can also be determined. In the future, based on the work presented here, the *L. monocytogenes* serovars can be separated using gradient-iDEP based on the difference in their biophysical properties. A physical model is employed and verified to assess the DEP trapping behavior and gives insights into the

origins of the differing behaviors of the analytes. Using this model may help to better understand the differences both between and within serovars. Changes in some of the experimental parameters, buffer compositions and applied potential (AC vs DC), could potentially help improve this separation capability. An investigation into the ability of iDEP to identify variants of the serovars, such a variant of 4b, termed 4bV or IVb-v1, would also be beneficial to further establish this technique.[8]

3.8 References

[1] Scallan, E., Hoekstra, R. M., Angulo, F. J., Tauxe, R. V., Widdowson, M.-A., Roy, S. L., Jones, J. L., Griffin, P. M., *Emerging Infectious Diseases* 2011, *17*, 7-15.

[2] Scallan, E., Griffin, P. M., Angulo, F. J., Tauxe, R. V., Hoekstra, R. M., *Emerging Infectious Diseases* 2011, *17*, 16.

[3] Ramaswamy, V., Cresence, V., Rejitha, J., Lekshmi, M., Dharsana, K., Prasad, S., Vijila, H., in: Ramaswamy, V. (Ed.) 2007, pp. 4-13.

[4] Goulet, V., King, L. A., Vaillant, V., de Valk, H., *BMC Infectious Diseases* 2013, *13*, 11.

[5] Jackson, B. R., Tarr, C., Strain, E., Jackson, K. A., Conrad, A., Carleton, H., Katz, L. S., Stroika, S., Gould, L. H., Mody, R. K., Silk, B. J., Beal, J., Chen, Y., Timme, R., Doyle, M., Fields, A., Wise, M., Tillman, G., Defibaugh-Chavez, S., Kucerova, Z., Sabol, A., Roache, K., Trees, E., Simmons, M., Wasilenko, J., Kubota, K., Pouseele, H., Klimke, W., Besser, J., Brown, E., Allard, M., Gerner-Smidt, P., *Clinical Infectious Diseases* 2016, *63*, 380-386.

[6] Ward, T. J., Gorski, L., Borucki, M. K., Mandrell, R. E., Hutchins, J., Pupedis, K., *Journal of Bacteriology* 2004, *186*, 4994-5002.

[7] Muñoz, P., Rojas, L., Bunsow, E., Saez, E., Sánchez-Cambronero, L., Alcalá, L., Rodríguez-Creixems, M., Bouza, E., *Journal of Infection*, *64*, 19-33.

[8] Bergholz, T. M., Shah, M. K., Burall, L. S., Rakic-Martinez, M., Datta, A. R., *Applied Microbiology and Biotechnology* 2018, *102*, 3475-3485.

[9] Rebuffo-Scheer, C. A., Schmitt, J., Scherer, S., *Applied and Environmental Microbiology* 2007, *73*, 1036.

[10] Borucki, M. K., Call, D. R., *Journal of Clinical Microbiology* 2003, *41*, 5537-5540.

[11] Seeliger, H. P. R., Höhne, K., in: Bergan, T., Norris, J. R. (Eds.), *Methods in Microbiology*, Academic Press 1979, pp. 31-49.

[12] Doumith, M., Buchrieser, C., Glaser, P., Jacquet, C., Martin, P., *Journal of Clinical Microbiology* 2004, *42*, 3819-3822.

[13] Bergholz, T. M., den Bakker, H. C., Katz, L. S., Silk, B. J., Jackson, K. A., Kucerova, Z., Joesph, L. A., Turnsek, M., Gladney, L. M., Halpin, J. L., Xavier, K., Gossack, J., Ward, T. J., Frace, M., Tarr, C. L., *Applied and Environmental Microbiology* 2016, *82*, 928-938.

[14] Jadhav, S., Bhave, M., Palombo, E. A., *Journal of Microbiological Methods* 2012, *88*, 327-341.

[15] Ronholm, J., Nasheri, N., Petronella, N., Pagotto, F., *Clinical Microbiology Reviews* 2016, *29*, 837-857.

[16] *Listeria, Listeriosis and Food Safety*, CRC Press, Boca Raton 2007.

[17] Timeline for Linking a Case of Listeria Infection to an Outbreak, in: H.S.S.-C.D.C. Prevention, 2016.

[18] Graves, L. M., Swaminathan, B., *International Journal of Food Microbiology* 2001, *65*, 55-62.

[19] Buchrieser, C., Brosch, R., Catimel, B., Rocourt, J., *Canadian Journal of Microbiology* 1993, *39*, 395-401.

[20] Gilmour, M. W., Graham, M., Van Domselaar, G., Tyler, S., Kent, H., Trout-Yakel, K. M., Larios, O., Allen, V., Lee, B., Nadon, C., *BMC Genomics* 2010, *11*, 120-120.

[21] Carp-Cărare, C., Vlad-Sabie, A., Florişţean, V.-C., *Romanian Review of Laboratory Medicine* 2013, p. 285.

[22] Liu, D., *Journal of Medical Microbiology* 2006, *55*, 6 45-659

[23] Seeliger, H. P. R., Langer, B., *International Journal of Food Microbiology* 1989, *8*, 245-248.

[24] Palumbo, J. D., Borucki, M. K., Mandrell, R. E., Gorski, L., *Journal of Clinical Microbiology* 2003, *41*, 564-571.

[25] D'Urso, O. F., Poltronieri, P., Marsigliante, S., Storelli, C., Hernández, M., Rodríguez-Lázaro, D., *Food Microbiology* 2009, *26*, 311-316.

[26] Chen, Y., Knabel, S. J., *Applied and Environmental Microbiology* 2007, *73*, 6299-6304.

[27] Kérouanton, A., Marault, M., Petit, L., Grout, J., Dao, T. T., Brisabois, A., *Journal of Microbiological Methods* 2010, *80*, 134-137.

[28] Jadhav, S., Sevior, D., Bhave, M., Palombo, E. A., *Journal of Proteomics* 2014, *97*, 100-106.

[29] Jadhav, S., Gulati, V., Fox, E. M., Karpe, A., Beale, D. J., Sevior, D., Bhave, M., Palombo, E. A., *International Journal of Food Microbiology* 2015, *202*, 1-9.

[30] Barbuddhe, S. B., Maier, T., Schwarz, G., Kostrzewa, M., Hof, H., Domann, E., Chakraborty, T., Hain, T., *Applied and Environmental Microbiology* 2008, *74*, 5402.

[31] Dingley, J., in: Photo-Tools, J. (Ed.), JD Photo-Tools 2014, pp. 1-89.

[32] Jones, P., Staton, S. R., Hayes, M., *Analytical and Bioanalytical Chemistry* 2011, *401*, 2103-2111.

[33] Jones, P. V., Hayes, M. A., *Electrophoresis* 2015, *36*, 1098-1106.

[34] Li, M., Li, W. H., Zhang, J., Alici, G., Wen, W., *Journal of Physics D: Applied Physics* 2014, *47*, 063001.

[35] LaLonde, A., Romero-Creel, M. F., Lapizco-Encinas, B. H., *Electrophoresis* 2015, *36*, 1479-1484.

[36] Labeed, F. H., Coley, H. M., Thomas, H., Hughes, M. P., *Biophysical Journal* 2003, *85*, 2028-2034.

[37] Perez-Gonzalez, V. H., Gallo-Villanueva, R. C., Cardenas-Benitez, B., Martinez-Chapa, S. O., Lapizco-Encinas, B. H., *Analytical Chemistry* 2018, *90*, 4310-4315.

[38] Luo, J., Abdallah, B. G., Wolken, G. G., Arriaga, E. A., Ros, A., *Biomicrofluidics* 2014, *8*, 021801.

[39] Su, Y.-H., Tsegaye, M., Varhue, W., Liao, K.-T., Abebe, L. S., Smith, J. A., Guerrant, R. L., Swami, N. S., *Analyst* 2014, *139*, 66-73.

[40] Swami, N., Chou, C.-F., Ramamurthy, V., Chaurey, V., *Lab on a Chip* 2009, *9*, 3212-3220.

[41] Pohl, H. A., *Journal of Applied Physics* 1951, *22*, 869-871.

[42] Hughes, M. P., Morgan, H., Rixon, F. J., Burt, J. P. H., Pethig, R., *Biochimica et Biophysica Acta (BBA) - General Subjects* 1998, *1425*, 119-126.

[43] Morgan, H., Hughes, M. P., Green, N. G., *Biophysical Journal*, *77*, 516-525.

[44] Mogi, K., Shirataki, C., Kihara, K., Kuwahara, H., Hongoh, Y., Yamamoto, T., *RSC Advances* 2016, *6*, 113000-113006.

[45] Pohl, H. A., Crane, J. S., *Biophysical Journal* 1971, *11*, 711-727.

[46] Chung, C., Pethig, R., Smith, S., Waterfall, M., *Electrophoresis* 2018, *39*, 989-997.

[47] Jones, P. V., DeMichele, A. F., Kemp, L., Hayes, M. A., *Analytical and Bioanalytical Chemistry* 2014, *406*, 183-192.

[48] Jones, P. V., Hilton, S. H., Davis, P. E., Yanashima, R., McLemore, R., McLaren, A., Hayes, M. A., *Analyst* 2015, *140*, 5152-5161.

[49] Chou, C.-F., Tegenfeldt, J. O., Bakajin, O., Chan, S. S., Cox, E. C., Darnton, N., Duke, T., Austin, R. H., *Biophysical Journal* 2002, *83*, 2170-2179.

[50] Abdallah, B. G., Chao, T.-C., Kupitz, C., Fromme, P., Ros, A., *ACS Nano* 2013, *7*, 9129-9137.

[51] Lapizco-Encinas, B. H., Simmons, B. A., Cummings, E. B., Fintschenko, Y., *Analytical Chemistry* 2004, *76*, 1571-1579.

[52] Cummings, E. B., Singh, A. K., *Analytical Chemistry* 2003, *75*, 4724-4731.

[53] Masuda, S., Washizu, M., Nanba, T., *Industry Applications, IEEE Transactions on* 1989, *25*, 732-737.

[54] Jones, P. V., Staton, S. J. R., Hayes, M. A., *Analytical and Bioanalytical Chemistry* 2011, *401*, 2103-2111.

[55] Braff, W. A., Willner, D., Hugenholtz, P., Rabaey, K., Buie, C. R., *PloS one* 2013, *8*, e76751.

[56] Crowther, C. V., Hayes, M. A., *Analyst* 2017, *142*, 1608-1618.

[57] Srivastava, S., Gencoglu, A., Minerick, A., *Analytical and Bioanalytical Chemistry* 2011, *399*, 301-321.

[58] Pohl, H. A., *Dielectrophoresis : the behavior of neutral matter in nonuniform electric fields*, Cambridge University Press, Cambridge; New York 1978.

[59] Pethig, R., *Biomicrofluidics* 2010, *4*, 022811.

[60] Clarke, R. W., Piper, J. D., Ying, L., Klenerman, D., *Physical Review Letters* 2007, *98*, 198102.

[61] Jones, T. B., *Electromechanics of Particles*, Cambridge University Press 1995.

[62] Cummings, E. B., *Engineering in Medicine and Biology Magazine, IEEE* 2003, *22*, 75-84.

[63] Kwon, J.-S., Maeng, J.-S., Chun, M.-S., Song, S., *Microfluidics and Nanofluidics* 2008, *5*, 23-31.

[64] Pysher, M. D., Hayes, M. A., *Analytical Chemistry* 2007, *79*, 4552-4557.

[65] Staton, S. J. R., Chen, K. P., Taylor, T. J., Pacheco, J. R., Hayes, M. A., *Electrophoresis* 2010, *31*, 3634-3641.

[66] Staton, S. J. R., Jones, P. V., Ku, G., Gilman, S. D., Kheterpal, I., Hayes, M. A., *Analyst* 2012, *137*, 3227-3229.

[67] Mack, C., *Fundamental principles of optical lithography: the science of microfabrication*, John Wiley & Sons 2008.

[68] Hilton, S. H., Hayes, M. A., *in preparation* 2018.

[69] Seeliger, H. P. R., Höhne, K., *Methods in Microbiology* 1979, *13*, 31-49.

[70] Schönberg, A., Bannerman, E., Courtieu, A. L., Kiss, R., McLauchlin, J., Shah, S., Wilhelms, D., *International Journal of Food Microbiology* 1996, *32*, 279-287.

[71] Bayer, M. E., Sloyer, J. L., *Journal of General Microbiology* 1990, *136*, 867-874.

[72] Bauer, J., *Journal of Chromatography B: Biomedical Sciences and Applications* 1987, *418*, 359-383.

[73] Mehrishi, J. N., Bauer, J., *Electrophoresis* 2002, *23*, 1984-1994.

[74] Chen, J.-Q., Regan, P., Laksanalamai, P., Healey, S., Hu, Z., *Food Science and Human Wellness* 2017, *6*, 97-120.

[75] Moura, A., Criscuolo, A., Pouseele, H., Maury, M. M., Leclercq, A., Tarr, C., Björkman, J. T., Dallman, T., Reimer, A., Enouf, V., Larsonneur, E., Carleton, H., Bracq-Dieye, H., Katz, L. S., Jones, L., Touchon, M., Tourdjman, M., Walker, M., Stroika, S., Cantinelli, T., Chenal-Francisque, V., Kucerova, Z., Rocha, E. P. C., Nadon, C., Grant, K., Nielsen, E. M., Pot, B., Gerner-Smidt, P., Lecuit, M., Brisse, S., *Nature Microbiology* 2016, *2*, 16185.

CHAPTER 4

EFFECTS OF SURFACE TREATMENTS ON TRAPPING WITH DC INSULATOR-BASED DIELECTROPHORESIS

4.1 Introduction

Complex biological mixtures of interest in science abound. Separation science finds applications in agriculture and food safety, pharmaceutical and vaccine development, forensics, blood-based diagnostics, viral isolation, and environmental samples. Many different techniques have been developed for the isolation of analytes of interest; each with their own advantages and disadvantages. The ability to precisely and accurately sort cells based on their biophysical properties has been at the forefront for the development of separation methods.[1-11]

Two commonly used techniques for cell sorting are fluorescence- and magnetic-activated cell sorting (FACS and MACS, respectively). Both methods use antibodies as a discriminator, making them highly accurate.[12] However, the labeling requirement limits the utility of these sorting techniques to cells of known properties.[13] MACS can capture a large number of cells in parallel but the purity of recovery is highly variable.[3] Furthermore, MACS and FACS instruments are prohibitively expensive for most labs.[12] Another important consideration is the affect that marker-based technologies can have on cell behavior, properties, and survival in downstream analysis.[14]

There are several label-free approaches to the problem of cell sorting.[15] Density-based methods include centrifugation and sedimentation.[2] Centrifugation is a common separation technique due to its user-friendliness and speed; however it has low specificity, as many cell populations do not differ enough in density to separate single

cell types.[9] Membrane filtration is similarly simple to use but has low specificity and can be prone to fouling.[16] Many microfluidic devices have been designed for hydrodynamic cell trapping, but these are geared toward separating specific cell types from known, low-complexity cell mixtures.[17] Optical tweezers are a highly specific label-free method of cell separation, however the system has a comparatively low-throughput.[8, 18, 19]

The use of electric fields to manipulate analytes of interest has gained popularity in recent years. As cell surfaces include positive and negative charges, the application of an electric field will cause some alignment of the cells with the field, which can be advantageous for achieving separations. Electrophoresis (EP), where a uniform electric field is used to manipulate charged analytes, has been used for many cell separations. However, EP systems can be complicated to use, do not influence neutral particles, and can be challenging to use with oppositely charged cells. [5, 20, 21] Dielectrophoresis (DEP) in contrast works on all particles based on their polarizability. DEP is the force which acts on a polarizable particle in a non-uniform electric field, which has the potential to improve existing separation strategies and open new avenues of research to discover and characterize microorganisms. The intrinsic biophysical properties, including conductivity, permittivity, and zeta potential of a cell, affect how a cell will behave in the presence of DEP. [2, 14, 22-26] Specifically, for the *E. coli* studied in this chapter, where modifications to the cell's surface are made, the properties of the cell which are associated with the surface are expected to be affected (Figure 4.1.). The ability to isolate a cell type of interest with high specificity, even if it is present in low concentrations, is a

major advantage to DEP separations.[24, 27, 28] Furthermore, DEP techniques preserve the viability of the cells after manipulation.[29-31]

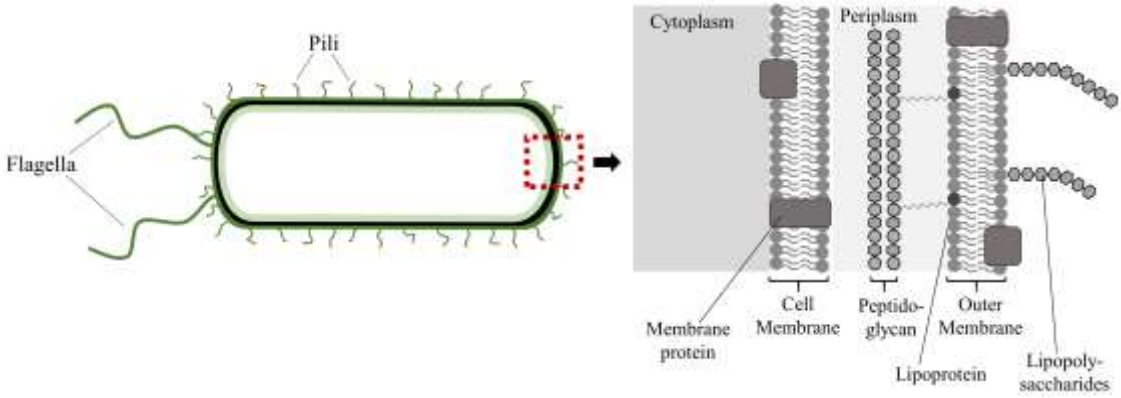

Figure 4.1. Illustration of physical structure of *E. coli*, a gram-negative bacterium, focusing on outer layers. Surface modifications can affect the biophysical properties of the cell and thus the electrokinetic and dielectrophoretic mobilities.

Many DEP systems utilize embedded electrodes, known as eDEP, to manipulate analytes of interest. Several applications of eDEP for the manipulation and separation of cells have been achieved.[4, 30, 32, 33] However, eDEP is subject to electrode fouling, undesirable electrolysis, and the DEP force is only effective near the electrodes where the high electric field gradients are achieved. In the early 2000s insulator-based dielectrophoresis (iDEP) was introduced, which uses insulating features to manipulate the shape of the electric field between distal electrodes, rather than using the placement of the electrodes.[23, 34, 35] The electrode placement in the distal reservoirs limits the effects of fouling and electrolysis. iDEP has been successful in manipulating, differentiating, and isolating various cells, including various strains of *E. coli* [36], antibiotic resistant and sensitive *Staphylococcus epidermidis* [2], *Bacillus subtilis* [37], and *Pseudomonas aeruginosa* and *Streptococcus mitis* [38].

The interaction of a cell with the outside world is determined by its surface properties (Figure 4.1.). Specifically the physiochemical properties are shaped by surface

biomolecules that are in turn shaped by gene expression.[39] Depending on the environment, a cell must use its membrane to sense nutrients and threats in the world around it and respond appropriately. For example, the pathogenic bacterium *Salmonella* regulates and modifies its membrane composition as needed for protection and host invasion.[40] Another example is that the physiochemical properties of the yeast cell wall determine its propensity for adhesion and flocculation.[41] Importantly, changes in cell surface functional groups influence a cell's electrophoretic mobility.[21] The ability for iDEP to detect changes in the both the internal and surface properties of cell have resulted in its growth as a field for interrogating and separating cells.[22, 42]

When working with *E. coli* in a DEP system, there are several different factors that must be considered. As *E. coli* is gram-negative, its cell wall is composed of an outer membrane, which is 7-8 nm in thickness, and a thin peptidoglycan layer, which is 1-3 nm in thickness (Figure 4.1.).[43, 44] This is in comparison to gram-positive bacteria, which has a peptidoglycan layer ranging from 20-80 nm in thickness.[43, 44] When *E. coli* is subjected to an electric field, the conductivities of the different cell layers can be taken into account, to better understand how the field will interact with bacteria. The conductivities of the cell wall and cell membrane have previously been reported as 5×10^{2} and $5 \times 10^{-5} \frac{\mu S}{mm}$, respectively.[45] The electric field can easily pass through the cell wall as it is highly conductive. Previous work has determined that with low frequencies applied, the cell interior is shielded by the cytoplasmic membrane as it is highly insulating, while at higher frequencies, above 100 kHz, the electric field can penetrate the cell membrane.[46] Furthermore, *E. coli* has a high density of negative charges on its surface, a net negative charge in physiological pH, and a higher

electrophoretic mobility than gram-positive bacteria.[47-49] Buszewki et al. determined, using capillary electrophoresis, that the electrokinetic and electroosmotic mobilities of *E. coli* do not differ significantly.[48] Jones et al. observed similar behavior, with DEP experiments, as the transportation of the bacteria in the microchannel was electroosmotically driven.[36] Furthermore, the zeta potential of *E. coli* must be taken into account, which can fluctuates, depending on pH, between -40 to -80 mV.[50] Lapizco et al. have previously used DEP successfully to manipulate live and dead *E. coli*, where the size, shape, morphological characteristics, electrokinetic mobility, etc. do not differ between the live and dead bacteria, however the conductivity of the cell membranes did differ.[34] Further work by Jones et al. demonstrated that DEP can be used to identify different serotypes of *E. coli*.[36] This must all be taken into consideration when determining the effect of various surface modification to the *E. coli*.

The work presented here seeks to further understand the effects that the relative contributions of surface chemistry vs. internal cell factors such as conductivity and permittivity have on trapping DEP cellular assessments. These two broad variables are difficult to isolate because differences in surface characteristics result from differences in gene expression, which in turn can alter the cell's internal physiochemical characteristics. In this study I have tested the effects of covalent surface modifications to the behavior of *E. coli* in an iDEP system and determined the effect on the electrokinetic mobility and dielectrophoretic mobility. The effect on the changes in mobility can be correlated to various changes in either the internal or external cell properties.

4.2 Theory

Insulator-based dielectrophoresis manipulates analytes based on the intrinsic properties of the analyte and the effects created in the microchannel by the dielectrophoretic and electrokinetic forces. In-depth development of the particle properties and forces are presented in several previous works and in Chapter 2 of this dissertation.[7, 25, 51-54] Pertinent information is reintroduced here for clarity.

The electrokinetic properties of a given analyte of interest can be describe by the electrokinetic mobility (μ_{EK}) which combines the effects of electrophoretic mobility (μ_{EP}) and electroosmosis (μ_{EO}).

$$\mu_{EK} = (\mu_{EO} + \mu_{EP}) = \frac{-\varepsilon_m \zeta_m}{\eta} + \frac{\varepsilon_m \zeta_p}{\eta} = \frac{-\varepsilon_m (\zeta_m - \zeta_p)}{\eta} \quad (1)$$

Where ε_m is the permittivity of the medium, ζ_m is the zeta potential of the medium, ζ_p is the zeta potential of the particle and η is the viscosity of the medium. Similarly, the dielectrophoretic mobility (μ_{DEP}) of an analyte can be described by the following:

$$\mu_{DEP} = \frac{\varepsilon_m r^2 f_{CM}}{3\eta} \quad (2)$$

Where *r* is the radius of the particle and f_{CM} is the Clausius-Mossotti factor, which is based on the conductivity of the particle and medium in DC fields.

The movement, flux ($\vec{j}$), of a given analyte in a the microchannel is a combination of the effects of diffusion (*D*), concentration (*C*), and the bulk ($\vec{v}_{Bulk}$), electrokinetic ($\vec{v}_{EK}$), and dielectrophoretic ($\vec{v}_{DEP}$) velocities. The $\vec{v}_{EK}$ and $\vec{v}_{DEP}$ relate their corresponding mobilities with the electric field ($\vec{E}$) or the gradient of the electric field squared ($\nabla\left|\vec{E}\right|^2$), respectively. The effects of *D* can be disregarded as *E. coli* is larger than 1 µm, and $\vec{v}_{Bulk}$ can be ignored as pressure driven flow is eliminated. Therefore, the movement of a given analytes in a microchannel can be described by the following.

$$\vec{J} = D\nabla C + C(\vec{v}_{Bulk} + \vec{v}_{EK} + \vec{v}_{DEP}) \approx C(\vec{v}_{EK} + \vec{v}_{DEP}) \quad (3)$$

The DEP force ($\vec{F}_{DEP}$) describes the force on a polarizable particle in a non-uniform electric field. Mathematically, for a spherical particle with a single monopole, the force can be described by:

$$\vec{F}_{DEP} = 2\pi\varepsilon_m r^3 f_{CM} \nabla \left| \vec{E} \right|^2 \quad (4)$$

The direction of the $\vec{F}_{DEP}$, depends on the sign of f_{CM} which will determine if the analyte of interest experiences either positive or negative dielectrophoresis. When a DC potential is applied, if the conductivity of the particle is greater than the conductivity of the media, the particle will be attracted to areas of high electric field strength, resulting in positive dielectrophoresis. Whereas, when the conductivity of the media is greater than that of particle, the particle is repelled from high electric field strengths, resulting in negative dielectrophoresis. The experimentation in this chapter results in negative dielectrophoretic trapping.

As *E. coli* is made up of several layers, including the cytoplasm, membrane, and cell wall, a better representation of the Clausius-Mossotti factor, which accounts for the the variations between the layers can be done using the multi-shell model.[55-58] This is done by assuming that concentric spheres represent the three layers of the cell including the cytoplasm (*cyto*), membrane (*mem*), and the cell wall (wall). The conductivity of the cytoplasm and membrane is given by:

$$\sigma_{2shell} = \sigma_{mem}\left[\frac{\left(\frac{r_{mem}}{r_{cyto}}\right)^3 + 2\left(\frac{\sigma_{cyto}-\sigma_{mem}}{\sigma_{cyto}+2\sigma_{mem}}\right)}{\left(\frac{r_{mem}}{r_{cyto}}\right)^3 - \left(\frac{\sigma_{cyto}-\sigma_{mem}}{\sigma_{cyto}+2\sigma_{mem}}\right)}\right] \quad (5)$$

where r is the respective layer's radius and σ is the respective layer's conductivity. Using this, the conductivities of the three shells can be represented by:

$$\sigma_{3shell} = \sigma_{wall}\left[\frac{\left(\frac{r_{wall}}{r_{mem}}\right)^3 + 2\left(\frac{\sigma_{2shell}-\sigma_{wall}}{\sigma_{2shell}+2\sigma_{wall}}\right)}{\left(\frac{r_{wall}}{r_{mem}}\right)^3 - \left(\frac{\sigma_{2shell}-\sigma_{wall}}{\sigma_{2shell}+2\sigma_{wall}}\right)}\right] \quad (6)$$

where the different cell layers will affect the overall conductivity of the cell.

As *E. coli* is rod shaped, the dielectrophoretic force for ellipsoidal particles must be considered to account for the effect of the cell's dimensions.[59, 60]

$$\vec{F}_{DEP} = \frac{4}{3}\pi abc\varepsilon_m\left(\frac{\sigma_p-\sigma_m}{Z\sigma_p+(1-Z)\sigma_m}\right)\nabla\left|\vec{E}\right|^2 \quad (7)$$

where the semi-principal axes of the ellipsoid are represented by a, b and c ($a > b = c$), Z is the depolarization factor, σ is the conductivity of the particle (p) or media (m).

Similar to the work done by Huang et al. and Castellarnau et. al, the dielectrophoretic force for an ellipsoid and the multi-shell model can be combined to describe the dielectrophoretic force on *E. coli*.[57, 58, 61]

DEP trapping of analytes occurs when the flux of the particle along the electric field lines is zero, $\vec{j}\cdot\vec{E} = 0$, which can be described using the EK and DEP mobilities base on Eq. 3.

$$\frac{\nabla|\vec{E}|^2}{E^2}\cdot\vec{E} \geq \frac{\mu_{EK}}{\mu_{DEP}} \quad (8)$$

The behavior of a given analyte in the microchannel can be used to assess their biophysical properties by understanding the EK and DEP mobilities.

4.3 Modeling

4.3.1 Finite Element Multiphysics

Finite element modeling (COMSOL, Inc., Burlington, MA) of the distribution of the electric field in the microchannel was done in the same manner as has been previously detailed.[51] The *AC/DC module* was used to interrogate the $\vec{E}$, $\nabla\left|\vec{E}\right|^2$, and $\frac{\nabla|\vec{E}|^2}{E^2}\cdot\vec{E}$ in an accurately scaled 2D model of the microchannel. The accuracy of the computations may be affected as the surface charge between PDMS and silica likely differ.

4.3.2 Data Model

A data model which correlates the various factors that affect trapping was implemented to further understand the behavior of a given analyte in the system.[22, 62] The data model assesses the number of particles which can arrive at a given gate of interest either with respect to magnitude of a potential or the length of time for which the potential has been applied. The data model for the microchannel utilized in this chapter has previously been developed.[62] Briefly, a time-dependent model, where the applied potential is held constant can be represented by:

$$SI = \frac{24V_A\gamma n\mu_{Ek}wh}{s}t \tag{9}$$

Where *SI* is the signal intensity, V_A is the applied potential, γ is the average *SI* per particle, *n* is the concentration of the analyte of interest, *w* is the average width of the microchannel an analyte experiences, *h* is the height of the microchannel, *s* is a stacking factor, and *t* is the time for which the potential has been applied.

When the time a given potential has been applied for is held constant, a voltage-dependent model can be developed. This is best described using a piecewise function:

$$SI(V_A) = \begin{cases} 0, if\ V_A < \frac{1}{1.0\times10^7}\left(\frac{\mu_{EK}}{\mu_{DEP}}\right) \\ 24\frac{\gamma n \mu_{Ek} wht}{s}\left[V_A - \frac{1}{1.0\times10^7}\left(\frac{\mu_{EK}}{\mu_{DEP}}\right)\right], if\ V_A \geq \frac{1}{1.0\times10^7}\left(\frac{\mu_{EK}}{\mu_{DEP}}\right) \end{cases} \quad (10)$$

where at potentials when no trapping occurs, there is no contribution to the *SI*, but after a given onset potential (*c*), the bacteria will collect in a linear fashion with respect to the applied potential.

4.4 Materials and Methods

4.4.1 Device Fabrication

Soft photolithography, microchannel fabrication, and bonding were performed according to established procedures. This work is similar to that which is included in Chapter 3 of this dissertation and is included here for simplicity. The V1 sawtooth microchannel geometry has been described in prior publications.[36, 63-65] Briefly, it consists of a 4.2 cm long microchannel, with an average depth of 17 μm, where equilateral triangles aligning both walls, forming opposing teeth that create constriction points, referred to hereafter as gates. The triangles increase in size from the inlet to the outlet, producing gates gradually decreasing in size, focusing toward the centerline. The initial gate width is 945 μm, with the sides of the equilateral triangles increasing by 40 μm after every six gates, resulting in a final gate width of 27 μm.

Polydimethylsiloxane (PDMS) microchannels were cast using Sylgard 184 silicone elastomer kit (Dow Silicones Corporation, Midland, MI USA) and cured at 70 °C for 1 hr. After curing, 3 mm reservoir holes were punched to form the inlet and outlet reservoirs. Microchannels were stored in airtight plastic bags in the freezer for up to two

weeks prior to use. For experimentation, PDMS casts were washed with isopropanol then 18 MΩ water followed by a 30 s sonication in 18 MΩ water, and then dried with air. Glass slides were cleaned in the same manner, except that an acetone wash preceded the isopropanol wash. Bonding of a completed microdevice was done by treating both the glass slides and the PDMS casts with oxygen plasma (PDC-32G, Harrick Plasma, Ithaca, NY) for 60 seconds at 18W.

4.4.2 Cell Culture and Surface Modification

Escherichia coli strain Bl21 DE3 Star with plasmid pET-29 expressing superfolder GFP (sfGFP) was grown on Lysogeny broth (LB) agar plates with 50 µg/mL kanamycin to maintain the plasmid. For each treatment, a single colony was inoculated into 10 mL of LB broth with 50 µg/mL kanamycin incubated overnight in shaker at 37 ° C to late log phase. Once the culture reached an OD_{600} between 0.8-1.1 the culture was inoculated with 1 mM isopropyl-b-D-1-thiogalactopyranosid (IPTG) to induce *lac* promoter expression of sfGFP. The bacteria was then stored at 4°C for at least an hour prior to labeling.

Siegmund and Wöstemeyer developed a surface modification technique for bacteria which was modified for this work.[66, 67] A carbodiimide (N-(3-Dimethylaminopropyl)-N′-ethylcarbodiimide hydrochloride (EDC)) is used to covalently link compounds to the cell's surface. The following molecules were used for surface modification: glycine, Bovine Serum Albumin (BSA), spermine, and 7-Amino-4-methyl-3-coumarinylacetic acid (AMCA-H). AMCA-H was used to visualize that a covalent bond was formed with the *E. coli* based on the additional fluorescence molecule.[66, 67]

Briefly, a solution of EDC (10 mg/mL) was made fresh with 18 MΩ water. 1 mL of the overnight culture was washed three times with 1 mL saline (9 g/L NaCl, 0.2 µm filtered) and resuspended in saline. EDC was added to the washed cells for a final concentration of 1 mg/mL with a total volume of 1mL and then incubated on shaker for 10 minutes at room temperature. The desired molecule for modification was then added for a final concentration of 1 mM, except in the case of BSA when a final concentration of 10 mg/mL was used. The pH was tested and adjusted using ~0.1 M phosphoric acid, pH ~5 to reach a pH between 4 and 6 to achieve optimal coupling. Adjustments in pH were only necessary for spermine modified cells. The reaction was then incubated for 20 additional minutes. The modified cells were then washed three times and resuspended in saline where a final concentration of 1 mM glycine was added to block any excess EDC. The mixture was incubated for 10 minutes. The cells were washed three times and resuspended with 2 mM phosphate buffer (PB), where the PB had measured conductivity of 330 µS/cm. The modified cells were stored at 4°C overnight. For experimentation, the next day, the modified cells were vortexed and a dilution of 200 µL of the modified cells and 800 µL of 2 mM PB made.

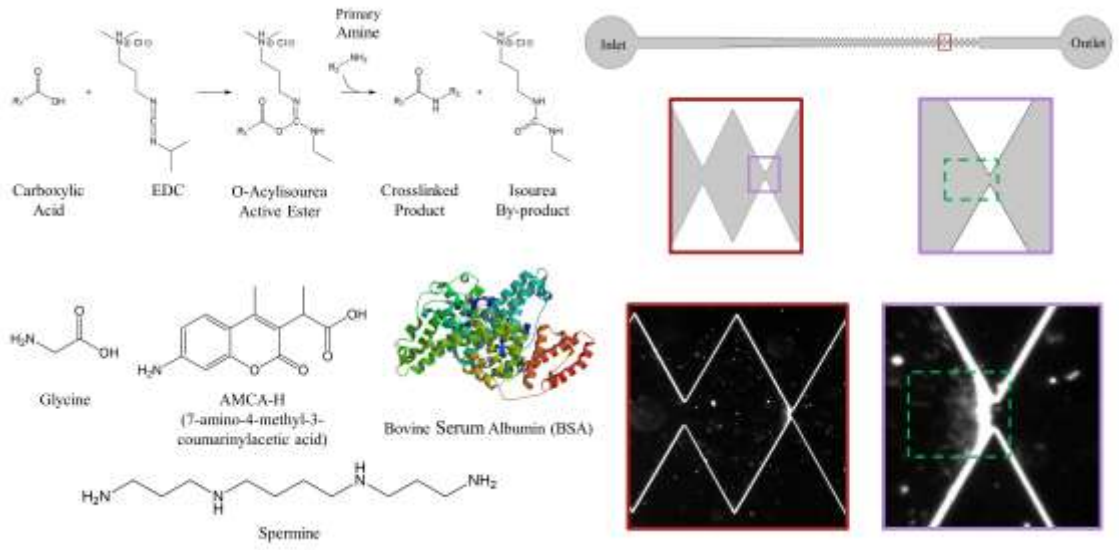

Figure 4.2. Amide coupling reaction for *E. coli* surface modifications (top left) and various molecules coupled to the *E. coli* (bottom left).[68] The right depicts example observed negative dielectrophoretic trapping at the first 27 µm gate in the microchannel. Specifically, the data depicted is of glycine modified *E. coli* after approximately 8 seconds with an applied potential of -500 V. The green box represents the ROI which was analyzed for signal intensity.

4.4.3 Experimental

A microdevice was washed and bonded on the day of use. The inlet and outlet reservoirs of the microchannel were filled with 15 µL of 2 mM PB and allowed to sit for 10 minutes. Platinum electrodes (0.404 mm external diameter 99.9% purity, Alfa Aesar, Ward Hill, MA, USA) were placed in both reservoirs and attached to a power supply (HVS 448 High Voltage Sequencers, LabSmith Inc., Livermore, CA, USA). The 2 mM PB was then removed and 15 µL of the modified diluted cell suspension was placed in the inlet reservoir allowing the cells to fill the channel by pressure driven flow for 5 minutes. The outlet reservoir was then filled with 15 µL of 2 mM PB to balance pressure driven flow. Fluorescence microscopy (Olympus IX70) with a mercury short arc lamp (H30 102 w/2, OSRAM) and an Olympus DAPI, FITC, Texas Red triple band pass cube

(Olympus, Center Valley, PA, USA) was used to check the presence of bacteria in the microchannel as the *E. coli*'s expression of sfGFP results in excitation/emission properties of 485/510 nm.[69] Experiments with the microchannel were monitored using bright field microscopy with a 4× objective. Voltages were sequentially applied from -100 V to -900 V for ~30 s to characterize how surface modifications affected the cell's behavior. Images were captured using Streampix V image capture software (Norpix, Inc., Montreal, QC) via a QICAM cooled CCD camera (QImaging, Inc., Surrey, BC).

Trials were run for each surface modification as a singular analyte, where the magnitude (V_A) and duration (t_A) of applied potential was varied. For each trial a new microdevice was utilized. Unmodified *E. coli* was tested as a control. A consistent gate position, the first 27 µm gate, was used to assess the behavior of the bacteria in the microchannel. Multiple replicate trials ($n \geq 9$) were run for each surface modification.

4.4.4 Image Analysis

To assess the trapping behavior of the bacteria in the microchannel the signal intensity (*SI*) for a defined region of interest (ROI) was monitored at the 27 µm gate both in response to the magnitude and length of time a potential was applied to the system. The ROI was defined as an 80 × 50 pixel box near the 27 µm gate where trapping characteristically is observed (Figure 4.2., green box). *SI* measurements were done using ImageJ (NIH freeware). The *SI* was normalized for *E. coli* concentration within each run and signal present prior to the application of voltage. A measurement 2 s after commencing data recording for the -100 V trial was used to for the measurement of the *SI*

with no applied voltage, as the voltage was not applied to system until ~5 s into recording.

The velocity of the modified cells was measured using particle tracing, where the path of individual bacterium was traced from frame-to-frame at or near the centerline just prior to the 27 μm gate. Each particle was traced until it could no longer be identified in the subsequent frame or reached a point where DEP could influence the particles velocity. For each surface modification the starting and ending location of fifteen cells and the time between locations measurements was done to assess velocity. Velocity determinations were done for three trials of each surface modification.

4.4.5 Safety Considerations

The bacteria used in this study is classified as Bio Safety Level 1 (BSL1). Experiments were conducted in accordance with the current version of the CDC/NIH BMBL publication in an approved BSL 1 laboratory.

4.5 Results

The biophysical behavior of *E. coli* with four different surface modifications was quantified using iDEP. Various compounds and a protein were covalently linked to the carboxyl groups on the surface of the *E. coli* using an amine coupling reaction, including glycine, spermine, BSA, and AMCA-H.

4.5.1 Velocity and Electrokinetic Mobility Determination

The velocity of the bacteria was determined using particle tracing in an area of the device where there was no evidence of trapping, in the more open portion of the microchannel, prior to the gate of interest (Figure 4.2.). A linear fit was used with respect to the applied voltage to more accurately determine μ_{EK} and confirm consistent behavior

over a range of velocities (Table 4.1.). The μ_{EK} values ranged from 3.0 to 5.1 $\times$ 10^{-8} $\frac{m^2}{Vs}$ with approximately 3% relative standard deviation, and all were significantly different. Based on previous work, where a difference in the conductivity of the cell membrane of live and dead *E.coli* resulted in their separation, it is possible that the surface labels are also altering the cell membrane's conductivity.[34] All values of μ_{EK} were in a similar range, close to 3.0 $\times$ 10^{-8} $\frac{m^2}{Vs}$, except for those modified with AMCA-H.

Surface Modification	$\boldsymbol{\mu_{EK}}$ $\left(\times\ \mathbf{10^{-8}}, \frac{\boldsymbol{m^2}}{\boldsymbol{Vs}}\right)$	**Trapping Onset Voltage (V)**	$\boldsymbol{\mu_{DEP}}$ $\left(\times\ \mathbf{10^{-17}}, \frac{\boldsymbol{m^4}}{\boldsymbol{V^2 s}}\right)$	$\frac{\boldsymbol{\mu_{EK}}}{\boldsymbol{\mu_{DEP}}}$ $\left(\times\ \mathbf{10^{9}}, \frac{\boldsymbol{V}}{\boldsymbol{m^2}}\right)$
None	3.0 ± 0.09	240 ± 66	1.2 ± 0.34	2.4 ± 0.66
Glycine	3.2 ± 0.07	270 ± 38	1.2 ± 0.17	2.7 ± 0.38
BSA	3.4 ± 0.1	310 ± 34	1.1 ± 0.12	3.1 ± 0.34
AMCA-H	5.1 ± 0.1	470 ± 46	1.1 ± 1.1	4.7± 0.46
Spermine	2.7 ± 0.09	460 ± 62	0.58 ± 0.081	4.6 ± 0.62

Table 4.1. Characteristic properties for each surface modification.

4.5.2 iDEP Trapping Experiments

Additional electrophysical behaviors of the various surface modified *E. coli* were quantified in the iDEP microdevice. Data sets were collected while varying both the magnitude of the applied potential (V_A) and the duration of application (t_A). In all cases the general structure of the capture was consistent with previous comparable work, in that a characteristic crescent shape of collected bacteria was observed a few microns prior to the first 27 µm gate on the inlet side. No observable trapping behavior was observed at the 90 µm or larger gates for any experiments.

Trapping DEP is a result of a ratio of channel effects balancing or exceeding the intrinsic biophysical property ratio of the analyte (Eq. 8). The specific threshold (c) of the applied potential which meets the trapping ratio results in the collection of the bacteria rather than its continued movement in the microchannel (Eq. 8). To evaluate the threshold, the *SI* in a defined region of interest (ROI) surrounding the typical point of trapping was assessed after 10 s of applied voltage from -100 to -900 V in increments of 100 V. The baseline for each surface modification experiment was determined using the following voltages: 0 to -200 V for no modification and glycine, 0 to -300 V for BSA, and 0 to -400 V for AMCA-H and spermine. Trapping was defined as when the measured *SI* was significantly different at the 95% CI than the baseline using a 2-tailed t-test. The *SI* initially increases linearly with applied potential at values higher than *c* (Figure 4.3.) and then plateaus except for the data from spermine and AMCA-H. All data sets were consistent with expected experimental results, based on previous work in the field, and provide sufficient linear ranges for statistical fitting, allowing for a determination of *c* including an estimate of error (Table 4.1.). Combining the value of *c* and COMSOL models of the microchannels, the ratio of mobilities for each of the surface modifications are determined (Table 4.1.). Utilizing the measured μ_{EK} and ratio of mobilities, μ_{DEP} is determined for each cell population (Table 4.1.).

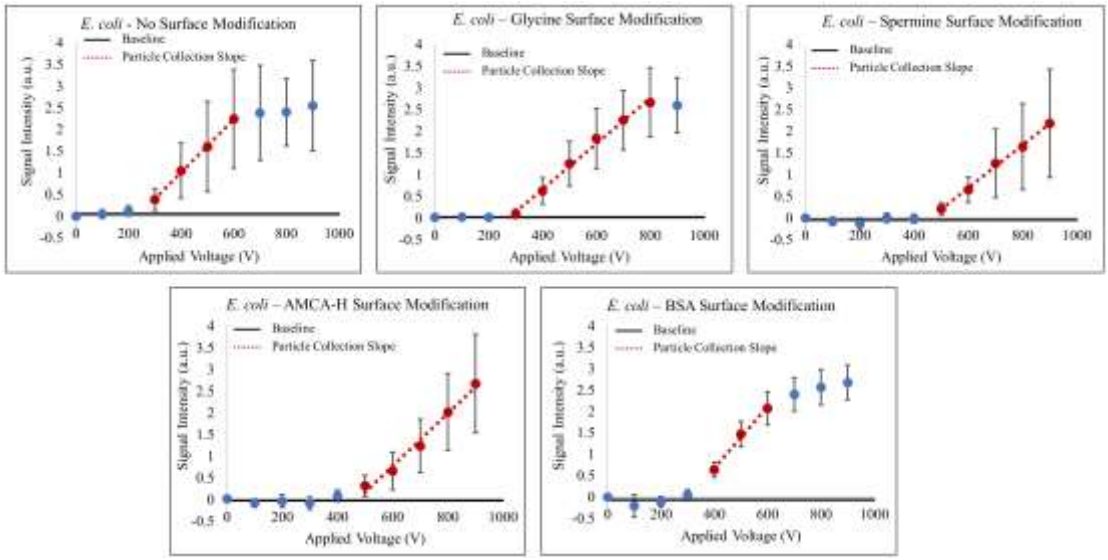

Figure 4.3. The effect of varying the voltage for the trapping behavior of surface modifications of *E. coli* was assessed 10 seconds after the application of potential. A linear fit of trapping behavior was assessed (dotted red line) when the signal was significantly different than the baseline and prior to a plateau in signal intensity (see text). The error bars represent the 95% CI. The absolute value of the applied potential is used for the plot.

4.5.3 Modeling of the Data

A data model was used to determine μ_{EK} based on the trapping data for each surface modification (separate from the velocity measurements). The time dependent model was then utilized to determine μ_{EK} (Eq. 9), as all the variables except μ_{EK} are known. Only the data considered as statistically significant and in the linear region of the voltage dependent data was utilized (red data points and linear fit, Figure 4.3.). Individual data points, where the *SI* for a given applied potential, which resulted in a negative intensity were removed as clearly no trapping was occurring. The following knowns were used: *t* as 10 s after the application of potential, *h* as 17 µm, and $\vec{E}_{ave}$ was determined using the applied potential and characteristic length of the microchannel. The average channel width that the bacteria will experience can be approximated as 0.2 ± 0.05 mm, depending on their velocity. Given the approximate size of *E. coli* and the channel height

the number of stacked bacteria is bound between 1-34 bacterium, however the exact number is dependent on the size and interactions of the bacteria. When a channel width of 0.2 mm is assumed the μ_{EK}, within the 95% CI of the μ_{EK} determined from the velocity measurements, for the unmodified, glycine and BSA modified bacteria can be determined by slightly varying the number of stacked particles. The μ_{EK} were determined to be 3.0 ± 0.9×10^{-8}, 3.3 ± 0.6×10^{-8}, and 3.5 ± 0.5×10^{-8} $\frac{m^2}{Vs}$ for the unmodified, glycine, and BSA modified bacteria respectively with 22, 26, and 24 respectively stacked bacterial particles. For the *E. coli* modified with spermine assuming a channel width of 0.15 mm and 24 stacked bacteria μ_{EK} is determined to be 2.6 ± 0.7×10^{-8} $\frac{m^2}{Vs}$ which is within the 95 % CI of the μ_{EK} determined using velocity. A comparable value for the μ_{EK} determined using the data model for the AMCA-H surface modified bacteria could not be determined within the bounds set for *w* and *s*.

4.6 Discussion

Chemically modifying the surface of *E. coli* causes measurable differences in its biophysical properties. The changes in the biophysical properties can be assessed by using iDEP to determine the μ_{EK} and μ_{DEP}(Figures 4.3. - 4.5. and Table 4.1.).

The $\vec{v}_{EK}$ for each surface modification was determined, and by extension the μ_{EK} (Table 4.1.). The μ_{EK} is a measure of the distribution of charge on the surface (Eq. 1). For each surface modification a statistically unique μ_{EK} was determined, meaning that the modifications to the surface of the bacteria are influencing or altering the biophysical properties of the analyte. This is expected as chemical modifications to the surface of the cell can cause alterations or changes to the surface charge density, the distribution of

charges, or multipoles present.[22] All of these factors will affect the zeta potential, which is a measure of how the particle interacts with the surrounding buffer, and in turn will alter the measurement of μ_{EK}.

To further understand how surface modifications can affect the biophysical properties of *E. coli*, the trapping behavior of the bacteria, in an iDEP microchannel, was assessed (Figure 4.3.). Many factors including the experimental conditions (buffer properties, channel coatings, voltage, analyte concentration, etc.), channel geometry, and the biophysical properties of the analyte will affect the trapping behavior of a given analyte (Figure 4.3.). Plateaus in the data may be a result of reaching the limit of detection for the CCD in the given ROI, material collecting outside the set ROI, or material collecting at the 60 µm gate. The behavior of the bacteria in the microchannel can be correlated to both the μ_{EK} and μ_{DEP}. Table 4.1. depicts that each modification alters both μ_{EK}, c, and the ratio of mobilities.

A comparison between the ratio of mobilities and each mobility individually is presented in Figure 4.4. Each of the surface modifications clearly has its own unique μ_{EK} (Figure 4.4., left), even though there is statistically overlap in the ratio of mobilities. In comparison, the μ_{DEP} is statistically unaffected when comparing the unmodified bacteria with the glycine or BSA modified bacteria; while those treated with spermine and AMCA-H result in statistically significant changes in μ_{DEP} (Figure 4.4., right).

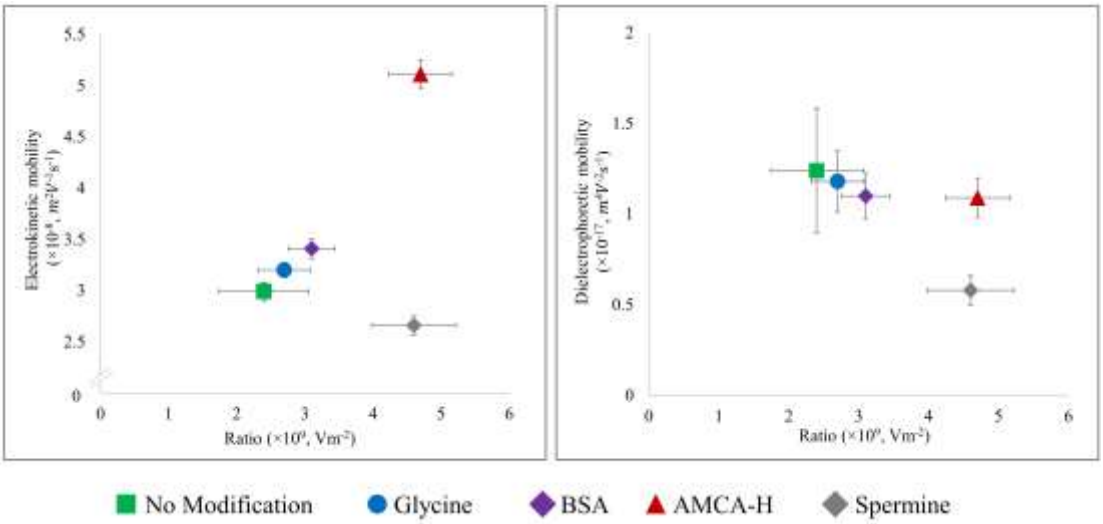

Figure 4.4. Comparison of the electrokinetic and dielectrophoretic mobilities versus their trapping ratio for each surface label (note vertical axes). Each surface modification results in notably different electrokinetic mobilities, while only the AMCA-H and spermine's dielectrophoretic mobilities are different.

The μ_{DEP} can be affected by both the external and internal properties of the cell. One specific issue that must be considered is that changes to the conductivity or permittivity of the cell will influence the μ_{DEP}. In the case of biological analytes the effect of conductivity and permittivity is generally assessed using the multi-shell model to account for the effect of the cytoplasm, membrane, and cell wall.[22, 55, 56, 61] The conductivity and permittivity relate to the ability for a given particle to conduct electricity and store electrical energy, respectively, which are related to both internal and external properties of the cell. This suggests that as spermine results in a statistically significant shift in μ_{DEP}, it is possible that this modification resulted in changes to both the external and internal properties of the bacteria. It should be noted that previous work correlated the difference in cell behavior to only the conductivity of the cell membrane, which would be an external cell property.[70] Furthermore, it is interesting that for all the

modified cells there is a decrease in the measured μ_{DEP} in comparison to the unmodified cells.

A model of the data was used to gain insight into the trapping behavior of the different analytes. The time dependent model was used to evaluate μ_{EK}. The μ_{EK} from the data model was compared with the μ_{EK} from the velocity measurements. In the case of the unmodified *E. coli* and those modified with glycine or BSA when all factors except the stacking factor, ranging from 22-26 particles, are held constant, the μ_{EK} determined from the data model falls within the 95% CI of those calculated based on velocity measurements. It is reasonable that variations in the surface properties of a cell will change the number of stacked particles because it will affect the particle-particle interactions. In the case of spermine, a smaller channel width is used when determining the μ_{EK} from the data model, which falls within the 95% CI of the μ_{EK} determined from the velocity measurements. Upon further inspection of the data this is logical as the spermine modified bacteria have the smallest $\vec{v}_{EK}$ and therefore will experience an overall smaller channel width. For the AMCA-H modified *E. coli*, no reasonable value for μ_{EK} could be determined using the data model with the set constraints on *w* and *s*. Potential factors which may be affecting this include the fact that the average $\vec{v}_{EK}$ and thus μ_{EK} was significantly higher than for any other treatment (Table 4.1.). Furthermore, the AMCA-H modified cells were prone to aggregation during trapping, which resulted in the aggregates leaving the initial gate of trapping, affecting the assessed *SI*. For each surface modification variation may be due to a low number of replicates ($n \geq 9$).

When determining the μ_{EK}, using either velocity measurements or the data model, the effect of residual pressure driven flow must be considered. Care was taken during

experimentation to minimize the effects; however, a perfect balance is not always possible with the current experimental set-up. In the case that pressure driven flow could not be completely eliminated, flow towards the outlet (forward flow) rather than inlet (backward flow) was preferred to prevent the reassessment of any previously trapped bacteria. In the case of velocity measurements forward pressure driven would artificially increase the assessed $\vec{v}_{EK}$ and thus μ_{EK}. Whereas in the case of the data model pressure driven flow would add to the electrokinetic effects in the channel resulting in a higher onset potential and therefore a larger ratio of mobilities. Furthermore, the presence of forward pressure driven flow would increase the rate of capture of bacteria artificially making the slope of the trapped data steeper (Figure 4.3.). All of these facts will affect the accuracy of the assessment of μ_{EK} using either velocity estimation or the data model.

Interpretation of the trapping iDEP data can be affected by several factors. Specifically, when defining the linear region (Figure 4.3.) an iterative process is used to determine the fit of statistically significant trapping. The linear fit ultimately incorporates the maximum amount of data where statistical trapping is occurring, while maintaining a realistic fit. In some cases, an obvious plateau in data is observed, which is the case for unmodified and glycine modified *E. coli* (Figure 4.3.). However, for the BSA modified *E. coli* the start of the plateau is semi-ambiguous. It should be noted that for the bacteria modified with BSA a total of 20 replicate trials were performed, whereas for all other surface modifications 9 -13 replicates were done. The data for -700 V can potentially be incorporated into the linear fit or deemed as part of the data plateau (Figure 4.5., top).

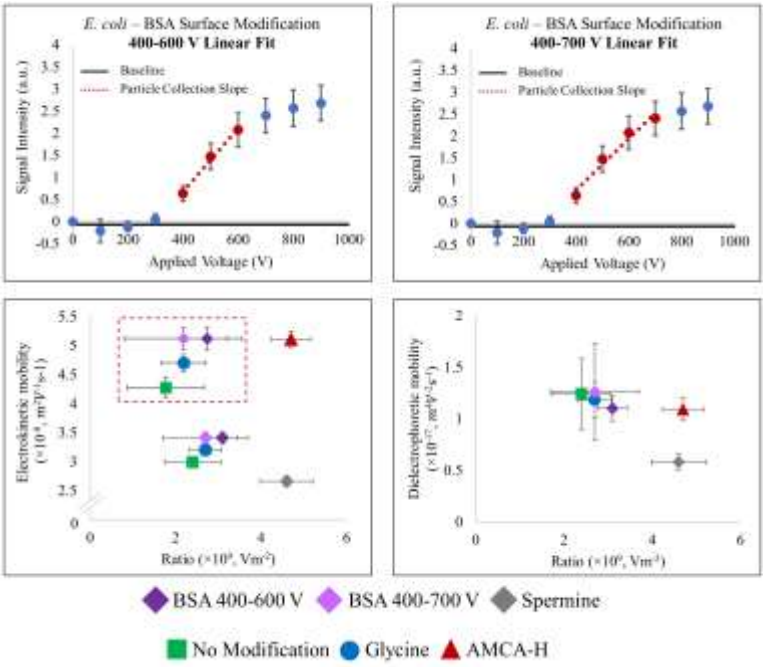

Figure 4.5. iDEP trapping results for BSA modified *E. coli*. (Top) The effect of various applied potentials at the first 27 µm gate where t_A is 10 s, where the error bars represent the 95 % CI. The absolute value of the applied potential is used for the plot. A linear fit either including or excluding V_A of -700 V can be assessed (see text for rationale). (Bottom) Graphs depicting the trapping ratio versus the electrokinetic and dielectrophoretic mobilities (note vertical axes). The inset in the electrokinetic mobility graph (bottom left) depicts the error bars for the relevant surface modifications.

Several factors come into play when determining the best fit. The coefficient of determination for the individual trials is slightly better for -400 to -600 V fit (R^2 = 0.58 vs 0.52). Furthermore, *c* was determined for both fits, and their 95% CI, resulting in -310 ± 34 V and -270 ± 100 V for the -400 to -600 V and the -400 to -700 V fit, respectively. Based on the slightly better fit and the smaller range for *c* the -400 to -600 V assessment is primarily discussed in this chapter. The smaller range of *c* is a logical choice as more replicates should decrease the range depicted by the 95% CI. In this case the -400 to -600 V interpretation has a 95% CI interval similar to the other surface modifications, while the -400 to -700 V fit results in the largest range.

Altering the linear fit will affect *c* and therefore the ratio of mobilities and μ_{DEP} (Figure 4.5., bottom). When looking at the μ_{EK} and ratio of mobilities (Figure 4.5., bottom left) the understanding of results do not significantly shift as each modification occupies its own unique space relative to the other modifications. Similarly, for the comparison of μ_{DEP} and the ratio of mobilities (Figure 4.5., bottom right) AMCA-H and spermine are still the only two modifications which are significantly altered and a significant shift in μ_{DEP} for BSA modified *E. coli* is not observed. For comparison μ_{DEP} is $1.1 \pm 0.12 \times 10^{-17}$ and $1.3 \pm 0.47 \times 10^{-17} \frac{m^4}{V^2 s}$ for the -400 to -600 V and the -400 to -700 V assessments, respectively. Data interpretation plays a key role in understanding dielectrophoretic assessments; for the BSA modified *E. coli* the choice in interpretation does not result in change in understanding of the results. To potentially improve upon the accuracy of the assessed values of *c* and μ_{DEP}, *SI* could be assessed every 50 V.

4.6 Conclusion

This work utilizes iDEP to understand the affect that surface modifications can have on analytes. Using the assessment of μ_{EK} and μ_{DEP}, insight into the changes in the biophysical properties of an analyte can be understood. Shifts in μ_{EK} are generally associated with the external properties of an analyte which is confirmed in the work presented in this chapter. Whereas, for μ_{DEP} both internal and external properties of the analyte will come into play. For the work presented here it is clear that surface modifications may potentially affect the internal properties of an analyte. In the future incorporating measurements of the zeta potential, conductivity, and permittivity would improve the understanding of how surface modifications affect properties of the cell. Furthermore, by incorporating the data model a better understanding of how the changes

to specific biophysical properties is possible. With the data presented in this chapter a separation of the various surface treatments should be possible using gradient-iDEP and incorporating slight changes to the experimental procedure (buffer composition, applied potential, etc.) may help optimize this. The ability for iDEP to rapidly probe how surface modifications can affect the biophysical properties of an analyte, in a non-destructive manner, gives new insight in the implications of surface labeling used in many scientific assessments.

4.8 References

[1] Ding, J., Woolley, C., Hayes, M. A., *Analytical and Bioanalytical Chemistry* 2017, *409*, 6405-6414.

[2] Jones, P. V., Hilton, S. H., Davis, P. E., Yanashima, R., McLemore, R., McLaren, A., Hayes, M. A., *Analyst* 2015, *140*, 5152-5161.

[3] Hu, X., Bessette, P. H., Qian, J., Meinhart, C. D., Daugherty, P. S., Soh, H. T., *Proceedings of the National Academy of Sciences of the United States of America* 2005, *102*, 15757.

[4] Johari, J., Hübner, Y., Hull, J. C., Dale, J. W., Hughes, M. P., *Physics in Medicine and Biology* 2003, *48*, N193.

[5] Bhagat, A. A. S., Bow, H., Hou, H. W., Tan, S. J., Han, J., Lim, C. T., *Medical & Biological Engineering & Computing* 2010, *48*, 999-1014.

[6] Bauer, J., *Journal of Chromatography B: Biomedical Sciences and Applications* 1987, *418*, 359-383.

[7] Gagnon, Z. R., *Electrophoresis* 2011, *32*, 2466-2487.

[8] Lee, K. H., Lee, K. S., Jung, J. H., Chang, C. B., Sung, H. J., *Applied Physics Letters* 2013, *102*, 141911.

[9] Tomlinson, M. J., Tomlinson, S., Yang, X. B., Kirkham, J., *Journal of Tissue Engineering* 2012, *4*, 2041731412472690.

[10] Roper, M. G., *Analytical Chemistry* 2016, *88*, 381-394.

[11] Sibbitts, J., Sellens, K. A., Jia, S., Klasner, S. A., Culbertson, C. T., *Analytical Chemistry* 2018, *90*, 65-85.

[12] Faraghat, S. A., Hoettges, K. F., Steinbach, M. K., van der Veen, D. R., Brackenbury, W. J., Henslee, E. A., Labeed, F. H., Hughes, M. P., *Proceedings of the National Academy of Sciences* 2017, *114*, 4591.

[13] Elvington, E. S., Salmanzadeh, A., Stremler, M. A., Davalos, R. V., *Journal of Visualized Experiments : JoVE* 2013, 50634.

[14] Pethig, R., *Biomicrofluidics* 2010, *4*, 022811.

[15] Zhu, H. W., Lin, X. G., Su, Y., Dong, H., Wu, J. H., *Biosensors & Bioelectronics* 2015, *63*, 371-378.

[16] Crowley, T. A., Pizziconi, V., *Lab on a Chip* 2005, *5*, 922-929.

[17] Gross, A., Schoendube, J., Zimmermann, S., Steeb, M., Zengerle, R., Koltay, P., *International Journal of Molecular Sciences* 2015, *16*, 16897-16919.

[18] Wang, M. M., Tu, E., Raymond, D. E., Yang, J. M., Zhang, H. C., Hagen, N., Dees, B., Mercer, E. M., Forster, A. H., Kariv, I., Marchand, P. J., Butler, W. F., *Nature Biotechnology* 2005, *23*, 83-87.

[19] Lange, J. R., Metzner, C., Richter, S., Schneider, W., Spermann, M., Kolb, T., Whyte, G., Fabry, B., *Biophysical Journal* 2017, *112*, 1472-1480.

[20] Akagi, T., Ichiki, T., *Analytical and Bioanalytical Chemistry* 2008, *391*, 2433.

[21] Hsu, J.-P., Hsieh, T.-S., Young, T.-H., Tseng, S., *Electrophoresis* 2003, *24*, 1338-1346.

[22] Hilton, S. H., Hayes, M. A., *in preparation* 2018.

[23] Cummings, E. B., Singh, A. K., *Analytical Chemistry* 2003, *75*, 4724-4731.

[24] Jones, P. V., Hayes, M. A., *Electrophoresis* 2015, *36*, 1098-1106.

[25] LaLonde, A., Gencoglu, A., Romero-Creel, M. F., Koppula, K. S., Lapizco-Encinas, B. H., *Journal of Chromatography A* 2014, *1344*, 99-108.

[26] Srivastava, S. K., Baylon-Cardiel, J. L., Lapizco-Encinas, B. H., Minerick, A. R., *Journal of Chromatography A* 2011, *1218*, 1780-1789.

[27] Kim, M., Jung, T., Kim, Y., Lee, C., Woo, K., Seol, J. H., Yang, S., *Biosensors and Bioelectronics* 2015, *74*, 1011-1015.

[28] LaLonde, A., Romero-Creel, M. F., Saucedo-Espinosa, M. A., Lapizco-Encinas, B. H., *Biomicrofluidics* 2015, *9*, 064113.

[29] Han, S.-I., Soo Kim, H., Han, A., *Biosensors and Bioelectronics* 2017, *97*, 41-45.

[30] Chen, X., Liang, Z., Li, D., Xiong, Y., Xiong, P., Guan, Y., Hou, S., Hu, Y., Chen, S., Liu, G., Tian, Y., *Biosensors and Bioelectronics* 2018, *99*, 416-423.

[31] LaLonde, A., Romero-Creel, M. F., Lapizco-Encinas, B. H., *Electrophoresis* 2015, *36*, 1479-1484.

[32] Li, H., Bashir, R., *Sensors and Actuators B: Chemical* 2002, *86*, 215-221.

[33] Gray, D. S., Tan, J. L., Voldman, J., Chen, C. S., *Biosensors and Bioelectronics* 2004, *19*, 1765-1774.

[34] Lapizco-Encinas, B. H., Simmons, B. A., Cummings, E. B., Fintschenko, Y., *Analytical Chemistry* 2004, *76*, 1571-1579.

[35] Chou, C.-F., Tegenfeldt, J. O., Bakajin, O., Chan, S. S., Cox, E. C., Darnton, N., Duke, T., Austin, R. H., *Biophysical Journal* 2002, *83*, 2170-2179.

[36] Jones, P. V., DeMichele, A. F., Kemp, L., Hayes, M. A., *Analytical and Bioanalytical Chemistry* 2014, *406*, 183-192.

[37] Lapizco-Encinas, B. H., Davalos, R. V., Simmons, B. A., Cummings, E. B., Fintschenko, Y., *Journal of Microbiological Methods* 2005, *62*, 317-326.

[38] Braff, W. A., Willner, D., Hugenholtz, P., Rabaey, K., Buie, C. R., *PloS one* 2013, *8*, e76751.

[39] Mehrishi, J. N., Bauer, J., *Electrophoresis* 2002, *23*, 1984-1994.

[40] Wagner, C., Hensel, M., in: Linke, D., Goldman, A. (Eds.), *Bacterial Adhesion: Chemistry, Biology and Physics*, Springer Netherlands, Dordrecht 2011, pp. 17-34.

[41] Mozes, N., Léonard, A., Rouxhet, P. G., *Biochimica et Biophysica Acta (BBA) - Biomembranes* 1988, *945*, 324-334.

[42] Wang, X. B., Huang, Y., Wang, X. J., Becker, F. F., Gascoyne, P. R. C., *Biophysical Journal* 1997, *72*, 1887-1899.

[43] Prescott, L. M. H., J. P.Klein, D.A., *Microbiology*, Wm. C. Brown Publishers, Dubuque, IAA 1996.

[44] Moat, A. G., Foster, J. W., Spector, M. P., *Microbial Physiology*, Wiley-Liss, New, York 2002.

[45] Suehiro, J., Hamada, R., Noutomi, D., Shutou, M., Hara, M., *Journal of Electrostatics* 2003, *57*, 157-168.

[46] Burt, J. P. H., Pethig, R., Gascoyne, P. R. C., Becker, F. F., *Biochimica et Biophysica Acta (BBA) - General Subjects* 1990, *1034*, 93-101.

[47] Sonohara, R., Muramatsu, N., Ohshima, H., Kondo, T., *Biophysical Chemistry* 1995, *55*, 273-277.

[48] Buszewski, B., Szumski, M., Kłodzińska, E., Dahm, H., *Journal of Separation Science* 2003, *26*, 1045-1049.

[49] Torimura, M., Ito, S., Kano, K., Ikeda, T., Esaka, Y., Ueda, T., *Journal of chromatography. B, Biomedical sciences and applications* 1999, *721*, 31-37.

[50] Kłodzińska, E., Szumski, M., Dziubakiewicz, E., Hrynkiewicz, K., Skwarek, E., Janusz, W., Buszewski, B., *Electrophoresis* 2010, *31*, 1590-1596.

[51] Crowther, C. V., Hayes, M. A., *Analyst* 2017, *142*, 1608-1618.

[52] Pohl, H. A., Crane, J. S., *Biophysical Journal* 1971, *11*, 711-727.

[53] Pohl, H. A., *Dielectrophoresis : the behavior of neutral matter in nonuniform electric fields*, Cambridge University Press, Cambridge; New York 1978.

[54] Srivastava, S., Gencoglu, A., Minerick, A., *Analytical and Bioanalytical Chemistry* 2011, *399*, 301-321.

[55] Irimajiri, A., Hanai, T., Inouye, A., *Journal of Theoretical Biology* 1979, *78*, 251-269.

[56] Bai, W., Zhao, K., Asami, K., *Colloids and Surfaces B: Biointerfaces* 2007, *58*, 105-115.

[57] Huang Ji-Ping and Yu Kin-Wah and Lei Jun and Sun, H., *Communications in Theoretical Physics* 2002, *38*, 113.

[58] Huang, J. P., Yu, K. W., Gu, G. Q., Karttunen, M., *Physical Review E* 2003, *67*, 051405.

[59] Jones, T. B., *Electromechanics of Particles*, Cambridge University Press 1995.

[60] Clarke, R. W., Piper, J. D., Ying, L., Klenerman, D., *Physical Review Letters* 2007, *98*, 198102.

[61] Castellarnau, M., Errachid, A., Madrid, C., Juárez, A., Samitier, J., *Biophysical Journal* 2006, *91*, 3937-3945.

[62] Crowther, C. V., Hilton, S. H., Kemp, L., Hayes, M. A., *Analytica Chimica Acta* 2018, In Submission.

[63] Pysher, M. D., Hayes, M. A., *Analytical Chemistry* 2007, *79*, 4552-4557.

[64] Staton, S. J. R., Chen, K. P., Taylor, J. P., Pacheco, J. R., Hayes, M. A., *Electrophoresis* **2010**, *31*, 3634-3641.

[65] Staton, S. J. R., Jones, P. V., Ku, G., Gilman, D. S., Kheterpal, I., Hayes, M. A., *Analyst* 2012, *137*, 3227-3229.

[66] Siegmund, L., Wostemeyer, J., *Understanding bacterial uptake by protozoa: A versatile technique for surface modification of bacteria*, 2016.

[67] Siegmund, L., Schweikert, M., Fischer Martin, S., Wöstemeyer, J., *Journal of Eukaryotic Microbiology* 2018, *0*.

[68] Majorek, K. A., Porebski, P. J., Dayal, A., Zimmerman, M. D., Jablonska, K., Stewart, A. J., Chruszcz, M., Minor, W., *Molecular Immunology* 2012, *52*, 174-182.

[69] Pédelacq, J.-D., Cabantous, S., Tran, T., Terwilliger, T. C., Waldo, G. S., *Nature Biotechnology* 2005, *24*, 79.

[70] Lapizco-Encinas, B. H., Simmons, B. A., Cummings, E. B., Fintschenko, Y., *Electrophoresis* 2004, *25*, 1695-1704.

CHAPTER 5

REFINEMENT OF INSULATOR-BASED DIELECTROPHORESIS

5.1 Introduction

In the last several years the exploitation of microfluidics as a method for analyte manipulation has grown rapidly, particularly for biological samples. This is driven by the limitations of current diagnostic methods, especially their need for large sample volumes, lengthy analysis times, and low resolution/sensitivity. Microfluidic devices have the potential to improve each of these figures of merit and provide increased portability. A wide range of bioparticles can be addressed, including animal cells[1], organelles[2], proteins[3, 4], DNA[5-7] and bacteria.[8-11]

One major division of microfluidics uses electrokinetic (EK) and the dielectrophoretic (DEP) forces on particles (molecules are considered particles for the purposes of this discussion). The EK forces allows for the manipulation of both the particle and the suspending medium, as it is the sum of electrophoresis and electroosmosis. DEP is the force, in its purest form, exerted on a polarizable particle present in a non-uniform electric field ($\vec{E}$). Utilizing EK and DEP forces, trapping and streaming of particles is possible. This allows for the separation of analytes based on their specific and subtle electrical physical properties.[10, 12-14]

Previous work on DEP separations has utilized electrode-based dielectrophoresis (eDEP), which has the advantage of being able to induce high field gradients with a low applied voltage.[15-22] Fabrication of eDEP devices can be difficult and is sometimes expensive. The electrodes are easily fouled, rendering the channels non-reusable. The

electrodes also induce electrolysis, creating bubbles and buffer alteration and the high gradients are limited to local volume near the conductive interface.

Insulator-based dielectrophoresis (iDEP) is an alternative to induce non–uniform electric fields in a microchannel. In contrast to eDEP, the electrodes are placed in distal inlet and outlet reservoirs and the electric field is defined by channel insulators and the conductive media. This resolves many of the issues encountered with eDEP (electrolysis, bubbles, fouling). Both AC and DC fields can be used with iDEP; DC fields drive overall particle movement since it induces EK and DEP transport and AC can refine separations influencing DEP only.[2, 6, 23-27] iDEP was theoretically conceived and proof of concept established in the early 2000s.[6, 28] Since then many different types of insulators have been utilized to achieve points of constriction[29] including single obstacles of various shapes[30, 31], oil menisci[32, 33], and insulating posts.[28, 34-36] Work has also been performed using height constrictions in microchannels and presents many unique opportunities for future developments.[37-40] The first separation to be demonstrated using iDEP was that of live and dead bacteria.[9, 10]

For all iDEP designs, the constriction geometry defines the overall performance, whether the basic shape is repeated or varies some characteristic dimension. The assessment here focuses on the constriction design, which is universal to all iDEP systems.[29] Examples of insulator shapes currently utilized include rectangle [14, 31, 41], triangle [25-27, 31], sawtooth[11, 23, 42, 43], circular posts [2, 10, 11, 27, 28, 35, 44], and diamond posts.[28, 45, 46] Trapping DEP leads to the isolation and concentration of analytes near the constriction points in the microchannels.[1-3, 6, 8, 10, 11, 25, 26, 28, 35] Separation can be achieved as a bipurification, where one analyte is

trapped and other analytes continue to flow through the microchannel[10], or multiple analytes can be trapped in the same microchannel.[11] Deflection techniques can also be used to achieve separations.[13, 47] Separation is possible in this case as the different mobilities of analytes results in different degrees of deflection when the particle passes the point of constriction in the microdevice.[48] Inducing the same behavior for a given particle type across all starting points will improve all existing iDEP systems.

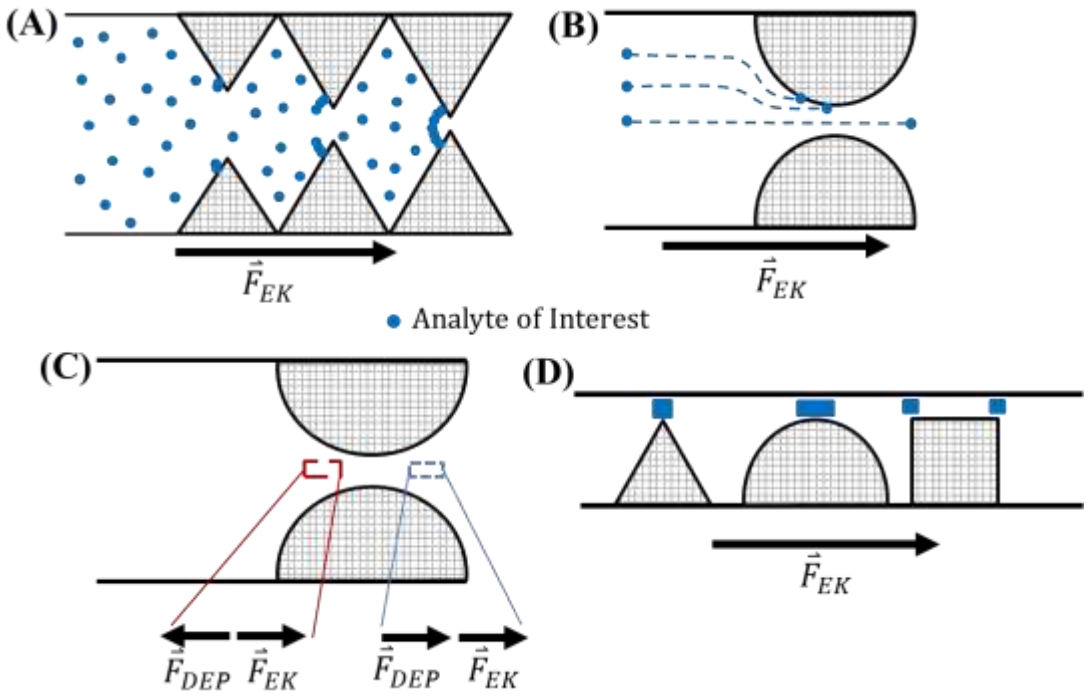

Figure 5.1. General illustration showing similar physical processes regardless of insulator geometry. For the purposes of this illustration, the bulk electrokinetic movement ($\vec{F}_{EK}$) for all the channels is from left to right. For (A) and (B) the blue spheres represent a single population of identical particles of interest experiencing nDEP. (A) Typical g-iDEP behavior, where some analytes are trapped near the point of greatest constriction at larger pitches before full cross-section sequestration occurs. (B) Identical particles experience different outcomes depending on initial pathline. In some cases, particles on centerline can traverse the gate, whereas those near the wall will be trapped. This results in like-particles being distributed throughout a range of gate pitches. (C) Near-centerline summation of forces for left-to-right $\vec{F}_{EK}$ and negative dielectrophoresis. (D) Various insulator shapes that are currently used that all allow variation in like-particle behavior depending on initial pathline. Blue rectangles depict the point of strongest DEP interaction for a particle in a DC field.

Each of these configurations creates different local environments for the analytes relative to the central longitudinal axis, depending on the initial lateral position in the channel (Figure 1). [1, 49, 50] This is true for local traps or elution strategies. For the purpose of high resolution separations, several factors come into play; including high values for the electric field and gradient[12] and the induction of all particles of an identical population to traverse the longitudinal axis in a similar fashion where the electric field strength and gradient intensity achieve separatory differentials (whether trapping, streaming (multi-outlet), or stochastic-based and chromatography-like elution-based strategies).[10, 11, 42, 43, 51-55] The identical or at least similar (accounting for diffusion and dispersion) movement of all particles of a homogeneous population is a core tenet of separations science. The manipulation of analytes by DEP is possible because each analyte has unique properties reflected by their electrophoretic (μ_{EP}) and dielectrophoretic (μ_{DEP}) mobilities. For all microchannels varying the constriction size, shape of the insulator, suspending medium, or the applied potential will alter the forces and thus the interaction of the particle with the microchannel.[3, 43, 56] Preliminary work has been performed to improve and optimize the current iDEP designs utilized for trapping DEP.[45, 57, 58] However, these works only manipulate the dimensions of currently-used shapes, and do not focus on streamlining the analytes thus eliminating extraneous trapping zones to help improve all types of DEP (trapping, deflection, and streaming). Several other works in DC and AC DEP have focused on generating a constant gradient, but these focus on the longitudinal axis or within limited zones of

interaction.[59-61] In contrast, this work is aimed at minimizing inhomogeneity across the lateral dimension.

This work seeks to develop a novel insulator geometry to improve the separation capabilities of iDEP. By iterative modeling of current and potential new designs using finite element software, a new multi-length scale insulator has been developed for negative DEP applications. The insulator design is calculated to streamline the particles, minimize the possibility for extraneous trapping zones, laterally homogenize the forces, while maintaining high gradients to allow for separation. Assurance that the models were physical was demonstrated using several experimental test probes.

5.2 Theory

Manipulation of the analytes is possible because of the influence of the EK and the DEP forces. Further development can be found in several previous works and Chapter 2 of this dissertation.[9, 10, 28, 62, 63] For continuity a short overview of theory is included here.

The electrokinetic velocity, $\vec{v}_{EK}$, is the combination of electrophoretic and electroosmotic velocities

$$\vec{v}_{EK} = \mu_{EK}\vec{E} = (\mu_{EOF} + \mu_{EP})\vec{E} \quad (1)$$

The DEP velocity, $\vec{v}_{DEP}$, can be represented in terms of dielectrophoretic mobility (μ_{DEP}) and the gradient of the electric field squared, $\nabla \left| \vec{E} \right|^2$. [62, 64, 65]

$$\vec{v}_{DEP} = -\mu_{DEP}\nabla \left| \vec{E} \right|^2 \quad (2)$$

Dielectrophoresis describes the force that is exerted on a polarizable particle present in a non-uniform electric field. For a spherical particle the force is described by the following: [62, 65]

$$\vec{F}_{DEP} = 2\pi\varepsilon_m r^3 f_{CM} \nabla \left| \vec{E} \right|^2 \quad (3)$$

where $\vec{F}_{DEP}$ is the DEP force, ε_m is the permittivity of the medium, r is the radius of the particle, and f_{CM} is the Clausius-Mossotti factor which is dependent on the conductivity of the particle and medium in DC fields. Depending upon the sign of f_{CM}, the particle of interest will either undergo positive or negative DEP. In positive DEP, the conductivity of the particle is greater than the conductivity of the media; meaning that the particle is attracted to areas of high electric field. In negative DEP, the conductivity of the media is larger than that of the particle so the particle is effectively repelled from the locations of high electric field strength.

The flow of analytes in a microfluidic channel is controlled by advection, diffusion and electrokinetic effects.[45] By eliminating pressure driven flow in the system advection can be ignored. For large particles (>1 μm) diffusion can be disregarded. Therefore, particle flow, $\vec{j}$, can be described by the following.[46, 66]

$$\vec{j} = D\nabla \mathrm{C} + C(\vec{v}_{Bulk} + \vec{v}_{EK} + \vec{v}_{DEP}) \approx C(\vec{v}_{EK} + \vec{v}_{DEP}) \quad (4)$$

Where *D* is the diffusion coefficient, *C* is the particle concentration, and $\vec{v}_{Bulk}$ is the motion of the fluid due to pressure driven flow. Therefore, particle flow is consequently only affected by the concentration of the analyte, EK, and DEP.

Dielectrophoretic forces are influenced by constrictions in the microchannel, as this is where the highest gradients are induced. Particle motion can be mostly attributed to EK when the particles are not near points of constriction in the microfluidic device, hence particle movement can be approximated by the electric field lines in these zones (Eq. 4).

Trapping of analytes occurs when the particle velocity along the field line is zero, $\vec{J} \cdot \vec{E} = 0$, such that $\vec{v}_{DEP}$is equal to $\vec{v}_{EK}$. A detailed determination of the trapping condition is included in Appendix A. Trapping of analytes can therefore be described using the EK and DEP mobilities:

$$\left(\mu_{EK}\vec{E} - \mu_{DEP}\nabla\left|\vec{E}\right|^2\right) \cdot \vec{E} \leq 0 \tag{5}$$

Eq. 7 can be rearranged such that dielectrophoretic trapping is described as:[67]

$$\frac{\nabla\left|\vec{E}\right|^2}{E^2} \cdot \vec{E} \geq \frac{\mu_{EK}}{\mu_{DEP}} \tag{6}$$

For streaming and sorting DEP the threshold for trapping is never achieved, but the particles are influenced by DEP (Eq. 4).

EK and DEP result in extremely complex systems, however the behavior can be classified as either streaming or trapping behaviors. Trapping behaviors occur when the interaction between the $\vec{E}$ and the slope of $\frac{\nabla\left|\vec{E}\right|^2}{E^2} \cdot \vec{E}$ meet at highly acute angles. Streaming DEP occurs where the $\vec{E}$ and the slope of $\frac{\nabla\left|\vec{E}\right|^2}{E^2} \cdot \vec{E}$ interact at glancing angles.

5.3 Mathematical Modeling

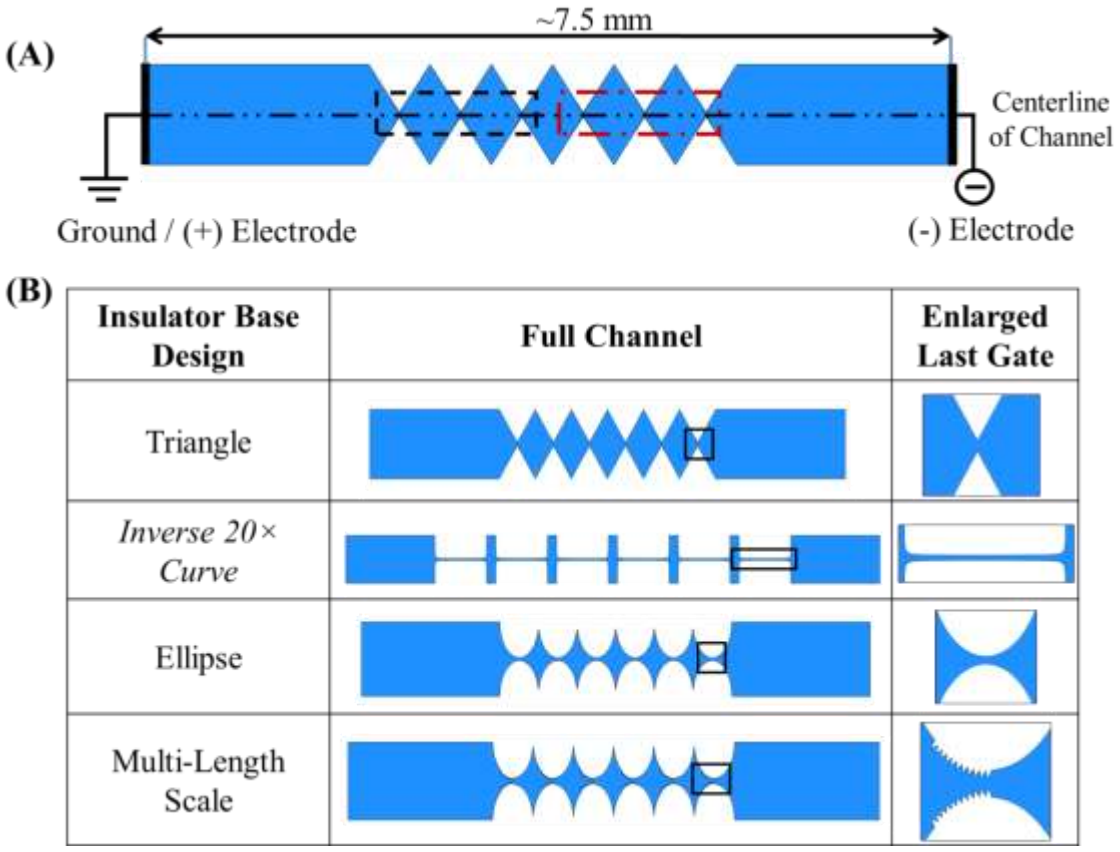

Figure 5.2. Illustration of generalized form of channels investigated computationally. (A) Enlarged sample schematic for one of the iDEP devices modeled. The approximate length of the channel and the constrictions were consistent for all models. The gate pitch of the first three gates is 36.37 μm and 34.10 μm for the second set of three gates. The only exception is for the *Inverse 20× Curve* where the channel was about 12 mm long. (B) Schematics of the some of the various insulator shapes and an enlarged view of the last gate. Other insulator shapes can be found in the Appendix A.

5.3.1 Microchannel Geometries

Six-constriction microchannels with various insulators were used in this study, where the gate pitch changed after 3 gates, resulting in 2 gate groupings. The gate pitches

were 36.37 μm and 34.10 μm (Figure 2A). The gate pitches were chosen to mimic measurements for a current channel design. The current channel measurements have been used for the manipulation and separation of several analytes including: polystyrene spheres, red blood cells, different serotypes of *Escherichia coli*, and different strains of *Staphylococcus epidermidis*.[1, 8, 11, 42] The channels modeled ranged in length from 7.5-12 mm (only the *Inverse 20× Curve* channels were on the upper end of this). A 500 V potential was applied so that the inlet wall was a ground and the outlet wall carried the potential (Figure 2A). AutoCAD 2014 (Autodesk, Inc., San Rafael, CA) was used to build the to-scale microchannels.

Insulator geometries were modeled to determine their effects on the local electric potential induced by distal electrodes. The insulator geometries focused on the following features: the effect of sharp features (triangular shape), flat designs (*Inverse 20× Curve* and rectangular insulators), rounded insulators (circular and elliptical shapes), and the addition of small insulator features to larger geometry elements near or at the point of highest constriction (Figure 2B). Several manipulations to the small insulating features were tested. Examples of these manipulations include: changing the height (ex. 20-30 μm), diminishing the insulator height, in-setting them into the base insulator, changing the width, increasing and decreasing the number of small insulators, altering the distribution of small insulators (over half the top or the full top of the base insulator), changing the shape (triangles, rectangles, curved fins, and ellipses). A sampling of these different geometries can be found in the Appendix A (Figure S1 & S2).

Fabrication limitations were not considered when testing the different variations of the multi-length scale designs. However, the multi-length scale insulator design

developed and discussed in this chapter was conceived to adhere to follow current fabrication limitations. The photomask has a tolerance for the critical dimension of 0.3 μm ± 10% with a maximum tolerance of 0.6 μm.[68] For the photomask the resolution over a 5.0 cm channel is 1.5 μm.[68] Wafers were made using standard photolithographic techniques; specifically using the photoresist AZ 3312 (AZ Electronic Materials) which can be used to create features less than 0.50 μm.[69] A microchannel depth of 20 μm with minimum feature size of a 2 μm is achievable using a Surface Technology Systems Deep Silicon Etch, which utilizes SF_6, C_4F_8, and O_2 to etch using the Bosch process for an anisotropic etch.[70] Therefore the final multi-length scale insulator shape discussed in this chapter was developed with a minimum critical dimension of 2.5 μm.

5.3.2 Finite Element Multiphysics Mathematical Models

The distribution of the electric potential was modeled using the finite-element multiphysics simulation software (COMSOL Multiphysics 5.1). The *AC/DC module* was specifically used to determine the distribution of the $\vec{E}$, $\nabla\left|\vec{E}\right|^2$, and $\frac{\nabla\left|\vec{E}\right|^2}{E^2}\cdot\vec{E}$.

Two-dimensional models of the microchannels were utilized as the electric potential is expected to vary minimally across the channel depth as the channels are relatively shallow compared to the other dimensions of the microchannel.[67] The insulating posts will distort the electric field of the entire depth of the microchannel as they are they full height of the microchannel. The same material properties and element size parameters were used for all microchannels for original comparison. The mesh was refined further for all designs discussed in this chapter.

The distribution of the electric potential was determined using the Laplace equation, where the electric potential (φ) within a microchannel is continuous:

$$\nabla^2\varphi = 0 \tag{7}$$

The boundaries are defined as the surfaces of the microchannel and insulators where the boundary conditions applied are as follows:

$$\vec{n} \cdot \vec{J} = 0 \text{ at the boundaries} \tag{8}$$

$$\varphi = V_{inlet} \tag{9}$$

$$\varphi = V_{outlet} \tag{10}$$

where $\vec{n}$ is the normal vector from the surface, $\vec{J}$ is the electrical current density, and V_{inlet} and V_{outlet} are the potentials applied at the inlet and outlet of the microchannel.

5.4 Materials and Methods

5.4.1 Microdevice fabrication

The multi-length scale insulator was developed into two different devices (Analyte and Larger) with varying sizes of gate sizes to achieve $\frac{\nabla|\vec{E}|^2}{E^2} \cdot \vec{E}$ ratios applicable to micron sized analytes. For both microchannels the width and depth were 1000 μm and 19.6 ± 0.7 μm (average between templates), respectively. The microchannels have circular, terminal reservoirs that defined the inlet and the outlet. The length of the microchannels is 3.69 cm and 3.52 cm for the Analyte and Larger designs, respectively. The channels vary based on the differential of the size between gates. The Analyte microchannel has 27 gates, where each gate size is replicated three times with a gate range of 37.01 μm to 12.27 μm. The Larger microchannel has 24 gates, with replicates of

three for each gate size, ranging from 20.4 μm to 17.6 μm. The microfluidic devices were fabricated as discussed previously.

Once the template wafers were prepared polydimethylsiloxane (PDMS) (Sylgard 184, Dow/Corning, Midland, MI) was poured on the wafers and cured at 70 °C for one hour. The PDMS casts were peeled from the templates, cut to size, and the terminal reservoirs access points were punched out with a diameter of 3 mm.

The microchannels were assembled by bonding the PDMS to a glass coverplate. Both were treated with oxygen plasma in a plasma cleaner (PDC-32G, Harrick Plasma, Ithaca, NY) for 60 seconds at 18W. The PDMS and glass coverplate sealed on contact forming the microchannel.

5.4.2 Microparticles and Suspending Medium

Experiments were performed using two different analytes. Sulfate-modified, 2.0 μm diameter, fluorescent yellow- green (ex/em 505/515) polystyrene spheres (Life Technologies, Eugene, OR) were suspended in DI-water, pH 6.3, to reach a desired particle concentration. 2.7 μm unlabeled silica spheres (Agilent Technologies, Santa Clara, CA) were suspended in 2 mM phosphate buffer, pH 7.4 with 3 mg/mL bovine serum albumin (BSA). All analytes were vortexed and sonicated before use to disrupt aggregates.

5.4.3 Experimental

Preliminary experiments were performed to ensure general features noted in the simulation were physical. Using an Olympus IX70 inverted microscope with 4× and 20× objectives, completed microdevices were observed. Approximately 20 μL of the either the polystyrene or silica spheres were pipetted into the inlet reservoir. A similar volume

was added to the outlet reservoir and used to balance pressure driven flow, confirmed by observing the elimination of longitudinal particle motion in the channel. Platinum electrodes with a diameter of 0.404 mm (Alfa Aesar, Ward Hill, MA) were inserted into the reservoirs and connected to a HVS448 3000D high voltage sequencer (Labsmith, Inc., Livermore, CA). The samples were illuminated using a combination of a mercury short arc lamp (H30 102 w/2, OSRAM) and Fiber-Lite High Intensity Illuminator (Model 170D, Dolan Jenner, Lawrence, MA). To observe the fluorescence a Texas Red triple bandpass cube (Olympus, Center Valley, PA) was utilized. A range of DC voltages, ~0-1000V, were applied across the device and used to manipulate both analytes. For the polystyrene sphere experiments color video was collected using a digital single-lens reflex Nikon D5000 camera (Nikon, Melville, NY). Videos and images of the silica spheres were collected using a monochrome QICAM cooled CCD camera (QImaging, Inc., Surrey, BC) and Streampix V image capture software (Norpix, Inc., Montreal, QC). ImageJ was used for file conversion and to assess, manipulate and quantify the images and generate data.

5.5 Results and Discussion

The shape of insulators in iDEP defines the ability to manipulate analytes within the microfluidic channel. The insulator induces the distribution of $\vec{E}$ and therefore the $\nabla \left| \vec{E} \right|^2$ and the streaming or trapping of the analyte. For trapping, streaming, and sorting it is desirable for each particle of a given physical makeup to experience the same environment to ensure consistent outcomes. Concurrently, the dielectrophoretic forces must be high enough to overcome transport and diffusional forces to generate an observable effect. This requires large gradients, resulting in large $\nabla \left| \vec{E} \right|^2$ values.[1, 12]

Depending on the geometric configuration and strength of the various forces, streaming or trapping can result. Sorting of particles in a continuous or semi-continuous mode has been an important use of dielectrophoresis. A common strategy is deflection using streaming DEP, but recent work has shown sorting by exploiting trapping or trapping-like mechanisms.[8, 11, 13, 47] For deflection techniques to operate most efficiently, similar principles apply, in that, all particles of a population should occupy a homogenous lateral environment during the deflection process. This suggests that all particles for each analyte population is influenced by the same $\frac{\nabla|\vec{E}|^2}{E^2} \cdot \vec{E}$ values within each zone throughtout the process.

The need for a gradient and to have all analytes experience equivalent forces as they traverse the system can be at odds with one another, by definition gradient means a change in the value where as there needs to be homogeniety in a lateral (or semilateral) dimension. This study probes a large variety of insulator shapes to create an environment where high gradient values are attained, while giving a homogeneous environment to all particles within a given analyte population exposed to the separatory system.

Several geometric constructs were probed, including the effect of different base insulators: triangle, rectangle, *Inverse 20× Curve*, circle, and ellipse (Figure 3). Futhermore the addition of small insulators to the base structure was tested; variables included the shape of the small insulator(s) (triangle, ellipse, rectangle, and curved fin), number of small insulator(s), location on the base insulator (across the whole top or half, insetting the insulators in the base insulator), and the dimensions of the small insulators (height, width variations at base and top). Examples of these different geometries that were tested can be found in the Appendix A (Figure S2). All of these geometries were

eliminated based on one or more of the following factors: not achieving $\nabla \left| \vec{E} \right|^2$ values comparable to currently utilized designs, inefficient streaming (presence of local traps) of analytes, and/or severe lateral field inhomogeniety (Appendix A Table S1). The multi-length scale insulator design was developed futher and was optimized to adhere to the fabrication limitations as noted.

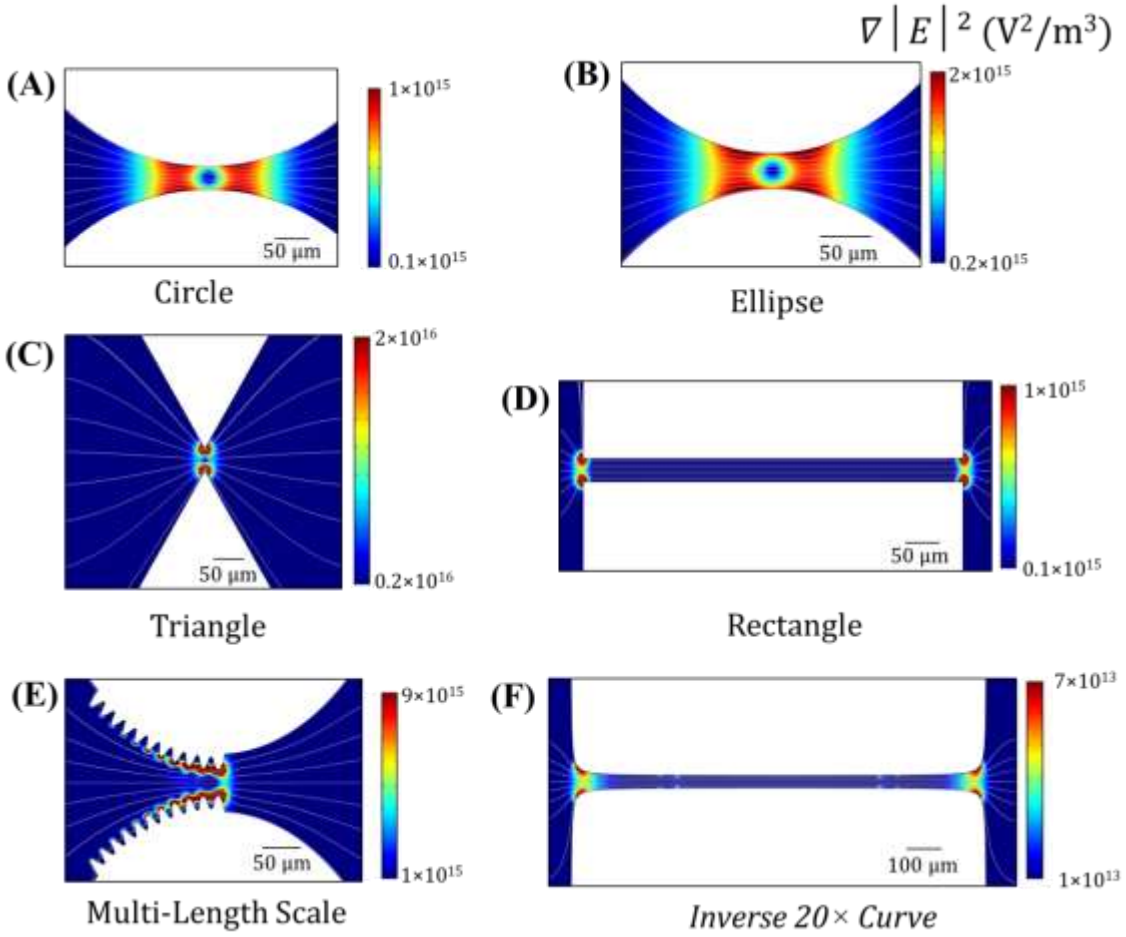

Figure 5.3. Study of general design options (others shown in Appendix A, Figure S2). Two dimensional plots of the $\nabla \left| \vec{E} \right|^2$ for different insulator shapes with electric field lines (grey). The absolute value for the color scale for each design differs to highlight the patterns that result from the specific insulator shape. Each image is of the first gate of 34.10 µm for the different designs with an applied global potential of 500 V.

To achieve high $\nabla \left| \vec{E} \right|^2$, the most effective insulator design has sharp points, demonstrated by the triangular insulator (Figure 3C). The radius of curvature of the

insulator for sharp features changes rapidly which, in turn, constricts the electric field and results in a high $\nabla \left| \vec{E} \right|^2$. The triangular insulator is representative of diamonds, sawteeth, and triangles used for insulators.[11, 23, 28, 31, 42, 43, 45] Along the centerline, the value for the gradient of the $\nabla \left| \vec{E} \right|^2$ is for the 34.10 μm gate is approximated to be 3.2×10^{16} V^2/m^3, which is the highest value of any of the insulator shapes examined. Particles will travel along the field line by EK forces in the absence of a significant gradient. However, these sharp features create local dielectrophoretic traps where the electric field line impinges the slope of the local gradient at an acute angle. This is seen at the lateral pathlines away from the centerline for these triangle designs, which are representative of this class of insulator shapes. In cases where trapping does not occur, particles are deflected in a highly non-linear fashion preventing consistent separations via deflection and streaming.

Circular insulators have smaller gradients (Figure 3 A & B) as the constriction of the electric field is more gradual as compared to triangular insulators. Therefore, only smaller $\nabla \left| \vec{E} \right|^2$ values are possible with the same constriction size compared to sharp insulators. The $\nabla \left| \vec{E} \right|^2$ along the centerline is 8.8×10^{14} and 1.85×10^{15} V^2/m^3 for the circular and ellipse shaped insulators respectively with a gate pitch of 34.10 μm.

Rectangular insulators are also used to alter the gradient of the electric field (Figure 3D)[14, 41]. The maximum $\nabla \left| \vec{E} \right|^2$ along the centerline is 6.3×10^{14} V^2/m^3 with a gate pitch of 34.10 μm. The gradient for rectangular and *Inverse 20× Curve* insulators (Figure 3 D&F) are smaller than for circular and triangular insulators as the constriction of the electric field is abrupt, so a high gradient is limited to the corners of the insulators.

These values are the lowest of any insulator shape, this could be increased by shortening the insulator or channel, however the $\nabla \left| \vec{E} \right|^2$ will still be lower than the other designs, leading to less influence on the particles in the channel.

The $\nabla \left| \vec{E} \right|^2$ value is not the same laterally for the triangular, circular, and rectangular insulators, so that particles will experience different forces based on their initial pathlines. Within each of these designs, particles starting at various vertical positions (as drawn, lateral position relative to the longitudinal axis of the device and applied external electric field) will be trapped at widely varying locations (Figure 1), meaning that trapping DEP will not occur at the same voltage for the different analyte pathlines.[49, 50] The rectangular and *Inverse 20× Curve* have the most laterally homogeneous electric field, however they do not have a strong enough gradient to trap analytes of typical interest.[12] For the case of sorting DEP methods having a low $\nabla \left| \vec{E} \right|^2$ will result in lower resolution separations as particles will not be deflected as much. This is compounded by the fact that like-particles along different pathlines will experience different forces, altering their deflection and thus the resolution of the separation. Streaming DEP is also affected by having low $\nabla \left| \vec{E} \right|^2$ values, and thus lower DEP forces, therefore the particles are not as effectively streamlined. The effects of inhomogeneous lateral fields are similar to the wall effect in chromatography, which results in lower resolution separations.[71]

The advantage to multi-length scale design is the small insulators alter the distribution of the electric field significantly at the points approaching the constriction resulting in higher values for the $\nabla \left| \vec{E} \right|^2$, while the elliptical base minimized lateral

heterogeneity. As the particles approach the point of constriction, under conditions of negative DEP, the analytes are pushed towards the center of the microchannel as they are repelled from the small insulators. The most useful insulator design from this study has an elliptically-shaped base insulator and small 20 μm-tall elliptically-shaped insulators across half the top of the base (Figure 3E). The $\nabla \left| \vec{E} \right|^2$ at the 34.10 μm gate pitch is 1.7×10^{15} V^2/m^3. This value is lower than for the triangular insulators and comparable to ellipse insulators, but higher than the other insulators.

All further comparisons made are between a triangular insulator, an elliptical insulator, and the new multi-length scale insulator. The triangular and elliptical insulators represent issues of partial trapping and an inhomogeneous lateral environment present for all other designs (circle and rectangle) and the triangular insulator has the highest $\nabla \left| \vec{E} \right|^2$ along the centerline. The elliptical insulator is also used for comparison to determine the effects of the addition of the small insulators for the multi-length insulator. Using the definition of trapping in an iDEP device defined in Eq. 4 particles are trapped based on the ratio of the μ_{EK} and μ_{DEP}. Using a known analyte (*Escherichia coli*), an established value for μ_{EK} is -1.0×10^{-8} m^2/Vs [8], noting that the analyte is rod shaped, but this is accounted for in the determination of μ_{EK}. The dielectrophoretic mobility can be calculated assuming the particle is between 0.1-1.0 μm, using the following relationship. [12]

$$\mu_{DEP} = \frac{\varepsilon_m r^2 f_{CM}}{3\eta} \tag{12}$$

where media permittivity (ε_m) is 10^{-9} F/m, the radius of the particle (r) is 10^{-6} to10^{-7} m, f_{CM} is -0.3, and solution viscosity (η) is $10^{-3}$$Ns/m^2$ [12]. This gives a range for μ_{DEP} of -

1.0×10^{-17} to -1.0×10^{-19} m^4/V^2s. Therefore, a range for the ratio of mobilities is 1.0×10^9 V/m^2 to 1.0×10^{11} V/m^2. These values reasonably coincides with the value determined for *Staphylococcus epidermidis* of $4.6 \pm 0.6\times10^9$ V/m^2 for gentamicin resistant and $9.2 \pm 0.4\times10^9$ V/m^2 for gentamicin sensitive. [11]

A direct visual 2D comparison of $\frac{\nabla|\vec{E}|^2}{E^2}\cdot\vec{E}$ within the three designs provides evidence for significantly different behaviors (Figure 4). The full range of $\frac{\nabla|\vec{E}|^2}{E^2}\cdot\vec{E}$ values depicts that a triangular insulator achieves the highest values followed by the multi-length scale and then elliptical insulator (Figure 4A, 4C, & 4E). In these representations, the intensity of the $\frac{\nabla|\vec{E}|^2}{E^2}\cdot\vec{E}$ value is plotted showing effect on a particle with various mobility ratios. Specific ratios were utilized as the various shapes with the same constrictions and voltage applied will trap particles with ratios between 5.4×10^9 and 1.7×10^{10} V/m^2 (Figure 4B, 4D, & 4F). The ratios were chosen to depict potential trapping conditions specific to the applied voltage, insulator shape, and gate pitch. A ratio of 5.6×10^9 V/m^2 was selected for the multi-length scale design selected to show trapping behavior at a slightly narrower gate (right) and complete passage of all particles at the wider gate (left) for the multi-length scale design (Figure 4F). The color scale toward red is the most repelling environment and the white areas completely exclude analytes with these properties. The portions with color define the area accessible to this analyte. This can be observed by noting that the white area completely bridges the gap on the right gate, indicating excluded area and trapping behavior.

Significantly different behaviors can be deduced for the triangular and ellipse insulators (Figures 4A, 4B, 4C, & 4D). For particles off the centerline, the electrokinetic

pathlines impinge upon the gradient at an acute angle, allowing for partial trapping at wider gates (Figures 4B & 4D). At the top (or bottom) the pathlines clearly impinge on the slope of the $\frac{\nabla|\vec{E}|^2}{E^2} \cdot \vec{E}$ at an acute angle. When full trapping across the gate occurs, an arc forms represented by the left edge of the white areas (Figures 4B & 4D). This arc structure has been observed in many experimental systems and is demonstrated computationally (Figures 5A, 5B, 5C, & 5D).[1, 3, 8-11, 45, 49, 50, 72] The net result is consistent with current experimental systems, where small collections of analytes are observed close to the point of greatest constriction of wide gates and full arcs form when complete trapping across the lateral dimension occurs. For a single particle population, some particles will trap on these wide gates, while other will continue on, which distributes that single population throughout the device.

The reason the multi-length scale system prevents these local traps at wide gates is the slope of the $\frac{\nabla|\vec{E}|^2}{E^2} \cdot \vec{E}$ impinges upon the electrokinetic lines at a glancing angles and simply streams particles that experience negative DEP toward the centerline. For the left, larger, gate particles not on the centerline will be influenced by the gradient near the white space (inaccessible area) first and be deflected towards the centerline, as this interaction does not occur at the highly acute angles necessary for trapping. As the particles interact near an inaccessible area first, and are deflected towards the centerline they will not interrogate the local minima between the small insulators (Figure 4F). If the centerline trapping forces are insufficient, no trapping occurs at that gate.

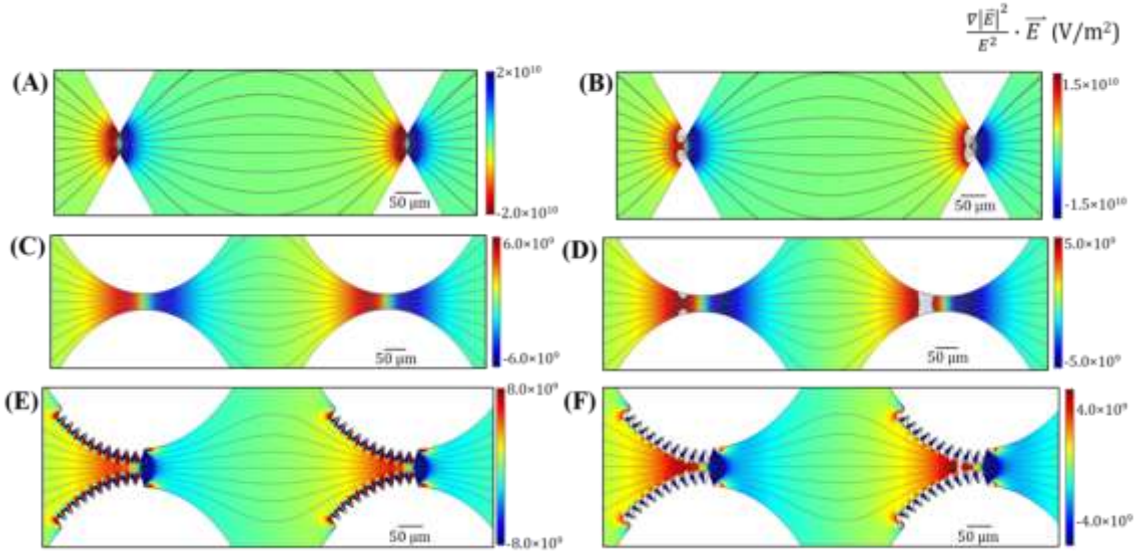

Figure 5.4. Study emphasizing differences between triangular, ellipse, and multi-length scale insulators at the critical transition to full trapping at second gate (non-trapping at left, trapping at right, panels B, D, & F). White areas indicate zones where the analyte is completely excluded (see text). Similar data in all six panels, with different representations to emphasize various transport and trapping features. Panels A, C, & E are the full distribution of $\frac{\nabla|\vec{E}|^2}{E^2}\cdot\vec{E}$. Electric field lines present in all panels. Panels B, D, & F illustrates the area that is accessible (colored region) to a particle that would be repelled (nDEP) with a given particle property (μ_{EK}/μ_{DEP}): 1.8×10^{10} V/m^2 – triangle, 5.4×10^{9} V/m^2 – ellipse, and 5.6×10^{9} V/m^2 – multi-length scale). At low $\frac{\nabla|\vec{E}|^2}{E^2}\cdot\vec{E}$ values, electric field lines are the pathlines of particles. Panels showing triangular insulator (A & B) show electric field lines off the centerline impinging the slope of the $\frac{\nabla|\vec{E}|^2}{E^2}\cdot\vec{E}$ (local direction of dielectrophoretic forces) at highly acute angles, creating a local trapping point. These lateral trapping areas are present at all sharp features and some rounded features (B & D). In this study, for the triangular and ellipse insulator given the analyte μ_{EK}/μ_{DEP} ratio of choice, the analyte is partially trapped at the first gate and fully trapped at the second gate. In contrast, the critical particle would pass the first gate completely and be trapped at the second gate for the multi-length scale insulator. Further, the multi-length scale insulator does not exhibit any lateral traps were the electric field lines impinge the $\frac{\nabla|\vec{E}|^2}{E^2}\cdot\vec{E}$ slope at extremely acute angles. The gate pitches are 36.37 µm and 34.10µm, left to right with an applied global potential of 500 V (A-F).

Predicted trapping locations for the different designs were determined, based on different mobilities ratio. For both the triangular and elliptically shaped insulators partial trapping is seen at the 36.37 µm gate (Figures 5A & 5C), while no trapping is seen for

multi-length insulator (Figure 5F). Complete trapping of an analyte is seen for all insulator shapes at the 34.10 μm gate (Figures 5B, 5D, & 5F). These results for the common insulator shapes agree with what many groups have seen computationally and experimentally.[9, 35, 45, 67]

One feature which promises improved results beyond the removal of local traps is that the assessable area limits the lateral variation in $\frac{\nabla|\vec{E}|^2}{E^2} \cdot \vec{E}$. At a trapping location (Figure 5F), the values are relatively constant across the entire gap. This is a direct result of the streamlining such that at the third small tooth (starting at the point of constriction working left) the channel width is 42.80 μm, however the accessible area to the analyte is only about 30 μm (Figure 5F). The particles are deflected towards the centerline of the channel, such that they will not interrogate the space close to the top or between the small insulators.

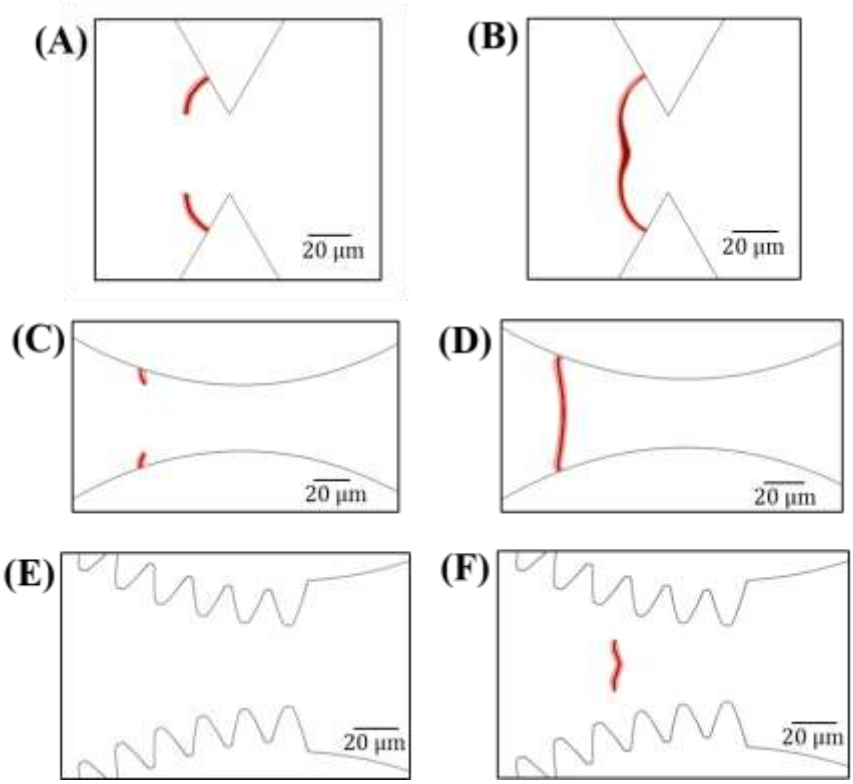

Figure 5.5. Depiction of trapping locations for various mobility ratios, where the dark red represents the trapping condition, and the pink is the region surrounding where trapping is also likely to occur. Partial trapping is depicted in A & C, while complete trapping of the analyte is present in B, D & F. The multi-length scale insulator does not have partial trapping as analytes deflected to the centerline, and then not trapped until the necessary conditions are met. A, C, & E are representative of 36.37 µm gates, while B, D, & F are representative of 34.10 µm gates. The mobility ratios depicted are as follows: A & B - 1.8×10^{10} V/m^2, C & D - 5.4×10^{9} V/m^2, E & F - 5.6×10^{9} V/m^2. All images are modelled such that the applied global potential is 500 V.

The multi-length scale insulator was fabricated and exploratory testing performed using two model analytes, polystyrene and silica spheres. Based on the preliminary results presented in Figure 6 the model was determined to be physical. This was based on the streaming effect of the analyte depicted in Figure 6 and Appendix A. The analytes are seen to be deflected away from the small insulators and pushed towards the centerline of the channel, (Figure 6 A-D). This ensures that the analytes will experience more similar forces as the analytes follow more similar pathlines. Looking at Figure 6 E & F both

analytes are trapped at the third tooth (starting at the point of constriction working left), which reflects what was predicted in the model (Figure 5F).

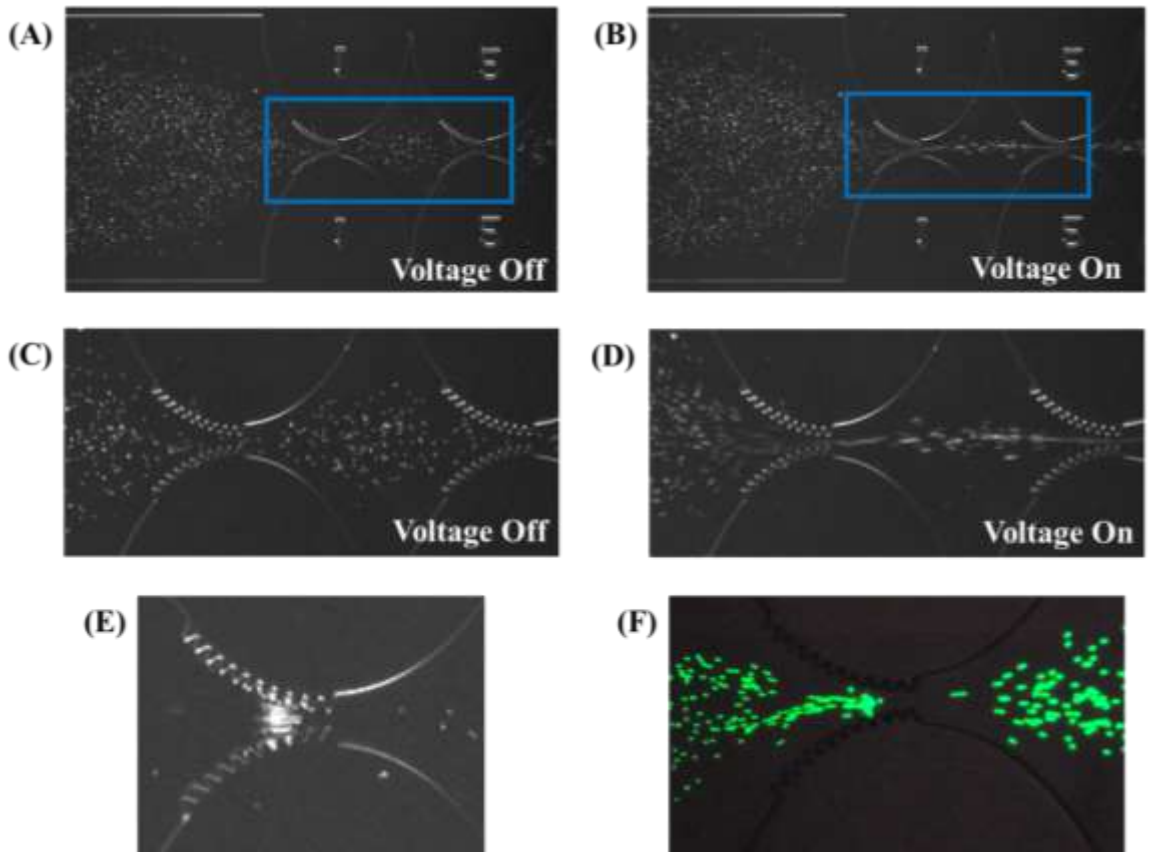

Figure 5.6. Examples of trapping and streaming of polystyrene and silica spheres using the multi-length scale insulators. Light field/dark field contrast enhanced image of (A-E) 2.7 μm silica particles. Fluorescence/bright field contrast enhanced image of (F) 2.0 μm yellow-green fluorescent polystyrene spheres. A-D depicts the streaming effect on the analyte with the applied voltage. C&D are enlarged images of the blue rectangles in A&B. With the voltage applied the analyte is pushed to the centerline of the channel and deflected away from the small insulators resulting in more effective streaming. E&F depict that the capture of different analytes is possible and correlates to the predicted capture location from the models. Gate sizes and applied potentials are as follows (A-D) 20.5 μm, -600 V (E) 18.0 μm, -1000 V (F) 18.7 μm, -400 V.

For the separation of mixed samples, the effect of analytes that experience positive DEP must be considered as they will be drawn to the drown-stream side of the small elliptical insulators. This is represented by the dark blue regions in Figure 4F. This may

result in unwanted behavior including clogging, distortion of forces, particle-particle interactions, etc. It is important to note that the majority of the analytes that experience positive DEP theoretically would be trapped at the preliminary gates in the microchannel and would therefore not influence separations at later gates. Some potential ways to address this concern would be by including a primary wide gate that would trap all the analytes that experience positive DEP, allowing for the separation of analytes that experience negative DEP in the rest of the microchannel. Additionally, to prevent clogging, the introduction of side channels may allow for the drain off desired analytes, including those that experience positive DEP.

For sorting and streaming techniques, in the region particles are predicted to interrogate, the forces are more uniform laterally with the multi-length scale insulator meaning that the particles will be repelled or deflected in more a similar manner as they will experience more similar forces. This lays the framework for the possibility of higher resolution separations as particles are deflected the same amount and better streaming will occur as the particles will be confined to a smaller area in the channel than with the other designs.

5.6 Conclusion

The development of a new multi-length scale insulator for iDEP insulator streamlines the analytes to ensure that like-particles experience similar environments as the $\vec{E}$ is more homogenous in the accessible area. This should minimize partial and extraneous trapping. The two factors are predicted to improve separation for both deflection and trapping techniques. Preliminary experimental evidence is consistent with

the model and this claim. This can all be accomplished while maintaining $\frac{\nabla|\vec{E}|^2}{E^2} \cdot \vec{E}$ values high enough to accomplish trapping.

5.7 References

[1] Jones, P. V., Staton, S. J. R., Hayes, M. A., *Analytical and Bioanalytical Chemistry* 2011, *401*, 2103-2111.

[2] Luo, J., Abdallah, B. G., Wolken, G. G., Arriaga, E. A., Ros, A., *Biomicrofluidics* 2014, *8*, 021801.

[3] Staton, S. J. R., Jones, P. V., Ku, G., Gilman, S. D., Kheterpal, I., Hayes, M. A., *Analyst* 2012, *137*, 3227-3229.

[4] Nakano, A., Camacho-Alanis, F., Ros, A., *Analyst* 2015, *140*, 860-868.

[5] Washizu, M., Kurosawa, O., *Industry Applications*, *IEEE Transactions on* 1990, *26*, 1165-1172.

[6] Chou, C.-F., Tegenfeldt, J. O., Bakajin, O., Chan, S. S., Cox, E. C., Darnton, N., Duke, T., Austin, R. H., *Biophysical Journal* 2002, *83*, 2170-2179.

[7] Martinez-Duarte, R., Camacho-Alanis, F., Renaud, P., Ros, A., *Electrophoresis* 2013, *34*, 1113-1122.

[8] Jones, P. V., DeMichele, A. F., Kemp, L., Hayes, M. A., *Analytical and Bioanalytical Chemistry* 2014, *406*, 183-192.

[9] Lapizco-Encinas, B. H., Simmons, B. A., Cummings, E. B., Fintschenko, Y., *Analytical Chemistry* 2004, *76*, 1571-1579.

[10] Lapizco-Encinas, B. H., Simmons, B. A., Cummings, E. B., Fintschenko, Y., *Electrophoresis* 2004, *25*, 1695-1704.

[11] Jones, P. V., Hilton, S. H., Davis, P. E., Yanashima, R., McLemore, R., McLaren, A., Hayes, M. A., *Analyst* 2015, *140*, 5152-5161.

[12] Jones, P. V., Hayes, M. A., *Electrophoresis* 2015, *36*, 1098-1106.

[13] Abdallah, B. G., Chao, T.-C., Kupitz, C., Fromme, P., Ros, A., *ACS Nano* 2013, *7*, 9129-9137.

[14] Srivastava, S. K., Baylon-Cardiel, J. L., Lapizco-Encinas, B. H., Minerick, A. R., *Journal of Chromatography A* 2011, *1218*, 1780-1789.

[15] Hughes, M. P., Morgan, H., Rixon, F. J., Burt, J. P. H., Pethig, R., *Biochimica et Biophysica Acta (BBA) - General Subjects* 1998, *1425*, 119-126.

[16] Crane, J. S., Pohl, H. A., *Journal of The Electrochemical Society* 1968, *115*, 584-586.

[17] Pohl, H. A., Crane, J. S., *Biophysical Journal* 1971, *11*, 711-727.

[18] Hoettges, K. F., Hughes, M. P., Cotton, A., Hopkins, N. A. E., McDonnell, M. B., *Engineering in Medicine and Biology Magazine, IEEE* 2003, *22*, 68-74.

[19] Johari, J., Hübner, Y., Hull, J. C., Dale, J. W., Hughes, M. P., *Physics in Medicine and Biology* 2003, *48*, N193.

[20] Morgan, H., Hughes, M. P., Green, N. G., *Biophysical Journal*, *77*, 516-525.

[21] Hughes, M. P., Morgan, H., *Analytical Chemistry* 1999, *71*, 3441-3445.

[22] Hughes, M. P., *Electrophoresis* 2002, *23*, 2569-2582.

[23] Chen, K. P., Pacheco, J. R., Hayes, M. A., Staton, S. J. R., *Electrophoresis* 2009, *30*, 1441-1448.

[24] Chaurey, V., Polanco, C., Chou, C.-F., Swami, N. S., *Biomicrofluidics* 2012, *6*, 012806.

[25] Swami, N., Chou, C.-F., Ramamurthy, V., Chaurey, V., *Lab on a Chip* 2009, *9*, 3212-3220.

[26] Su, Y.-H., Tsegaye, M., Varhue, W., Liao, K.-T., Abebe, L. S., Smith, J. A., Guerrant, R. L., Swami, N. S., *Analyst* 2014, *139*, 66-73.

[27] Gencoglu, A., Camacho-Alanis, F., Nguyen, V. T., Nakano, A., Ros, A., Minerick, A. R., *Electrophoresis* 2011, *32*, 2436-2447.

[28] Cummings, E. B., Singh, A. K., *Analytical Chemistry* 2003, *75*, 4724-4731.

[29] Srivastava, S., Gencoglu, A., Minerick, A., *Analytical and Bioanalytical Chemistry* 2011, *399*, 301-321.

[30] Keshavamurthy, S. S., Leonard, K. M., Burgess, S. C., Minerick, A. R., *NSTI-Nanotech, Boston, MA* 2008, 401-404.

[31] Kang, Y., Li, D., Kalams, S., Eid, J., *Biomedical Microdevices* 2008, *10*, 243-249.

[32] Barbulovic-Nad, I., Xuan, X., Lee, J. S. H., Li, D., *Lab on a Chip* 2006, *6*, 274-279.

[33] Thwar, P. K., Linderman, J. J., Burns, M. A., *Electrophoresis* 2007, *28*, 4572-4581.

[34] Lapizco-Encinas, B. H., Davalos, R. V., Simmons, B. A., Cummings, E. B., Fintschenko, Y., *Journal of Microbiological Methods* 2005, *62*, 317-326.

[35] Sabounchi, P., Morales, A., Ponce, P., Lee, L., Simmons, B., Davalos, R., *Biomedical Microdevices* 2008, *10*, 661-670.

[36] Regtmeier, J., Duong, T. T., Eichhorn, R., Anselmetti, D., Ros, A., *Analytical Chemistry* 2007, *79*, 3925-3932.

[37] Braff, W. A., Pignier, A., Buie, C. R., *Lab on a Chip* 2012, *12*, 1327-1331.

[38] Braff, W. A., Willner, D., Hugenholtz, P., Rabaey, K., Buie, C. R., *PloS one* 2013, *8*, e76751.

[39] Barrett, L. M., Skulan, A. J., Singh, A. K., Cummings, E. B., Fiechtner, G. J., *Analytical Chemistry* 2005, *77*, 6798-6804.

[40] Zellner, P., Shake, T., Hosseini, Y., Nakidde, D., Riquelme, M. V., Sahari, A., Pruden, A., Behkam, B., Agah, M., *Electrophoresis* 2015, *36*, 277-283.

[41] Kang, K. H., Kang, Y., Xuan, X., Li, D., *Electrophoresis* 2006, *27*, 694-702.

[42] Staton, S. J. R., Chen, K. P., Taylor, T. J., Pacheco, J. R., Hayes, M. A., *Electrophoresis* 2010, *31*, 3634-3641.

[43] Pysher, M. D., Hayes, M. A., *Analytical Chemistry* 2007, *79*, 4552-4557.

[44] Gallo-Villanueva, R. C., Rodríguez-López, C. E., Díaz-de-la-Garza, R. I., Reyes-Betanzo, C., Lapizco-Encinas, B. H., *Electrophoresis* 2009, *30*, 4195-4205.

[45] LaLonde, A., Gencoglu, A., Romero-Creel, M. F., Koppula, K. S., Lapizco-Encinas, B. H., *Journal of Chromatography A* 2014, *1344*, 99-108.

[46] Cummings, E. B., *Engineering in Medicine and Biology Magazine, IEEE* 2003, *22*, 75-84.

[47] Srivastava, S. K., Artemiou, A., Minerick, A. R., *Electrophoresis* 2011, *32*, 2530-2540.

[48] Abdallah, B. G., Roy-Chowdhury, S., Coe, J., Fromme, P., Ros, A., *Analytical Chemistry* 2015, *87*, 4159-4167.

[49] Gallo-Villanueva, R. C., Sano, M. B., Lapizco-Encinas, B. H., Davalos, R. V., *Electrophoresis* 2014, *35*, 352-361.

[50] Saucedo-Espinosa, M. A., Lapizco-Encinas, B. H., *Electrophoresis* 2015, *36*, 1086-1097.

[51] Giddings, J. C., *Unified Separation Science*, John Wiley & Sons, Inc., New York 1991.

[52] Morton, K. J., Loutherback, K., Inglis, D. W., Tsui, O. K., Sturm, J. C., Chou, S. Y., Austin, R. H., *Proceedings of the National Academy of Sciences* 2008, *105*, 7434-7438.

[53] Huang, L. R., Cox, E. C., Austin, R. H., Sturm, J. C., *Science* 2004, *304*, 987-990.

[54] Streek, M., Schmid, F., Duong, T. T., Ros, A., *Journal of Biotechnology* 2004, *112*, 79-89.

[55] Ros, A., Hellmich, W., Regtmeier, J., Duong, T. T., Anselmetti, D., *Electrophoresis* 2006, *27*, 2651-2658.

[56] Ozuna-Chacón, S., Lapizco-Encinas, B. H., Rito-Palomares, M., Martínez-Chapa, S. O., Reyes-Betanzo, C., *Electrophoresis* 2008, *29*, 3115-3122.

[57] Pesch, G. R., Kiewidt, L., Du, F., Baune, M., Thöming*, J., *Electrophoresis* 2016, *37*, 291-301.

[58] Saucedo-Espinosa, M. A., Lapizco-Encinas, B. H., *Journal of Chromatography A* 2015, *1422*, 325-333.

[59] Weiss, N. G., Jones, P. V., Mahanti, P., Chen, K. P., Taylor, T. J., Hayes, M. A., *Electrophoresis* 2011, *32*, 2292-2297.

[60] Humble, P. H., Kelly, R. T., Woolley, A. T., Tolley, H. D., Lee, M. L., *Analytical Chemistry* 2004, *76*, 5641-5648.

[61] Allen, D. J., Accolla, R. P., Williams, S. J., *Electrophoresis* 2017, *38*, 1441-1449.

[62] Pohl, H. A., *Dielectrophoresis : the behavior of neutral matter in nonuniform electric fields*, Cambridge University Press, Cambridge; New York 1978.

[63] Pethig, R., *Biomicrofluidics* 2010, *4*, 022811.

[64] Probstein, R. F., *Physicochemical Hydrodynamics: An Introduction*, John Wiley & Sons, Inc. 1994, pp. 1-8.

[65] Jones, T. B., *Electromechanics of Particles*, Cambridge University Press 1995.

[66] Kwon, J.-S., Maeng, J.-S., Chun, M.-S., Song, S., *Microfluidics and Nanofluidics* 2008, *5*, 23-31.

[67] Baylon-Cardiel, J. L., Lapizco-Encinas, B. H., Reyes-Betanzo, C., Chavez-Santoscoy, A. V., Martinez-Chapa, S. O., *Lab on a Chip* 2009, *9*, 2896-2901.

[68] Dingley, J., in: Photo-Tools, J. (Ed.), JD Photo-Tools 2014, pp. 1-89.

[69] AZ Electronic Materials: AZ® 3300 Series Crossover Photoresists 2005.

[70] Bhardwaj, J., Ashraf, H., McQuarrie, A., *Proc. Symp. Microstructures and Microfabricated Systems*, *ECS* 1997.

[71] Shalliker, R. A., Broyles, B. S., Guiochon, G., *Journal of Chromatography A* 2000, *888*, 1-12.

[72] Staton, S. J. R., Chen, K. P., Taylor, J. P., Pacheco, J. R., Hayes, M. A., *Electrophoresis* **2010**, *31*, 3634-3641.

CHAPTER 6

SEPARATING PROTISTS PRESENT IN A TERMITE'S HINDGUT

6.1 Introduction

Termites survive by consuming cellulose or dead plant matter, examples of which include wood and leaf litter. The reason that "lower" termites (all families except Termitidae) can survive on this diet is due to their symbiotic relationship with the protists that reside in their hindgut. Specifically, the protists are part of the Phylum Parabasalia and Phylum Preaxostyla. These phyla are primarily made up of protists which inhabit the guts of both invertebrate and vertebrate animals. The majority of the protists from these phyla reside in hindguts of termites, where they are conveyed from generation to generation by proctodeal feeding.[1] As is implied by a symbiotic relationship, neither the termites nor protists would survive without the other. The termites rely on the protist to assist in the digestion of wood, while the protists cannot survive outside of the termites hindgut. [2] The symbiotic relationship of the termites and protists goes back 150-200 million years. [3, 4] Protists can range in size from a few microns up to hundreds of microns (Figure 6.1.).[5] The hindgut communities of different termite species also varies wildly as some termites only have a few protists species, while other termites will have a much more diverse community. Figure 6.1. demonstrates the diversity of the hindgut contents found in a *Reticulitermes tibialis* worker hindgut.

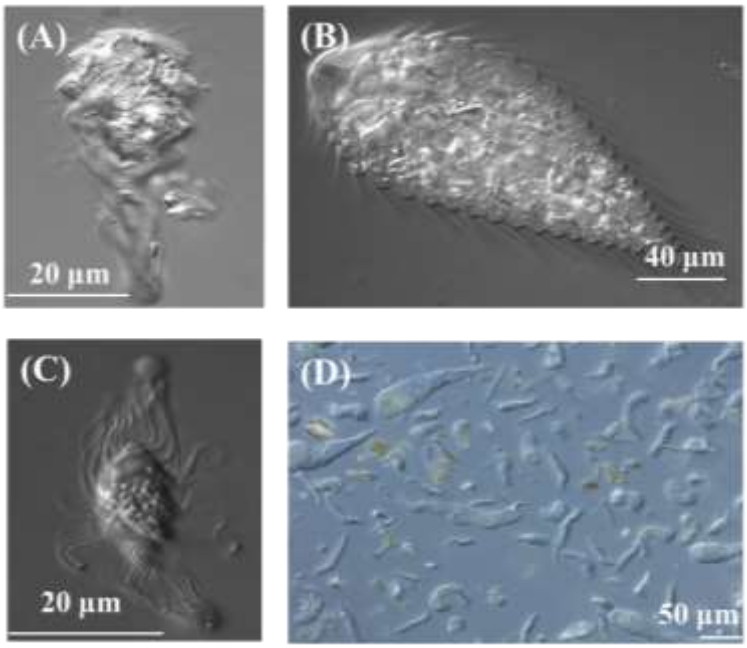

Figure 6.1. Example protists present in a termite. A-C are differential interference contrast (DIC) micrographs of various protists; specifically, A) *Pyrsonympha* (Phylum Preaxostyla) B) *Teranympha* (Phylum Parabasalia) C) *Holomastigotes* (Phylum Parabasalia). D) is a DIC light micrograph of the hindgut contents of *Reticulitermes tibialis* depicting the variety of shapes and sizes of protists present. The hindgut contents are diluted 100 times. All images are courtesy of Dr. Gillian Gile.

The relationship between the parabasalids and their hosts is intriguing for many reasons. It is apparent on a broad scale that there has been co-evolution of the wood-digesting parabasalids across termite species, where in some cases parabasalid families are restricted to specific termite families. Parabasalids can also co-speciate with their hosts, which is the case for *Pseudotrichonympha* and its Rhinotermitidae hosts.[6, 7] Although, in many cases there are incongruities between the phylogenies of the termites and parabasalids.[4, 5, 8] Furthermore, the evolutionary development that lead to the wood-digesting capability in the termite-protist symbiosis is an intriguing aspect.[9, 10] Some theories to explain the evolutionary dynamics in this symbiotic relationship include: 1) parabasalids are evolving faster than their hosts 2) resource partitioning or new symbioses with bacteria are driving speciation 3) transfer of the parabasalids

between termite species results in speciation-by-isolation relative to the host. Previous works have demonstrated that parabasalids are capable of surviving in distantly related host termites, however in nature lateral symbiont transfer has not been directly observed.[6, 11] Furthermore, additional previous work has focused on the composition of the hindgut community for a specific termite or the phylogenetic affinity of particular parabasalids.[12, 13] While, both of these approaches look at different aspects of the symbiosis, neither provides insight on its evolutionary dynamics.

To enable a better understanding of the termite-parabasalid symbiosis and their evolutionary dynamics of speciation and transmission, a rapid method for characterizing the parabasalids present in a termite's hindgut is necessary. Currently, to determine the number of protist species in a termite's hindgut and their phylogenetic position, cells are manually isolated for morphological and molecular characterization, which is extremely time consuming and subject to human bias. This is made even more difficult as the protists are anaerobes, and once removed from a termite's hindgut will deform within 10 minutes to 3 hours. These factors make sequestering hundreds of parabasalids on a large scale impractical. The development of a dielectrophoretic (DEP) microfluidic device capable of isolating the various protists present in a termite's hindgut in mere minutes would enable comparative genomics studies of the protists to better understand their evolution and wood-digestion capability. However, an insulator-based dielectrophoretic (iDEP) trapping device capable of working with samples from tens to hundreds of microns has yet to be developed. The focus of this work is to develop and fabricate a device capable of separating and isolating the various protists present in the hindgut of a termite.

6.2 DEP Trapping Conditions for Protists

To start developing a device capable of trapping protists present in the hindgut of termites, the channel parameters necessary to achieve trapping must be assessed. As is outlined in Chapter 2 of this dissertation the dielectrophoretic trapping condition (*TC*) can be mathematically described as:

$$\frac{\nabla|\vec{E}|^2}{E^2} \cdot \vec{E} \geq \frac{\mu_{EK}}{\mu_{DEP}} \tag{1}$$

When the field characteristics, left side of equation 1, are greater than or equal to the intrinsic analyte properties, right side of equation 1, trapping of the analyte of interest will occur. The electrokinetic and dielectrophoretic mobilities, μ_{EK} and μ_{DEP}, can be defined by the following equations:

$$\mu_{EK} = \frac{-\varepsilon_m(\zeta_m - \zeta_p)}{\eta} \tag{2}$$

$$\mu_{DEP} = \frac{\varepsilon_m r^2 f_{CM}}{3\eta} \tag{3}$$

where ε_m represent the media permittivity, r is the radius of the analyte, ζ is the zeta potential of the media (*m*) or particle (*p*), and η is the solution viscosity. Measurements of the μ_{EK} have previously been reported between 9.0 $\times 10^{-9}$ and $2.0 \times 10^{-8} \frac{m^2}{Vs}$. [14, 15] An approximate μ_{DEP} and *TC* for various analyte radii were estimated with the following assumptions: $\mu_{EK} = 2.8 \times 10^{-8} \frac{m^2}{Vs}$, : $\varepsilon_m = 1.0 \times 10^{-8} \frac{F}{m}$, f_{CM}= - 0.3, and $\eta = 1.0 \times 10^{-3} \frac{Ns}{m^2}$ (Table 6.1). [16] It should be noted that these values only serve as an approximation based on the size of the analyte. This approximation does not account for several other factors including, but not limited to, the effect of various suspending buffers, the

conductivity of the analyte versus surrounding medium, etc. However, it serves as an initial starting point for device prototyping, which can later be refined.

Analyte Radius (μm)	Dielectrophoretic Mobility, $\mu_{DEP}\ \left(\frac{m^4}{Vs}\right)$	Ratio of Mobilities, $\frac{\mu_{EK}}{\mu_{DEP}}\ \left(\frac{V}{m^2}\right)$
1.0	1.0×10^{-18}	2.8×10^{10}
10	1.0×10^{-16}	2.8×10^{8}
50	2.5×10^{-15}	1.1×10^{7}
100	1.0×10^{-14}	2.8×10^{6}
150	2.3×10^{-14}	1.2×10^{6}
200	4.0×10^{-14}	7.0×10^{5}
250	6.3×10^{-14}	4.5×10^{5}
300	9.0×10^{-14}	3.1×10^{5}

Table 6.1. Approximate dielectrophoretic mobility and ratio of mobilities for particles based on their size.

Based on the approximate *TC*s in Table 6.1. a prototype microchannel was designed to isolate and separate protists from approximately 5 to 200 μm in size. Several different geometries were designed, and the distribution of the electric field was modeled using finite element software (COMSOL Multiphysics). The specifics of modeling parameters are described in Chapter 5 and Appendix B of this dissertation. Based on the fabrication limitations that are discussed in section 6.3 a gradient-iDEP (g-iDEP) microdevice was designed to have five different gates sizes which range from 220 to 750 μm, where each gate size was repeated twice (Figure 6.2.). This allows for the simultaneous sequestration of up to six different analytes, where five would be trapped at the various gates and one would be able to flow freely through the microdevice. However, the need for collection of analytes post trapping must be addressed. Current,

iDEP devices designed for trapping have used various channel and reservoirs designs for the collection of trapped analytes, but in all of these cases the channels or reservoirs are present only before or after the insulating features.[14, 16-26] Meaning that extraction of the trapped analytes could be difficult to impossible without dilution and/or mixing of the various analytes back together. Most of these systems can achieve a bipurification, where one analyte is trapped and the other flows through the microchannel. For g-iDEP the various analytes can be separated but removing the analytes from the system is challenging.

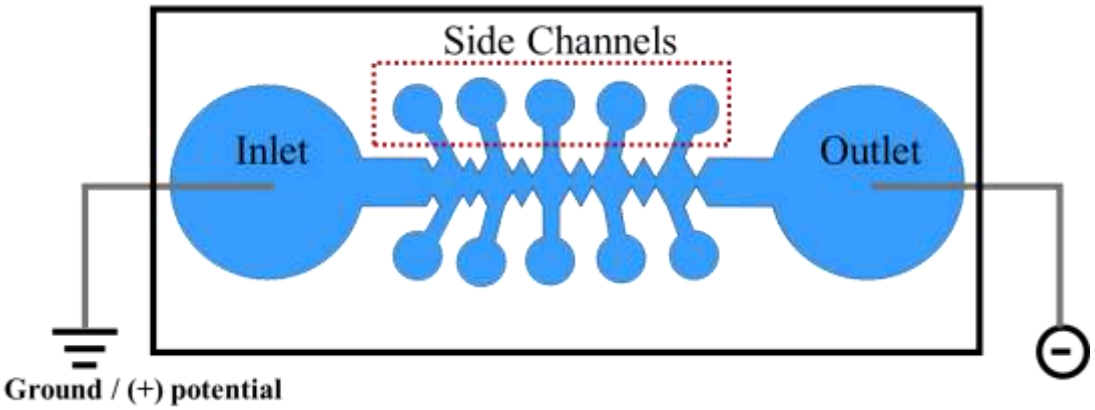

Figure 6.2. Schematic representation of a microdevice design for the separation of protists that reside in a termite's hindgut. The white space is representative of the insulating material that makes up the microchannel. The blue space represents the microchannel. The inlet reservoir is where the sample of interest is introduced to the microdevice. A potential is applied across the device, allowing for sample to travel from inlet to outlet in the main channel. Constrictions for dielectrophoretic trapping are depicted by the triangular insulators. Dielectrophoretic trapping of the analyte's can occur at the various constrictions in the microdevice, based on the analytes unique biophysical properties. Smaller side reservoirs (red box), which are connected to the main channel, are included to allow for the recovery of trapped species. The constrictions, made up by the triangular insulators, vary from 220 μm to 750 μm, where the constriction size is duplicated, before and after each of the side channels.

To allow for easy removal of the various trapped analytes, side channels were introduced between the similarly sized gates (Figure 6.2.) With an applied potential the various protists will be transported by electrokinetic effects from inlet to outlet.

Depending upon the applied potential, which will alter the trapping conditions throughout the microchannel, the various analytes can be trapped at different gates in the microchannel. Once the separation is complete the potential applied to the microdevice can be altered so that potential is applied to the smaller side channels resulting in the trapped analytes being sequestered in the smaller side reservoirs (Figure 6.3.). It may be necessary when performing separation experiments to apply a low applied potential to the side channels. This will repel analytes from the side channels, ensuring they stay in the main channel for potential separation.

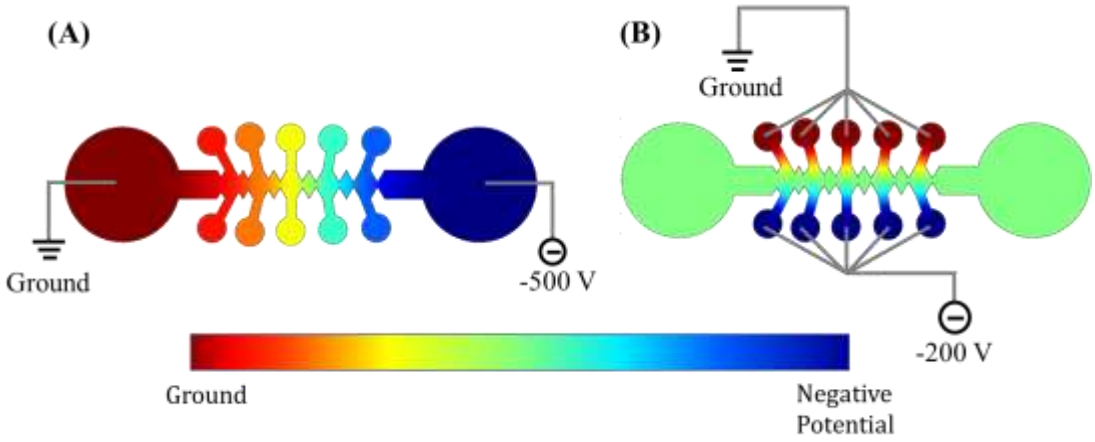

Figure 6.3. Mathematical model of the distribution of the electric field in the microdevice based on where potential is applied. All analytes of interest in this model would be assumed to travel toward a negative potential. A) Depicts the application of potential to allow for separation of microparticles using dielectrophoretic trapping. B) Trapped analytes can be removed from the microchannel by applying potential to the side channels, resulting in the sequestered analytes traveling to reservoirs respective to their gate size.

The *TC* within the microchannel was also modelled using finite element software, to ensure that the various sized protists would trap at desired locations in the microchannel. Initial device designs were modeled depicting the *TC* along the centerline and the gate size was adjusted to achieve the desired conditions (Table 6.1), which

resulted in the microchannel depicted in this chapter. A 2D representation of a specific trapping ratio, $\frac{\mu_{EK}}{\mu_{DEP}} = 5.7 \times 10^8 \frac{V}{m^2}$, was also modeled (Figure 6.4.).

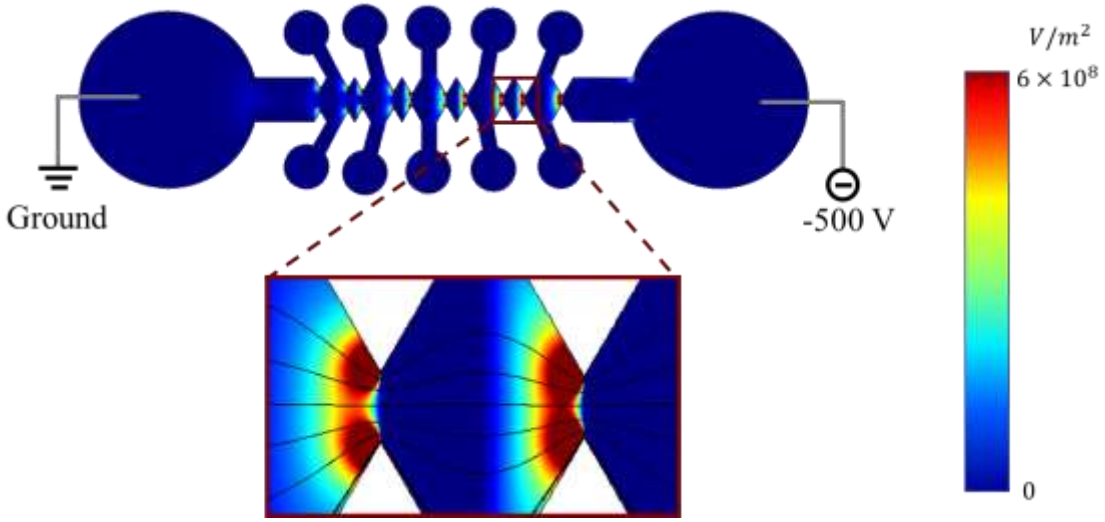

Figure 6.4. Mathematical model of trapping conditions in the microdevice. The red coloring in the model is representative of a trapping ratio consistent with the following ratio of mobilities, $\frac{\mu_{EK}}{\mu_{DEP}} = 5.7 \times 10^8 \frac{V}{m^2}$. The two gates depicted from left to right are 250 µm and 220 µm. The black lines represent the electric field lines, which can be approximated as particle pathlines. For the left gate, as the red coloring does not stretch across the entire width of the channel, analytes with the aforementioned ratio of mobilities will continue in the microdevice. Whereas the right gate achieves the desired ratio across the entire microchannel, which will result in dielectrophoretic trapping of analytes with the aforementioned ratio.

The close-up image in Figure 6.4. depicts the previously defined trapping ratio, red color, at the last two gate sizes in the microchannel, 250 and 220 µm, respectively. The trapping ratio does not cover the entire width of the microchannel at the left, 250 µm, gate, so analytes with intrinsic particle properties matching this ratio will continue in the microchannel. Whereas at the right gate, 220 µm, the trapping ratio stretches across the entire microchannel, resulting in the sequestration of analytes with the defined *TC*.

6.3 Fabrication Strategies

A microchannel capable of interrogating protists would need a greater depth than currently utilized iDEP systems. This falls outside the limits of many traditional methods of fabrication via photolithography. It should be noted the negative photoresist SU-8 can be used to fabricate microstructures up to 450 μm in depth.[27, 28] However, negative photoresists are not utilized in the readily accessible cleanroom. Therefore, other fabrication possibilities capable of achieving features in the desired size range were considered. Specifically, laser ablation and 3D printing can be used to make a microfluidic device or a master template for use with soft lithographic strategies.

6.3.1 3D Printing

The process of making three-dimensional (3D) object by additive manufacturing, layer-by-layer, using precise control is commonly referred to as 3D printing. For the creation of microfluidic devices there are three commonly utilized techniques: fused deposition modeling (FDM), multi jet modeling (MJM), and stereolithography (SLA).

FDM utilizes nozzles to deposit thermoplastic material onto a substrate going point-to-point and then adding layers.[29-31] This method has been further developed such that 3D structures can be printed with “inks” that do not require a thermal processing step, known as direct ink writing (DIW).[32, 33] Many of the commercially available desktop do-it-yourself 3D printers utilize the FDM technique. FDM printed objects are known to have low structural strength as the adjacent layers are not fused together well; this results in weak seals which is not ideal for microchannel applications.[31] Furthermore, FDM typically uses filaments that are larger than common channel dimensions.[31] In a study by MacDonald et al. looking at the accuracy and precision of 3D printed objects with FDM

printing that uses a ~300 µm-wide extrusion nozzle there was ~600 µm peak-to-peak surface abnormalities. This increases the surface area for laminar flow and can result in unintended mixing.[30, 34] While FDM prints can be done quickly the loss in feature resolution and size limitations can be prohibitive for applications in microfluidic manufacturing.[30]

In contrast to FDM, MJM utilizes multiple parallel microscale inkjets to deposit microdroplets of photopolymer/photoplastic materials in a line-by-line, layer-by-layer process, where continual UV photocuring produces the 3D objects. MJM can print several materials simultaneously, including a sacrificial support layer, which can be removed with post-processing procedures. This has enabled the creation of the most complex geometries of any additive manufacturing method.[30, 31] Advantages of MJM technologies include print speed, geometric versatility, multi-material integration, and build volumes. However, a limited number of proprietary materials are available, many of which are not biocompatible. [30, 31, 35, 36] Improvements to biocompatibility have been made by preventing leaching of cytotoxic monomers into fluids.[30] Another complexity of MJM is the need for sacrificial support materials to make internal voids during the 3D printing process, which results in the need for time-consuming post processing. Removal of this sacrificial layer can be sped up by the introduction of additional ports. Furthermore, in many cases the sacrificial layer is water-soluble, and therefore its removal is diffusion limited, which significantly lengthens the time for post processing.[30, 31]

Stereolithography takes a different approach to 3D printing where the 3D object is built by exposing a liquid-phase photo-curable polymer. Specifically, a bath of liquid-phase photoreactive material is photocured by a focused light, building the 3D object point-by-

point, layer-by-layer.[30, 31] Both UV and LED light sources are used with SLA.[37] 3D objected printed using SLA have been proven to be more reliably and accurately replicated and have lower surface roughness when compared to FDM and MJM. This has led to SLA being the predominant method used by researchers for complete microfluidic systems.[30] The minimum feature size of SLA depends on the absorption spectra of the photoresin and the laser spot size.[38] An extension of SLA is Direct Laser Writing (DLW) where two-photon absorption is used for spatially-controlled photopolymerization at a single point in space. This method has achieved the highest resolution for 3D printing, enabling prints down to the 100 nm range.[32] One consideration for SLA structures is that they need to be entirely self-supporting or have incorporated support structures, which may need to be removed once the print is complete; however this is not always easy or feasible.[30] For the 3D printed objects presented in this chapter a SLA 3D printer was used.

6.3.2 Laser Micromachining

Laser micromachining results in the selective removal of material when exposed to short and ultrashort laser pulses. A wide variety of both solid and gas lasers are used with resulting wavelengths ranging from the mid-infrared to the deep ultraviolet.[39] Laser ablation is one of the most commonly utilized methods for micromachining, although laser cutting and drilling are also prevalent. [39]

Laser ablation is a common method of making microfluidic channels. Ablation of material occurs when the fluence of the laser, the optical energy delivered per unit area, exceeds ablation threshold of the material.[39, 40] The ablation threshold and mechanism of a given material are affected by properties of both the material and laser. Specifically, the material properties, absorption mechanism, and presence of defects combined with the

wavelength, pulse duration, and fluence of the laser all have an effect on the ablation of a given material.[39, 40] The ablation of material happens at low fluences when evaporation and sublimation occur by photothermal mechanisms; whereas at high laser fluence normal boiling occurs which results from heterogenous nucleation of vapor bubbles.[39, 40]

The development of ultrafast lasers in the last few decades has resulting in their use for micromachining. Ultrafast lasers have nano- to atto-seconds pulses, which characteristically result in high peak intensities and interact with materials on a time scale faster than lattice disorder and heat diffusion. The result is that materials can very precisely be controlled and manipulated.[39, 40] The use of these instruments is growing as they become more user- and cost- friendly[40], however the cost can still be prohibitive and are they are not always readily accessible.[41, 42]

In comparison standard-grade CO_2 laser ablation systems are relatively inexpensive and commercially available. Epilog Laser, Universal Laser Systems, and Teledyne CETAC Technologies all make commercially available laser ablation systems which CO_2 lasers that operate in the mid infrared range.[39, 42] For CO_2 lasers the minimum feature size possible is determined by the focusing optics which control the beam shape.[43] Microfluidic devices have been fabricated using CO_2 lasers from serval different materials including PDMS[44], PMMA[45-49], paper[50, 51], and glass[42]. The wide array of possible materials, rapid fabrication for prototypes, and a readily accessible system resulted in several prototype templates for this project.

6.4 Microfluidic Templates

Prototype microfluidic channels templates were made using laser ablation. Specifically, a Universal Laser Systems VLS 4.60 CO_2 60W (10.6 μm) laser with a 2.0”

lens (Scottsdale, AZ) was used for prototyping devices. The laser spot size when all the optics are clean and aligned is approximately 130 µm; this was taken to be the absolute minimum feature size. In reality, the minimum feature size is dependent on the material and the laser parameters; meaning that to ensure that multiple materials and methods could be used 200 µm was used as the minimum feature size. Even with this imposed size limitation the desired ratio of mobilities could be achieved for dielectrophoretic trapping (Figure 6.4 and Table 6.1).

A wide variety of methods and materials were utilized to create the templates. Various material and thicknesses of polyester (1.9 and 0.82 mm), polymethyl methacrylate (PMMA) (1.56, 17.1 mm), and a glass microscope slide were all tested. Depending upon the material various approaches of manipulating the material were utilized. In all cases the laser system has preset recommended settings depending on the material to either cut (vector) or ablate (raster) the material, however these do not necessarily result in the desired microchannel depth of 500 µm. There are three readily adjustable parameters for the laser which will affect the overall depth and resolution of the product; they are the percent of laser power, percent of full speed, and the laser pulses per inch (ppi), which maxes out at 1000. Changing the laser power affects how much material is ablated, however this also depends on the speed as the faster the laser moves the less energy is delivered to a specific location on the material. This is all affected by the ppi, as with fewer pulses less material is ablated and less heat is transferred, with a higher ppi pulses more material is ablated, however the likelihood of melting or burning the material increases. This is a common issue previously seen, which results in issues bonding microfluidic devices.[42, 46] One method of optimizing this process was to do multiple passes of the same design, to limit

the undesired effects. Glass, most commonly soda lime, is known to be extremely difficult to work with for laser ablation due to a significant coefficient of thermal expansion and low thermal conductivity. This leads to low quality microdevices and/or cracking of the glass. [42]

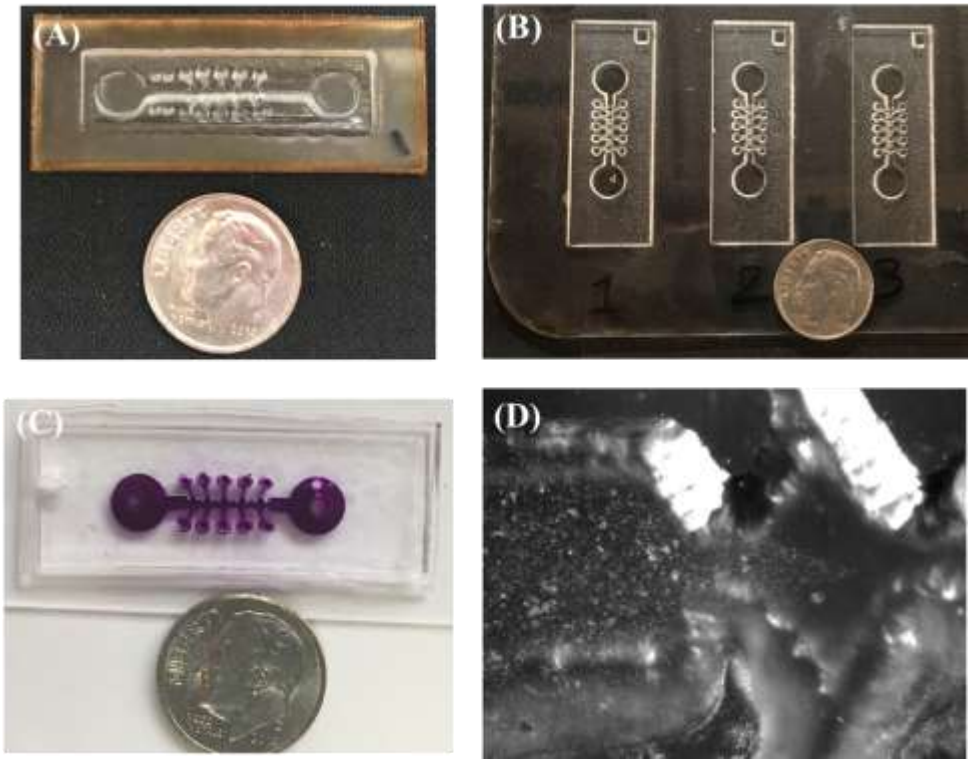

Figure 6.5. Prototype large scale microfluidic devices. A) and B) represent microfluidic molds in A) 0.76 mm polyester and B) 3.0 mm PMMA. The gate sizes range from 750 to 220 µm. C) The resulting microfluidic device from the mold in B) were the channel was sealed to partially cured PDMS made at a ratio of 16:1 elastomer to hardener. The channel is filled with Crystal Violet for easy visualization. Specific parameters of the device can be found in the text. D) Brightfield micrograph of the whole gut content filling the larger DEP device.

When working with the polyester, issues with the heat from the laser warping the plastic were common (Figure 6.5.). Furthermore, the ablation of the polyester resulted in a wavy texture to the material; which is not ideal as the integrity of the microchannel is not upheld and bonding the microchannels can be difficult due to a build-up of ablated material

at the edges. With standard glass slides a few challenges became apparent as ablating to a 500 µm depth would not be easy, and the desired resolution of the microfeatures would not be achievable without serious modifications to the process. Channels templates ablated in PMMA resulted in better defined features, however the issue of waviness from the ablation process persisted, and issues with inconsistencies in the microstructures became apparent with close inspection.

Preliminary work to create a template by 3D printing for use with soft lithography was also pursued. Specifically, a Form 1+ 3D Printer (Form Labs, Somerville, MA) was used. A completed template was not achieved due to adhesion problems between the cured resin and the build platform. Further complications were experienced when the 3D printed template was not completed during the print due to issues with the resin. Due to time and cost constraints no further testing of the 3D printed devices was pursued.

6.5 Preliminary Experimental Work

Preliminary tests were done with smaller microchannels similar to those used the rest of this dissertation[16-18, 52] to ensure the common buffer solutions used with protists, Ringer's solution (8.5 g NaCl, 0.20 g KCl, 0.20 g $CaCl_2$, $NaHCO_3$ per liter, HiMedia Laboratories) or Trager U saline solution [53], were compatible with PDMS microchannels. For both solutions the application of voltage did not result in PDMS break down or bubble formation in the microchannel with the applied potentials necessary for separation.

Soft lithographic strategies were implemented with the PMMA template, made by laser ablation, to create PDMS microfluidic devices for preliminary testing (Figure 6.5). A 3 mm punch was used on the main inlet and outlet reservoirs, while a smaller 1.5 mm punch

was used for the side channel reservoirs. The PDMS casts were kept in a freezer prior to use.

As the face of the channel which needed to be bonded to make a complete microfluidic device was not entirely flat, due to the undesirable effects from laser ablation, partially cured PDMS was used to complete the device. Specifically, a 16:1 ratio of elastomer to hardener was used instead of the normal 10:1 ratio. The mixture was poured over a clean blank silicon wafer and left to sit on the lab bench for 10 minutes and was then transferred to a 70°C oven. After approximately 20 minutes small pieces of cured PDMS were used to test if they sank in the PDMS or adhered to the surface. In the case that the small PDMS piece sank, the PDMS was left in the oven to cure further. When the small PDMS piece adhered to the surface without sinking the PDMS channel mold was then adhered to the surface. This was done to complete the microdevice and ensure that the height of the channels was consistent between devices. The completed microdevice was then left in the oven for approximately 40 more minutes, at which point the microdevice was removed from the silicon wafer.

Various approaches to fill the microchannel were tested. The optimum method involved treating the device with oxygen plasma and then preliminarily filling the microdevice with approximately 100 μL of 18 MΩ water. To ensure the complete microdevice was filled, solution was added first to the inlet reservoir, then the outlet reservoirs, and finally to all the side channel reservoirs. This resulted in a rapid fill of the device with no undesirable remaining air pockets. Once, the complete microdevice had been filled, the 18 MΩ water was removed, and the channel was filled with either Ringer's or Trager U. Preliminary trials with the contents of a termite's hindgut suspended in

Ringer's were performed. The application of voltage resulted in flow of protists in the microchannel, however the concentration of protists was extremely high. Furthermore, electrolysis at both the inlet and outlet resulting in bubble formation throughout the microchannel and potentials above 150 V resulted in currents exceeding those which the power supply could provide. Potential ridges in the PDMS and incompletely formed insulating features resulting from laser ablation of the template molds may contribute to some of the challenges. Furthermore, both Trager's U and Ringer's solution have a much higher salt concentration, and therefore conductivity, than currently utilized buffers. This will contribute to issues with electrolysis, bubble formation, and high currents.

6.6 Potential Future Improvements

To overcome some of the challenges that have arisen from experimentation, there are several potential options. For laser ablation, making the devices using a glass slide that is coated with wax has been proven.[42] The wax coating prevents cracking and breaking of the slide while still achieving the desired channel features. Another option would be to change the laser ablation system which is being utilized. A lower powered laser, such as a 30 W (9.3 μm) CO_2 laser would significantly reduce heating effects resulting in higher resolution templates. Furthermore, when working with laser ablation to ensure the best quality before every template is made the focus of the laser, cleanliness of optics, and airflow around the laser should be checked. Poor air flow can result in ablated material collecting on the optics or material resulting in lower resolution products. Additionally, when setting up the parameters for ablation, the frame raster could be altered, to shift how quickly the laser ablates a given area. Using the same power level for frame rastering is desirable for triangular insulators as it ensures that the material is given a time to cool

before more ablation occurs. However, altering this parameter in the future could be advantageous when refining the ablation process.

The option of 3D printing to make the master templates or completed microdevices can also be pursued. To improve upon past results where a completed template was not achieved there are several options. In order for the print to adhere to the build platform, ensuring a level unscratched platform is important. Replacing the build platform may improve issues with the prints not adhering. Another option would be to coat the build platform in polydimethylsiloxane (PDMS), to ensure a level surface, and allow for easy removal of the print.[31] To improve the features that are printed as desired the resin basin should be checked for small pieces of cured resin from previous prints. This can be done by either replacing the resin or using a fine-tooth comb to remove them should result in a successfully printed 3D object. By implementing these adjustments to the fabrication process a template or completed microdevice should be achievable for the separation of the protists present in the hindgut of a termite.

6.7 References

[1] Nalepa, C. A., *Ecological Entomology* 2015, *40*, 323-335.

[2] Cleveland, L. R., *The Biological Bulletin* 1925, *48*, 309-[326]-301.

[3] Ware, J. L., Grimaldi, D. A., Engel, M. S., *Arthropod Structure & Development* 2010, *39*, 204-219.

[4] Bourguignon, T., Lo, N., Cameron, S. L., Šobotník, J., Hayashi, Y., Shigenobu, S., Watanabe, D., Roisin, Y., Miura, T., Evans, T. A., *Molecular Biology and Evolution* 2015, *32*, 406-421.

[5] Noda, S., Mantini, C., Meloni, D., Inoue, J.-I., Kitade, O., Viscogliosi, E., Ohkuma, M., *PLOS ONE* 2012, *7*, e29938.

[6] Kitade, O., *Microbes and Environments* 2004, *19*, 215-220.

[7] Noda, S., Kitade, O., Inoue, T., Kawai, M., Kanuka, M., Hiroshima, K., Hongoh, Y., Constantino, R., Uys, V., Zhong, J., Kudo, T., Ohkuma, M., *Molecular Ecology* 2007, *16*, 1257-1266.

[8] Yamin, M. A., *Sociobiology* 1979, 4:3-117.

[9] Inward, D., Beccaloni, G., Eggleton, P., *Biology Letters* 2007, *3*, 331-335.

[10] Gile, G. H., Slamovits, C. H., *Protist* 2012, *163*, 274-283.

[11] Light, S., Sanford, M., *University of California Publications in Zoology* 1928, *31*, 269-274.

[12] Gerbod, D., Edgcomb, V. P., Noël, C., Delgado-Viscogliosi, P., Viscogliosi, E., *International microbiology : the official journal of the Spanish Society for Microbiology* 2000, *3*, 165-172.

[13] Saldarriaga, J. F., Gile, G. H., James, E. R., HorÁK, A., Scheffrahn, R. H., Keeling, P. J., *Journal of Eukaryotic Microbiology* 2011, *58*, 487-496.

[14] Jones, P. V., DeMichele, A. F., Kemp, L., Hayes, M. A., *Analytical and Bioanalytical Chemistry* 2014, *406*, 183-192.

[15] Crowther, C. V., Hilton, S. H., Kemp, L., Hayes, M. A., *Analytica Chimica Acta* 2018, In Submission.

[16] Crowther, C. V., Hayes, M. A., *Analyst* 2017, *142*, 1608-1618.

[17] Jones, P. V., Staton, S. J. R., Hayes, M. A., *Analytical and Bioanalytical Chemistry* 2011, *401*, 2103-2111.

[18] Jones, P. V., Hilton, S. H., Davis, P. E., Yanashima, R., McLemore, R., McLaren, A., Hayes, M. A., *Analyst* 2015, *140*, 5152-5161.

[19] Abdallah, B. G., Chao, T.-C., Kupitz, C., Fromme, P., Ros, A., *ACS Nano* 2013, *7*, 9129-9137.

[20] Luo, J., Abdallah, B. G., Wolken, G. G., Arriaga, E. A., Ros, A., *Biomicrofluidics* 2014, *8*, 021801.

[21] Nakano, A., Camacho-Alanis, F., Ros, A., *Analyst* 2015, *140*, 860-868.

[22] LaLonde, A., Gencoglu, A., Romero-Creel, M. F., Koppula, K. S., Lapizco-Encinas, B. H., *Journal of Chromatography A* 2014, *1344*, 99-108.

[23] Lapizco-Encinas, B. H., Simmons, B. A., Cummings, E. B., Fintschenko, Y., *Electrophoresis* 2004, *25*, 1695-1704.

[24] Saucedo-Espinosa, M. A., Lapizco-Encinas, B. H., *Electrophoresis* 2015, *36*, 1086-1097.

[25] Saucedo-Espinosa, M. A., LaLonde, A., Gencoglu, A., Romero-Creel, M. F., Dolas, J. R., Lapizco-Encinas, B. H., *Electrophoresis* 2016, *37*, 282-290.

[26] Ding, J., Woolley, C., Hayes, M. A., *Analytical and Bioanalytical Chemistry* 2017, *409*, 6405-6414.

[27] Leester-Schadel, M., Lorenz, T., Jurgens, F., Richter, C., in: Dietzel, A. (Ed.), *Microsystems for Pharmatechnology*, Springer 2016, pp. 23-57.

[28] Lorenz, H., Despont, M., Fahrni, N., LaBianca, N., Renaud, P., Vettiger, P., *Journal of Micromechanics and Microengineering* 1997, *7*, 121.

[29] Crump, S. S., Stratasys Inc 1992.

[30] Sochol, R. D., Sweet, E., Glick, C. C., Wu, S.-Y., Yang, C., Restaino, M., Lin, L., *Microelectronic Engineering* 2018, *189*, 52-68.

[31] Bhattacharjee, N., Urrios, A., Kang, S., Folch, A., *Lab on a Chip* 2016, *16*, 1720-1742.

[32] Lewis, J. A., *Advanced Functional Materials* 2006, *16*, 2193-2204.

[33] Gratson, G. M., Xu, M., Lewis, J. A., *Nature* 2004, *428*, 386.

[34] Macdonald, N. P., Cabot, J. M., Smejkal, P., Guijt, R. M., Paull, B., Breadmore, M. C., *Analytical Chemistry* 2017, *89*, 3858-3866.

[35] Au, A. K., Huynh, W., Horowitz, L. F., Folch, A., *Angewandte Chemie International Edition* 2016, *55*, 3862-3881.

[36] Walczak, R., Adamski, K., *Journal of Micromechanics and Microengineering* 2015, *25*, 085013.

[37] Waldbaur, A., Rapp, H., Länge, K., Rapp, B. E., *Analytical Methods* 2011, *3*, 2681-2716.

[38] Fang, N., Sun, C., Zhang, X., *Applied Physics A* 2004, *79*, 1839-1842.

[39] Mishra, S., Yadava, V., *Optics and Lasers in Engineering* 2015, *73*, 89-122.

[40] Phillips, K. C., Gandhi, H. H., Mazur, E., Sundaram, S. K., *Advances in Optics and Photonics* 2015, *7*, 684-712.

[41] Nisar, S., Li, L., Sheikh, M., *Laser Glass Cutting Techniques - A Review*, 2013.

[42] da Costa, E. T., Santos, M. F. S., Jiao, H., do Lago, C. L., Gutz, I. G. R., Garcia, C. D., *Electrophoresis* 2016, *37*, 1691-1695.

[43] Fiorini, G. S., Chiu, D. T., *BioTechniques* 2005, *38*, 429-446.

[44] Fogarty, B. A., Heppert, K. E., Cory, T. J., Hulbutta, K. R., Martin, R. S., Lunte, S. M., *Analyst* 2005, *130*, 924-930.

[45] Hong, T.-F., Ju, W.-J., Wu, M.-C., Tai, C.-H., Tsai, C.-H., Fu, L.-M., *Microfluidics and Nanofluidics* 2010, *9*, 1125-1133.

[46] Gabriel, E. F. M., Coltro, W. K. T., Garcia, C. D., *Electrophoresis* 2014, *35*.

[47] Mazher, I. M. a. M. N. H. Z. A. a. A. K. a. I. G., *Journal of Micromechanics and Microengineering* 2017, *27*, 015021.

[48] Jensen, M. F., Noerholm, M., Christensen, L. H., Geschke, O., *Lab on a Chip* 2003, *3*, 302-307.

[49] Snakenborg, D., Klank, H., Kutter, J., *Journal of Micromechanics and Microengineering* 2004, *14*, 182.

[50] Evans, E., Gabriel, E. F. M., Benavidez, T. E., Coltro, W. K. T., Garcia, C. D., *The Analyst* 2014, *139*, 5560-5567.

[51] Evans, E., Gabriel, E. F. M., Coltro, W. K. T., Garcia, C. D., *The Analyst* 2014, *139*, 2127-2132.

[52] Ding, J., Lawrence, R. M., Jones, P. V., Hogue, B. G., Hayes, M. A., *Analyst* 2016, *141*, 1997-2008.

[53] Trager, W., *The Biological Bulletin* 1934, *66*, 182-190.

CHAPTER 7

SUMMARY AND CONCLUSIONS

7.1 Biological Analytics Utilizing Dielectrophoresis

Since Pohl first described dielectrophoresis (DEP) in the 1950s the field has quickly grown. Early applications focused on electrode-based systems (eDEP) for manipulation of particles of interest. While eDEP stands as a pillar for DEP research and is still used today, the limitations and challenges that eDEP faces for certain applications are numerable. In the early 2000s the field of insulator-based DEP (iDEP) was established to address some of the limitations of eDEP and several potential applications of iDEP have since been implemented. Insulator-based systems excel in comparison to eDEP systems for their inexpensive nature, ease of fabrication, and inherent ability to limit the electrochemical reactions between solutions and the electrodes. These systems have been established as a method to manipulate and interrogate a wide variety of analytes, including, but not limited to, cancer cells, proteins, bacteria, and viruses.

The introduction of gradient iDEP (g-iDEP) enabled the investigation of multi-analyte separations. DEP is exploited, in the case of g-iDEP, to achieve rapid and high-resolution separations where the analytes of interest are both isolated and concentrated. The technique stands out for its potential to rapidly and accurately separate extremely similar bioparticles. Furthermore, insight into the biophysical properties of the analytes can be assessed based on the behavior of the analytes in the microchannels. This dissertation demonstrates some of the unique capabilities and potential applications of iDEP and g-iDEP systems for both detection and interrogation of a wide range of analytes. The possibility of quickly gathering the epidemiology of the different serovars

of *Listeria monocytogenes* and incorporating a data model to assess biophysical properties are explored in Chapter 3. The ability to detect changes to the surface chemistry of *E. coli* was measured and resulted in a better understanding of how surface modifications can affect the biophysical make-up of bacterial cells (Chapter 4). To enable high-resolution separations and address some of the challenges of current insulators a novel insulator design was developed and tested (Chapter 5). In Chapter 6, the scope of applications for trapping iDEP was expanded by developing a device capable of assessing larger analytes (10-250 μm).

7.2 Future Directions

The potential ability for iDEP to revolutionize methods of separation and interrogation of analytes stands as an exciting prospect for the future of science. The ability to achieve rapid, high-resolution, and inexpensive analyses of various samples opens the door to a wide array of possibilities. In order to take iDEP systems to the next level there are several challenges which need to be addressed.

In the case of separations, a high-throughput system may be desirable for the rapid isolation of several analytes, or the processing of large volumes. One strategy to overcome this hurdle would be to develop a system with several microchannels; where the channels can be run sequentially or in parallel. In both cases pneumatic valves may be incorporated to section off various parts of the system as is deemed necessary. The development and refinement of pneumatic valves for use in microfluidic systems has recently been pursued by several research groups. Sequential channels may be desirable to sequester many different analytes of interest while parallel channels may enable the processing of larger volumes. The combination of these strategies may also be beneficial

as the ability to sequester many analytes from large sample volumes is desirable. In all cases fine-tuning of the microchannels can be done with several different strategies including, but not limited to, alterations of the channel design(s), variations in surface coating(s), or altering the applied potential (both AC vs DC and overall magnitude/frequency).

Another potential method for processing larger volume of samples would be to develop 3D insulators, such that instead of extruding the plane of a 2D geometry to achieve the third dimension the 2D geometry would be rotated around a central axis to achieve a column-type channel (Figure 7.1.); similar in shape to some nanopores. Three dimensional designs (Figure 7.1. right), on the same length scale as those currently utilized for iDEP, would be extremely complicated or impossible to make using traditional photolithography techniques. However, the rise and accuracy of 3D printing has enabled the fabrication of structures such as this.

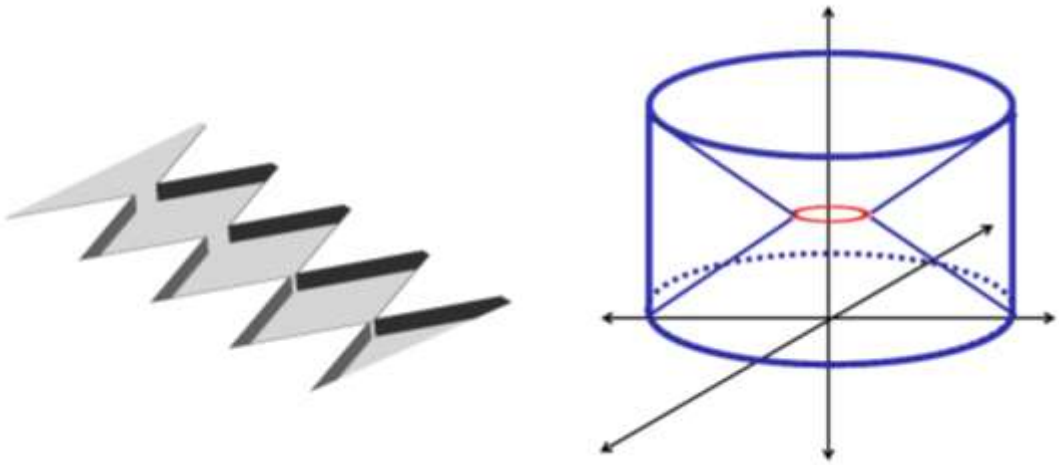

Figure 7.1. Channel designs for iDEP. The left schematic represents the current extrusion of a 2D plane while the right schematic depicts the equivalent of a singular constriction (red oval) in a 3D column channel.

The design of a microfluidic channel and the optimum insulator design comes with several challenges, many of which were addressed in Chapter 5. Specifically, as the fields of iDEP and g-iDEP continue to grow various insulator shapes may be desirable for different applications. Several factors come into play when designing insulators including limitations of the fabrication method, the ability to achieve the desired DEP forces, and limiting the effects of both the heterogenous electric fields and dispersive effects. Another consideration which needs to be addressed is the removal of analytes from the system after the DEP analysis is complete. This idea is introduced in Chapter 6, where the side channels are introduced between gates to allow for removal of trapped analytes. Another option would be to introduce side channels perpendicular to the channel, which would allow for the removal of trapped analytes, while not requiring the separation of the gates from each other. Furthermore, multiplexing the device, such that it can perform several techniques is desirable for a totally self-contained system. Several preliminary steps have been taken towards achieving this goal; although there are still engineering hurdles that need to be overcome to create these devices. The field has been rapidly expanding and improving current techniques, resulting in more accurate and precise designs. This has resulted in the fabrication limitations of even a few years ago are being rapidly surpassed.

A further understanding of how different biophysical properties affect dielectrophoretic trapping is introduced in Chapters 3 and 4, where a combination of finite-element modeling and various analysis techniques are utilized to determine both the electrokinetic and dielectrophoretic mobilities. The data model introduced in Chapter 3 describes some of the various factors which effect trapping, however there is a need to

delve further into how specific biophysical properties, such as the deformability and polarizability, affect trapping behavior.

This work lays the foundation for using iDEP and g-iDEP for biological analyses of a wide variety of samples. There are still many potential applications for this work which may benefit the scientific community. Some examples that come to mind include using iDEP to quantify the amount of protein in a cell without the need to lyse the cell; for example, this could be done with green fluorescent protein at different points in of cell growth. Another application would be to use this system to sequester desired analytes from complex real-world samples.

7.3 Scientific Outlook

The work presented in this dissertation delves into some of the many possibilities for utilizing DEP for biological analytics. The implications for this work are far reaching, because of this technique's unique ability to isolate and concentrate analytes while probing their biophysical properties. Rapid, portable, and cost-effective analysis of a wide variety of nano- and micro- particles becomes a reality through this technique. The potential for applications across the biological realm is only touched upon in this dissertation. A portable simplistic test capable of rapidly identifying pathogenic bacteria, while simultaneously collecting epidemiological information about the analytes is easily envisioned. This application alone would revolutionize both the food and health care industries. The ability to quickly assess and separate analytes based on their unique properties could enable a myriad of novel scientific pursuits.

REFERENCES

CHAPTER 1

[1] Raven, P., Johnson, G., Mason, K., Losos, J., Singer, S., *Biology*, McGraw Hill Education 2017.

[2] Fleming, A., *British journal of experimental pathology* 1929, *10*, 226-236.

[3] Willyard, C., *Nature* 2017, *543*, 15.

[4] Watson, J. D., Crick, F. H. C., *Nature* 1953, *171*, 737-738.

[5] Liu, X., Zhang, F., Jing, X., Pan, M., Liu, P., Li, W., Zhu, B., Li, J., Chen, H., Wang, L., Lin, J., Liu, Y., Zhao, D., Yan, H., Fan, C., *Nature* 2018, *559*, 593-598.

[6] Yager, P., Edwards, T., Fu, E., Helton, K., Nelson, K., Tam, M. R., Weigl, B. H., *Nature* 2006, *442*, 412.

[7] Toner, M., Irimia, D., *Annual Review of Biomedical Engineering* 2005, *7*, 77-103.

[8] Ho, C. M. B., Ng, S. H., Li, K. H. H., Yoon, Y.-J., *Lab on a Chip* 2015, *15*, 3627-3637.

[9] *Difco & BBL Manual: Manual of Microbiological Culture Media*, BD Diagnostics, Sparks, MD 2009.

[10] Palumbo, J. D., Borucki, M. K., Mandrell, R. E., Gorski, L., *Journal of Clinical Microbiology* 2003, *41*, 564-571.

[11] Doumith, M., Buchrieser, C., Glaser, P., Jacquet, C., Martin, P., *Journal of Clinical Microbiology* 2004, *42*, 3819-3822.

[12] Ng, P. C., Kirkness, E. F., in: Barnes, M. R., Breen, G. (Eds.), *Genetic Variation: Methods and Protocols*, Humana Press, Totowa, NJ 2010, pp. 215-226.

[13] Barbuddhe, S. B., Maier, T., Schwarz, G., Kostrzewa, M., Hof, H., Domann, E., Chakraborty, T., Hain, T., *Applied and Environmental Microbiology* 2008, *74*, 5402.

[14] Jadhav, S., Sevior, D., Bhave, M., Palombo, E. A., *Journal of Proteomics* 2014, *97*, 100-106.

[15] Heck, A. J. R., *Nature Methods* 2008, *5*, 927.

[16] Belgrader, P., Benett, W., Hadley, D., Richards, J., Stratton, P., Mariella, R., Milanovich, F., *Science* 1999, *284*, 449.

[17] Whitesides, G. M., *Nature* 2006, *442*, 368.

[18] Squires, T. M., Quake, S. R., *Reviews of Modern Physics* 2005, *77*, 977-1026.

[19] Sackmann, E. K., Fulton, A. L., Beebe, D. J., *Nature* 2014, *507*, 181.

[20] Bhagat, A. A. S., Bow, H., Hou, H. W., Tan, S. J., Han, J., Lim, C. T., *Medical & Biological Engineering & Computing* 2010, *48*, 999-1014.

[21] Sibbitts, J., Sellens, K. A., Jia, S., Klasner, S. A., Culbertson, C. T., *Analytical Chemistry* 2018, *90*, 65-85.

[22] Roper, M. G., *Analytical Chemistry* 2016, *88*, 381-394.

[23] Dittrich, P. S., Manz, A., *Nature Reviews Drug Discovery* 2006, *5*, 210.

[24] Abdallah, B. G., Chao, T.-C., Kupitz, C., Fromme, P., Ros, A., *ACS Nano* 2013, *7*, 9129-9137.

[25] Srivastava, S. K., Baylon-Cardiel, J. L., Lapizco-Encinas, B. H., Minerick, A. R., *Journal of Chromatography A* 2011, *1218*, 1780-1789.

[26] Subramanian, S., Tolstaya, E. I., Winkler, T. E., Bentley, W. E., Ghodssi, R., *ACS Applied Materials & Interfaces* 2017, *9*, 31362-31371.

[27] Martin, W. E., Ge, N., Srijanto, B. R., Furnish, E., Collier, C. P., Trinkle, C. A., Richards, C. I., *ACS Omega* 2017, *2*, 3858-3867.

[28] Li, L., Zhang, Y., Zhang, L., Ge, S., Liu, H., Ren, N., Yan, M., Yu, J., *Analytical Chemistry* 2016, *88*, 5369-5377.

[29] Son, K. J., Rahimian, A., Shin, D.-S., Siltanen, C., Patel, T., Revzin, A., *Analyst* 2016, *141*, 679-688.

[30] Stone, H. A., Kim, S., *AIChE Journal* 2004, *47*, 1250-1254.

[31] Jones, P. V., Hayes, M. A., *Electrophoresis* 2015, *36*, 1098-1106.

[32] Jones, P. V., DeMichele, A. F., Kemp, L., Hayes, M. A., *Analytical and Bioanalytical Chemistry* 2014, *406*, 183-192.

[33] Jones, P. V., Hilton, S. H., Davis, P. E., Yanashima, R., McLemore, R., McLaren, A., Hayes, M. A., *Analyst* 2015, *140*, 5152-5161.

[34] Johari, J., Hübner, Y., Hull, J. C., Dale, J. W., Hughes, M. P., *Physics in Medicine and Biology* 2003, *48*, N193.

[35] Labeed, F. H., Coley, H. M., Thomas, H., Hughes, M. P., *Biophysical Journal* 2003, *85*, 2028-2034.

[36] Braff, W. A., Willner, D., Hugenholtz, P., Rabaey, K., Buie, C. R., *PloS one* 2013, *8*, e76751.

[37] Lapizco-Encinas, B. H., Simmons, B. A., Cummings, E. B., Fintschenko, Y., *Analytical Chemistry* 2004, *76*, 1571-1579.

[38] LaLonde, A., Romero-Creel, M. F., Lapizco-Encinas, B. H., *Electrophoresis* 2015, *36*, 1479-1484.

[39] Wang, M. M., Tu, E., Raymond, D. E., Yang, J. M., Zhang, H. C., Hagen, N., Dees, B., Mercer, E. M., Forster, A. H., Kariv, I., Marchand, P. J., Butler, W. F., *Nature Biotechnology* 2005, *23*, 83-87.

[40] Bhattacharya, S., Chao, T.-C., Ariyasinghe, N., Ruiz, Y., Lake, D., Ros, R., Ros, A., *Analytical and Bioanalytical Chemistry* 2014, *406*, 1855-1865.

[41] Luo, J., Abdallah, B. G., Wolken, G. G., Arriaga, E. A., Ros, A., *Biomicrofluidics* 2014, *8*, 021801.

[42] Ding, J., Woolley, C., Hayes, M. A., *Analytical and Bioanalytical Chemistry* 2017, *409*, 6405-6414.

[43] Srivastava, S. K., Artemiou, A., Minerick, A. R., *Electrophoresis* 2011, *32*, 2530-2540.

[44] Hughes, M. P., Morgan, H., Rixon, F. J., Burt, J. P. H., Pethig, R., *Biochimica et Biophysica Acta (BBA) - General Subjects* 1998, *1425*, 119-126.

[45] Ding, J., Lawrence, R. M., Jones, P. V., Hogue, B. G., Hayes, M. A., *Analyst* 2016, *141*, 1997-2008.

[46] Gallo-Villanueva, R. C., Rodríguez-López, C. E., Díaz-de-la-Garza, R. I., Reyes-Betanzo, C., Lapizco-Encinas, B. H., *Electrophoresis* 2009, *30*, 4195-4205.

[47] Martinez-Duarte, R., Camacho-Alanis, F., Renaud, P., Ros, A., *Electrophoresis* 2013, *34*, 1113-1122.

[48] Swami, N., Chou, C.-F., Ramamurthy, V., Chaurey, V., *Lab on a Chip* 2009, *9*, 3212-3220.

[49] Gan, L., Chao, T.-C., Camacho-Alanis, F., Ros, A., *Analytical Chemistry* 2013, *85*, 11427-11434.

[50] Nakano, A., Camacho-Alanis, F., Ros, A., *Analyst* 2015, *140*, 860-868.

[51] Lapizco-Encinas, B. H., Ozuna-Chacón, S., Rito-Palomares, M., *Journal of Chromatography A* 2008, *1206*, 45-51.

CHAPTER 2

[1] Ohanian, H. C., Markert, J. T., *Physics for Engineers and Scientists*, W. W. Norton & Company, New York 2007.

[2] Pohl, H. A., *Dielectrophoresis : the behavior of neutral matter in nonuniform electric fields*, Cambridge University Press, Cambridge; New York 1978.

[3] Kirby, B. J., *Micro-and nanoscale fluid mechanics: transport in microfluidic devices*, Cambridge University Press 2010.

[4] Ren, X., Bachman, M., Sims, C., Li, G. P., Allbritton, N., *J. Chromatogr. B* 2001, *762*, 117-125.

[5] Kleinstreuer, C., *Microfluidics and nanofluidics : theory and selected applications*, Hoboken, New Jersey : Wiley 2014.

[6] Probstein, R. F., *Physicochemical Hydrodynamics: An Introduction*, John Wiley & Sons, Inc. 1994, pp. 1-8.

[7] von Smoluchowski, M., *Elektrische endosmose und stromungsstrome. In Handbuch der Elektrizitat und des Magnetimus*, Leipzig 1914.

[8] Jones, T. B., *Electromechanics of Particles*, Cambridge University Press 1995.

[9] Pohl, H. A., *Journal of Applied Physics* 1951, *22*, 869-871.

[10] Clarke, R. W., Piper, J. D., Ying, L., Klenerman, D., *Physical Review Letters* 2007, *98*, 198102.

[11] Pethig, R., *Biomicrofluidics* 2010, *4*, 022811.

[12] Cummings, E. B., Singh, A. K., *Analytical Chemistry* 2003, *75*, 4724-4731.

[13] Cummings, E. B., *Engineering in Medicine and Biology Magazine, IEEE* 2003, *22*, 75-84.

[14] Lapizco-Encinas, B. H., Simmons, B. A., Cummings, E. B., Fintschenko, Y., *Analytical Chemistry* 2004, *76*, 1571-1579.

[15] Jones, P. V., Staton, S. J. R., Hayes, M. A., *Analytical and Bioanalytical Chemistry* 2011, *401*, 2103-2111.

[16] Abdallah, B. G., Chao, T.-C., Kupitz, C., Fromme, P., Ros, A., *ACS Nano* 2013, *7*, 9129-9137.

[17] Saucedo-Espinosa, M. A., Lapizco-Encinas, B. H., *Electrophoresis* 2015, *36*, 1086-1097.

[18] Abdallah, B. G., Roy-Chowdhury, S., Coe, J., Fromme, P., Ros, A., *Analytical Chemistry* 2015, *87*, 4159-4167.

[19] Baylon-Cardiel, J. L., Lapizco-Encinas, B. H., Reyes-Betanzo, C., Chavez-Santoscoy, A. V., Martinez-Chapa, S. O., *Lab on a Chip* 2009, *9*, 2896-2901.

[20] Srivastava, S. K., Baylon-Cardiel, J. L., Lapizco-Encinas, B. H., Minerick, A. R., *Journal of Chromatography A* 2011, *1218*, 1780-1789.

[21] LaLonde, A., Gencoglu, A., Romero-Creel, M. F., Koppula, K. S., Lapizco-Encinas, B. H., *Journal of Chromatography A* 2014, *1344*, 99-108.

[22] Jones, P. V., Hilton, S. H., Davis, P. E., Yanashima, R., McLemore, R., McLaren, A., Hayes, M. A., *Analyst* 2015, *140*, 5152-5161.

[23] Kwon, J.-S., Maeng, J.-S., Chun, M.-S., Song, S., *Microfluidics and Nanofluidics* 2008, *5*, 23-31.

[24] Crowther, C. V., Hayes, M. A., *Analyst* 2017, *142*, 1608-1618.

[25] Lapizco-Encinas, B. H., Simmons, B. A., Cummings, E. B., Fintschenko, Y., *Electrophoresis* 2004, *25*, 1695-1704.

[26] Pohi, H. A., Hawk, I., *Science* 1966, *152*, 647-649.

[27] Crane, J. S., Pohl, H. A., *Journal of The Electrochemical Society* 1968, *115*, 584-586.

[28] Pohl, H. A., Crane, J. S., *Biophysical Journal* 1971, *11*, 711-727.

[29] Golan, S., Elata, D., Orenstein, M., Dinnar, U., *Electrophoresis* 2006, *27*, 4919-4926.

[30] Chaurey, V., Polanco, C., Chou, C.-F., Swami, N. S., *Biomicrofluidics* 2012, *6*, 012806.

[31] Price, J. A. R., Burt, J. P. H., Pethig, R., *Biochimica et Biophysica Acta (BBA) - General Subjects* 1988, *964*, 221-230.

[32] Huang, Y., Pethig, R., *Measurement Science and Technology* 1991, *2*, 1142.

[33] Pethig, R., Huang, Y., Wang, X.-b., Burt, J. P. H., *Journal of Physics D: Applied Physics* 1992, *25*, 881.

[34] Washizu, M., Kurosawa, O., *Industry Applications, IEEE Transactions on* 1990, *26*, 1165-1172.

[35] Washizu, M., Nanba, T., Masuda, S., *Industry Applications, IEEE Transactions on* 1990, *26*, 352-358.

[36] Hoettges, K. F., Hughes, M. P., Cotton, A., Hopkins, N. A. E., McDonnell, M. B., *Engineering in Medicine and Biology Magazine, IEEE* 2003, *22*, 68-74.

[37] Gonzalez, C. F., Remcho, V. T., *Journal of Chromatography A* 2009, *1216*, 9063-9070.

[38] Martinez-Duarte, R., Camacho-Alanis, F., Renaud, P., Ros, A., *Electrophoresis* 2013, *34*, 1113-1122.

[39] Hughes, M. P., Morgan, H., *Analytical Chemistry* 1999, *71*, 3441-3445.

[40] Labeed, F. H., Coley, H. M., Thomas, H., Hughes, M. P., *Biophysical Journal* 2003, *85*, 2028-2034.

[41] Hughes, M. P., Morgan, H., Rixon, F. J., Burt, J. P. H., Pethig, R., *Biochimica et Biophysica Acta (BBA) - General Subjects* 1998, *1425*, 119-126.

[42] Johari, J., Hübner, Y., Hull, J. C., Dale, J. W., Hughes, M. P., *Physics in Medicine and Biology* 2003, *48*, N193.

[43] Chou, C.-F., Tegenfeldt, J. O., Bakajin, O., Chan, S. S., Cox, E. C., Darnton, N., Duke, T., Austin, R. H., *Biophysical Journal* 2002, *83*, 2170-2179.

[44] Srivastava, S., Gencoglu, A., Minerick, A., *Analytical and Bioanalytical Chemistry* 2011, *399*, 301-321.

[45] Hsiao, F.-B., Jen, C.-P., Chen, H.-Y., Hsu, H.-L., Lee, Y.-C., Chuang, C.-H., Wang, C.-H., IEEE 2008, pp. 951-954.

[46] Chen, K. P., Pacheco, J. R., Hayes, M. A., Staton, S. J. R., *Electrophoresis* 2009, *30*, 1441-1448.

[47] Gencoglu, A., Minerick, A., *Lab on a Chip* 2009, *9*, 1866-1873.

[48] Masuda, S., Washizu, M., Nanba, T., *Industry Applications, IEEE Transactions on* 1989, *25*, 732-737.

[49] Staton, S. J. R., Chen, K. P., Taylor, J. P., Pacheco, J. R., Hayes, M. A., *Electrophoresis* 2010, *31*, 3634-3641.

[50] Luo, J., Abdallah, B. G., Wolken, G. G., Arriaga, E. A., Ros, A., *Biomicrofluidics* 2014, *8*, 021801.

[51] Nakano, A., Ros, A., *Electrophoresis* 2013, *34*, 1085-1096.

[52] Nakano, A., Camacho-Alanis, F., Ros, A., *Analyst* 2015, *140*, 860-868.

[53] Staton, S. J. R., Jones, P. V., Ku, G., Gilman, S. D., Kheterpal, I., Hayes, M. A., *Analyst* 2012, *137*, 3227-3229.

[54] Regtmeier, J., Duong, T. T., Eichhorn, R., Anselmetti, D., Ros, A., *Analytical Chemistry* 2007, *79*, 3925-3932.

[55] Jones, P. V., DeMichele, A. F., Kemp, L., Hayes, M. A., *Analytical and Bioanalytical Chemistry* 2014, *406*, 183-192.

[56] Zhu, J., Tzeng, T.-R., Hu, G., Xuan, X., *Microfluidics and Nanofluidics* 2009, *7*, 751-756.

[57] Barbulovic-Nad, I., Xuan, X., Lee, J. S. H., Li, D., *Lab on a Chip* 2006, *6*, 274-279.

[58] Thwar, P. K., Linderman, J. J., Burns, M. A., *Electrophoresis* 2007, *28*, 4572-4581.

[59] Kang, K. H., Kang, Y., Xuan, X., Li, D., *Electrophoresis* 2006, *27*, 694-702.

[60] Kang, Y., Li, D., Kalams, S., Eid, J., *Biomedical Microdevices* 2008, *10*, 243-249.

[61] Ozuna-Chacón, S., Lapizco-Encinas, B. H., Rito-Palomares, M., Martínez-Chapa, S. O., Reyes-Betanzo, C., *Electrophoresis* 2008, *29*, 3115-3122.

[62] Pysher, M. D., Hayes, M. A., *Analytical Chemistry* 2007, *79*, 4552-4557.

[63] Jones, P., Staton, S. R., Hayes, M., *Analytical and Bioanalytical Chemistry* 2011, *401*, 2103-2111.

[64] Perez-Gonzalez, V. H., Gallo-Villanueva, R. C., Cardenas-Benitez, B., Martinez-Chapa, S. O., Lapizco-Encinas, B. H., *Analytical Chemistry* 2018, *90*, 4310-4315.

[65] Braff, W. A., Willner, D., Hugenholtz, P., Rabaey, K., Buie, C. R., *PloS one* 2013, *8*, e76751.

[66] Jones, P. V., Hayes, M. A., *Electrophoresis* 2015, *36*, 1098-1106.

[67] Staton, S. J. R., Chen, K. P., Taylor, T. J., Pacheco, J. R., Hayes, M. A., *Electrophoresis* 2010, *31*, 3634-3641.

[68] Ding, J., Woolley, C., Hayes, M. A., *Analytical and Bioanalytical Chemistry* 2017, *409*, 6405-6414.

[69] Becker, H., Locascio, L. E., *Talanta* 2002, *56*, 267-287.

[70] Leester-Schadel, M., Lorenz, T., Jurgens, F., Richter, C., in: Dietzel, A. (Ed.), *Microsystems for Pharmatechnology*, Springer 2016, pp. 23-57.

[71] McDonald, J. C., Duffy, D. C., Anderson, J. R., Chiu, D. T., Wu, H., Schueller, O. J. A., Whitesides, G. M., *Electrophoresis* 1999, *21*, 27-40.

[72] Xia, Y., Whitesides, G. M., *Annual Review of Materials Science* 1998, *28*, 153-184.

[73] Sochol, R. D., Sweet, E., Glick, C. C., Wu, S.-Y., Yang, C., Restaino, M., Lin, L., *Microelectronic Engineering* 2018, *189*, 52-68.

[74] Lucas, N., Demming, S., Jordan, A., Sichler, P., S., B., *Journal of Micromechanics and Microengineering* 2008, *18*, 075037.

[75] Toepke, M. W., Beebe, D. J., *Lab on a Chip* 2006, *6*, 1484-1486.

[76] Lorenz, H., Despont, M., Fahrni, N., LaBianca, N., Renaud, P., Vettiger, P., *Journal of Micromechanics and Microengineering* 1997, *7*, 121.

[77] da Costa, E. T., Santos, M. F. S., Jiao, H., do Lago, C. L., Gutz, I. G. R., Garcia, C. D., *Electrophoresis* 2016, *37*, 1691-1695.

[78] Dingley, J., in: Photo-Tools, J. (Ed.), JD Photo-Tools 2014, pp. 1-89.

[79] AZ Electronic Materials: AZ® 3300 Series Crossover Photoresists 2005.

[80] Mack, C., *Fundamental principles of optical lithography: the science of microfabrication*, John Wiley & Sons 2008.

[81] Bhardwaj, J., Ashraf, H., McQuarrie, A., *Proc. Symp. Microstructures and Microfabricated Systems, ECS* 1997.

CHAPTER 3

[1] Scallan, E., Hoekstra, R. M., Angulo, F. J., Tauxe, R. V., Widdowson, M.-A., Roy, S. L., Jones, J. L., Griffin, P. M., *Emerging Infectious Diseases* 2011, *17*, 7-15.

[2] Scallan, E., Griffin, P. M., Angulo, F. J., Tauxe, R. V., Hoekstra, R. M., *Emerging Infectious Diseases* 2011, *17*, 16.

[3] Ramaswamy, V., Cresence, V., Rejitha, J., Lekshmi, M., Dharsana, K., Prasad, S., Vijila, H., in: Ramaswamy, V. (Ed.) 2007, pp. 4-13.

[4] Goulet, V., King, L. A., Vaillant, V., de Valk, H., *BMC Infectious Diseases* 2013, *13*, 11.

[5] Jackson, B. R., Tarr, C., Strain, E., Jackson, K. A., Conrad, A., Carleton, H., Katz, L. S., Stroika, S., Gould, L. H., Mody, R. K., Silk, B. J., Beal, J., Chen, Y., Timme, R., Doyle, M., Fields, A., Wise, M., Tillman, G., Defibaugh-Chavez, S., Kucerova, Z., Sabol, A., Roache, K., Trees, E., Simmons, M., Wasilenko, J., Kubota, K., Pouseele, H., Klimke, W., Besser, J., Brown, E., Allard, M., Gerner-Smidt, P., *Clinical Infectious Diseases* 2016, *63*, 380-386.

[6] Ward, T. J., Gorski, L., Borucki, M. K., Mandrell, R. E., Hutchins, J., Pupedis, K., *Journal of Bacteriology* 2004, *186*, 4994-5002.

[7] Muñoz, P., Rojas, L., Bunsow, E., Saez, E., Sánchez-Cambronero, L., Alcalá, L., Rodríguez-Creixems, M., Bouza, E., *Journal of Infection*, *64*, 19-33.

[8] Bergholz, T. M., Shah, M. K., Burall, L. S., Rakic-Martinez, M., Datta, A. R., *Applied Microbiology and Biotechnology* 2018, *102*, 3475-3485.

[9] Rebuffo-Scheer, C. A., Schmitt, J., Scherer, S., *Applied and Environmental Microbiology* 2007, *73*, 1036.

[10] Borucki, M. K., Call, D. R., *Journal of Clinical Microbiology* 2003, *41*, 5537-5540.

[11] Seeliger, H. P. R., Höhne, K., in: Bergan, T., Norris, J. R. (Eds.), *Methods in Microbiology*, Academic Press 1979, pp. 31-49.

[12] Doumith, M., Buchrieser, C., Glaser, P., Jacquet, C., Martin, P., *Journal of Clinical Microbiology* 2004, *42*, 3819-3822.

[13] Bergholz, T. M., den Bakker, H. C., Katz, L. S., Silk, B. J., Jackson, K. A., Kucerova, Z., Joesph, L. A., Turnsek, M., Gladney, L. M., Halpin, J. L., Xavier, K., Gossack, J., Ward, T. J., Frace, M., Tarr, C. L., *Applied and Environmental Microbiology* 2016, *82*, 928-938.

[14] Jadhav, S., Bhave, M., Palombo, E. A., *Journal of Microbiological Methods* 2012, *88*, 327-341.

[15] Ronholm, J., Nasheri, N., Petronella, N., Pagotto, F., *Clinical Microbiology Reviews* 2016, *29*, 837-857.

[16] *Listeria, Listeriosis and Food Safety*, CRC Press, Boca Raton 2007.

[17] Timeline for Linking a Case of Listeria Infection to an Outbreak, in: H.S.S.-C.D.C. Prevention, 2016.

[18] Graves, L. M., Swaminathan, B., *International Journal of Food Microbiology* 2001, *65*, 55-62.

[19] Buchrieser, C., Brosch, R., Catimel, B., Rocourt, J., *Canadian Journal of Microbiology* 1993, *39*, 395-401.

[20] Gilmour, M. W., Graham, M., Van Domselaar, G., Tyler, S., Kent, H., Trout-Yakel, K. M., Larios, O., Allen, V., Lee, B., Nadon, C., *BMC Genomics* 2010, *11*, 120-120.

[21] Carp-Cărare, C., Vlad-Sabie, A., Florişţean, V.-C., *Romanian Review of Laboratory Medicine* 2013, p. 285.

[22] Liu, D., *Journal of Medical Microbiology* 2006, *55*, 6 45-659

[23] Seeliger, H. P. R., Langer, B., *International Journal of Food Microbiology* 1989, *8*, 245-248.

[24] Palumbo, J. D., Borucki, M. K., Mandrell, R. E., Gorski, L., *Journal of Clinical Microbiology* 2003, *41*, 564-571.

[25] D'Urso, O. F., Poltronieri, P., Marsigliante, S., Storelli, C., Hernández, M., Rodríguez-Lázaro, D., *Food Microbiology* 2009, *26*, 311-316.

[26] Chen, Y., Knabel, S. J., *Applied and Environmental Microbiology* 2007, *73*, 6299-6304.

[27] Kérouanton, A., Marault, M., Petit, L., Grout, J., Dao, T. T., Brisabois, A., *Journal of Microbiological Methods* 2010, *80*, 134-137.

[28] Jadhav, S., Sevior, D., Bhave, M., Palombo, E. A., *Journal of Proteomics* 2014, *97*, 100-106.

[29] Jadhav, S., Gulati, V., Fox, E. M., Karpe, A., Beale, D. J., Sevior, D., Bhave, M., Palombo, E. A., *International Journal of Food Microbiology* 2015, *202*, 1-9.

[30] Barbuddhe, S. B., Maier, T., Schwarz, G., Kostrzewa, M., Hof, H., Domann, E., Chakraborty, T., Hain, T., *Applied and Environmental Microbiology* 2008, *74*, 5402.

[31] Dingley, J., in: Photo-Tools, J. (Ed.), JD Photo-Tools 2014, pp. 1-89.

[32] Jones, P., Staton, S. R., Hayes, M., *Analytical and Bioanalytical Chemistry* 2011, *401*, 2103-2111.

[33] Jones, P. V., Hayes, M. A., *Electrophoresis* 2015, *36*, 1098-1106.

[34] Li, M., Li, W. H., Zhang, J., Alici, G., Wen, W., *Journal of Physics D: Applied Physics* 2014, *47*, 063001.

[35] LaLonde, A., Romero-Creel, M. F., Lapizco-Encinas, B. H., *Electrophoresis* 2015, *36*, 1479-1484.

[36] Labeed, F. H., Coley, H. M., Thomas, H., Hughes, M. P., *Biophysical Journal* 2003, *85*, 2028-2034.

[37] Perez-Gonzalez, V. H., Gallo-Villanueva, R. C., Cardenas-Benitez, B., Martinez-Chapa, S. O., Lapizco-Encinas, B. H., *Analytical Chemistry* 2018, *90*, 4310-4315.

[38] Luo, J., Abdallah, B. G., Wolken, G. G., Arriaga, E. A., Ros, A., *Biomicrofluidics* 2014, *8*, 021801.

[39] Su, Y.-H., Tsegaye, M., Varhue, W., Liao, K.-T., Abebe, L. S., Smith, J. A., Guerrant, R. L., Swami, N. S., *Analyst* 2014, *139*, 66-73.

[40] Swami, N., Chou, C.-F., Ramamurthy, V., Chaurey, V., *Lab on a Chip* 2009, *9*, 3212-3220.

[41] Pohl, H. A., *Journal of Applied Physics* 1951, *22*, 869-871.

[42] Hughes, M. P., Morgan, H., Rixon, F. J., Burt, J. P. H., Pethig, R., *Biochimica et Biophysica Acta (BBA) - General Subjects* 1998, *1425*, 119-126.

[43] Morgan, H., Hughes, M. P., Green, N. G., *Biophysical Journal*, *77*, 516-525.

[44] Mogi, K., Shirataki, C., Kihara, K., Kuwahara, H., Hongoh, Y., Yamamoto, T., *RSC Advances* 2016, *6*, 113000-113006.

[45] Pohl, H. A., Crane, J. S., *Biophysical Journal* 1971, *11*, 711-727.

[46] Chung, C., Pethig, R., Smith, S., Waterfall, M., *Electrophoresis* 2018, *39*, 989-997.

[47] Jones, P. V., DeMichele, A. F., Kemp, L., Hayes, M. A., *Analytical and Bioanalytical Chemistry* 2014, *406*, 183-192.

[48] Jones, P. V., Hilton, S. H., Davis, P. E., Yanashima, R., McLemore, R., McLaren, A., Hayes, M. A., *Analyst* 2015, *140*, 5152-5161.

[49] Chou, C.-F., Tegenfeldt, J. O., Bakajin, O., Chan, S. S., Cox, E. C., Darnton, N., Duke, T., Austin, R. H., *Biophysical Journal* 2002, *83*, 2170-2179.

[50] Abdallah, B. G., Chao, T.-C., Kupitz, C., Fromme, P., Ros, A., *ACS Nano* 2013, *7*, 9129-9137.

[51] Lapizco-Encinas, B. H., Simmons, B. A., Cummings, E. B., Fintschenko, Y., *Analytical Chemistry* 2004, *76*, 1571-1579.

[52] Cummings, E. B., Singh, A. K., *Analytical Chemistry* 2003, *75*, 4724-4731.

[53] Masuda, S., Washizu, M., Nanba, T., *Industry Applications, IEEE Transactions on* 1989, *25*, 732-737.

[54] Jones, P. V., Staton, S. J. R., Hayes, M. A., *Analytical and Bioanalytical Chemistry* 2011, *401*, 2103-2111.

[55] Braff, W. A., Willner, D., Hugenholtz, P., Rabaey, K., Buie, C. R., *PloS one* 2013, *8*, e76751.

[56] Crowther, C. V., Hayes, M. A., *Analyst* 2017, *142*, 1608-1618.

[57] Srivastava, S., Gencoglu, A., Minerick, A., *Analytical and Bioanalytical Chemistry* 2011, *399*, 301-321.

[58] Pohl, H. A., *Dielectrophoresis : the behavior of neutral matter in nonuniform electric fields*, Cambridge University Press, Cambridge; New York 1978.

[59] Pethig, R., *Biomicrofluidics* 2010, *4*, 022811.

[60] Clarke, R. W., Piper, J. D., Ying, L., Klenerman, D., *Physical Review Letters* 2007, *98*, 198102.

[61] Jones, T. B., *Electromechanics of Particles*, Cambridge University Press 1995.

[62] Cummings, E. B., *Engineering in Medicine and Biology Magazine, IEEE* 2003, *22*, 75-84.

[63] Kwon, J.-S., Maeng, J.-S., Chun, M.-S., Song, S., *Microfluidics and Nanofluidics* 2008, *5*, 23-31.

[64] Pysher, M. D., Hayes, M. A., *Analytical Chemistry* 2007, *79*, 4552-4557.

[65] Staton, S. J. R., Chen, K. P., Taylor, T. J., Pacheco, J. R., Hayes, M. A., *Electrophoresis* 2010, *31*, 3634-3641.

[66] Staton, S. J. R., Jones, P. V., Ku, G., Gilman, S. D., Kheterpal, I., Hayes, M. A., *Analyst* 2012, *137*, 3227-3229.

[67] Mack, C., *Fundamental principles of optical lithography: the science of microfabrication*, John Wiley & Sons 2008.

[68] Hilton, S. H., Hayes, M. A., *in preparation* 2018.

[69] Seeliger, H. P. R., Höhne, K., *Methods in Microbiology* 1979, *13*, 31-49.

[70] Schönberg, A., Bannerman, E., Courtieu, A. L., Kiss, R., McLauchlin, J., Shah, S., Wilhelms, D., *International Journal of Food Microbiology* 1996, *32*, 279-287.

[71] Bayer, M. E., Sloyer, J. L., *Journal of General Microbiology* 1990, *136*, 867-874.

[72] Bauer, J., *Journal of Chromatography B: Biomedical Sciences and Applications* 1987, *418*, 359-383.

[73] Mehrishi, J. N., Bauer, J., *Electrophoresis* 2002, *23*, 1984-1994.

[74] Chen, J.-Q., Regan, P., Laksanalamai, P., Healey, S., Hu, Z., *Food Science and Human Wellness* 2017, *6*, 97-120.

[75] Moura, A., Criscuolo, A., Pouseele, H., Maury, M. M., Leclercq, A., Tarr, C., Björkman, J. T., Dallman, T., Reimer, A., Enouf, V., Larsonneur, E., Carleton, H., Bracq-Dieye, H., Katz, L. S., Jones, L., Touchon, M., Tourdjman, M., Walker, M., Stroika, S.,

Cantinelli, T., Chenal-Francisque, V., Kucerova, Z., Rocha, E. P. C., Nadon, C., Grant, K., Nielsen, E. M., Pot, B., Gerner-Smidt, P., Lecuit, M., Brisse, S., *Nature Microbiology* 2016, *2*, 16185.

CHAPTER 4

[1] Ding, J., Woolley, C., Hayes, M. A., *Analytical and Bioanalytical Chemistry* 2017, *409*, 6405-6414.

[2] Jones, P. V., Hilton, S. H., Davis, P. E., Yanashima, R., McLemore, R., McLaren, A., Hayes, M. A., *Analyst* 2015, *140*, 5152-5161.

[3] Hu, X., Bessette, P. H., Qian, J., Meinhart, C. D., Daugherty, P. S., Soh, H. T., *Proceedings of the National Academy of Sciences of the United States of America* 2005, *102*, 15757.

[4] Johari, J., Hübner, Y., Hull, J. C., Dale, J. W., Hughes, M. P., *Physics in Medicine and Biology* 2003, *48*, N193.

[5] Bhagat, A. A. S., Bow, H., Hou, H. W., Tan, S. J., Han, J., Lim, C. T., *Medical & Biological Engineering & Computing* 2010, *48*, 999-1014.

[6] Bauer, J., *Journal of Chromatography B: Biomedical Sciences and Applications* 1987, *418*, 359-383.

[7] Gagnon, Z. R., *Electrophoresis* 2011, *32*, 2466-2487.

[8] Lee, K. H., Lee, K. S., Jung, J. H., Chang, C. B., Sung, H. J., *Applied Physics Letters* 2013, *102*, 141911.

[9] Tomlinson, M. J., Tomlinson, S., Yang, X. B., Kirkham, J., *Journal of Tissue Engineering* 2012, *4*, 2041731412472690.

[10] Roper, M. G., *Analytical Chemistry* 2016, *88*, 381-394.

[11] Sibbitts, J., Sellens, K. A., Jia, S., Klasner, S. A., Culbertson, C. T., *Analytical Chemistry* 2018, *90*, 65-85.

[12] Faraghat, S. A., Hoettges, K. F., Steinbach, M. K., van der Veen, D. R., Brackenbury, W. J., Henslee, E. A., Labeed, F. H., Hughes, M. P., *Proceedings of the National Academy of Sciences* 2017, *114*, 4591.

[13] Elvington, E. S., Salmanzadeh, A., Stremler, M. A., Davalos, R. V., *Journal of Visualized Experiments : JoVE* 2013, 50634.

[14] Pethig, R., *Biomicrofluidics* 2010, *4*, 022811.

[15] Zhu, H. W., Lin, X. G., Su, Y., Dong, H., Wu, J. H., *Biosensors & Bioelectronics* 2015, *63*, 371-378.

[16] Crowley, T. A., Pizziconi, V., *Lab on a Chip* 2005, *5*, 922-929.

[17] Gross, A., Schoendube, J., Zimmermann, S., Steeb, M., Zengerle, R., Koltay, P., *International Journal of Molecular Sciences* 2015, *16*, 16897-16919.

[18] Wang, M. M., Tu, E., Raymond, D. E., Yang, J. M., Zhang, H. C., Hagen, N., Dees, B., Mercer, E. M., Forster, A. H., Kariv, I., Marchand, P. J., Butler, W. F., *Nature Biotechnology* 2005, *23*, 83-87.

[19] Lange, J. R., Metzner, C., Richter, S., Schneider, W., Spermann, M., Kolb, T., Whyte, G., Fabry, B., *Biophysical Journal* 2017, *112*, 1472-1480.

[20] Akagi, T., Ichiki, T., *Analytical and Bioanalytical Chemistry* 2008, *391*, 2433.

[21] Hsu, J.-P., Hsieh, T.-S., Young, T.-H., Tseng, S., *Electrophoresis* 2003, *24*, 1338-1346.

[22] Hilton, S. H., Hayes, M. A., *in preparation* 2018.

[23] Cummings, E. B., Singh, A. K., *Analytical Chemistry* 2003, *75*, 4724-4731.

[24] Jones, P. V., Hayes, M. A., *Electrophoresis* 2015, *36*, 1098-1106.

[25] LaLonde, A., Gencoglu, A., Romero-Creel, M. F., Koppula, K. S., Lapizco-Encinas, B. H., *Journal of Chromatography A* 2014, *1344*, 99-108.

[26] Srivastava, S. K., Baylon-Cardiel, J. L., Lapizco-Encinas, B. H., Minerick, A. R., *Journal of Chromatography A* 2011, *1218*, 1780-1789.

[27] Kim, M., Jung, T., Kim, Y., Lee, C., Woo, K., Seol, J. H., Yang, S., *Biosensors and Bioelectronics* 2015, *74*, 1011-1015.

[28] LaLonde, A., Romero-Creel, M. F., Saucedo-Espinosa, M. A., Lapizco-Encinas, B. H., *Biomicrofluidics* 2015, *9*, 064113.

[29] Han, S.-I., Soo Kim, H., Han, A., *Biosensors and Bioelectronics* 2017, *97*, 41-45.

[30] Chen, X., Liang, Z., Li, D., Xiong, Y., Xiong, P., Guan, Y., Hou, S., Hu, Y., Chen, S., Liu, G., Tian, Y., *Biosensors and Bioelectronics* 2018, *99*, 416-423.

[31] LaLonde, A., Romero-Creel, M. F., Lapizco-Encinas, B. H., *Electrophoresis* 2015, *36*, 1479-1484.

[32] Li, H., Bashir, R., *Sensors and Actuators B: Chemical* 2002, *86*, 215-221.

[33] Gray, D. S., Tan, J. L., Voldman, J., Chen, C. S., *Biosensors and Bioelectronics* 2004, *19*, 1765-1774.

[34] Lapizco-Encinas, B. H., Simmons, B. A., Cummings, E. B., Fintschenko, Y., *Analytical Chemistry* 2004, *76*, 1571-1579.

[35] Chou, C.-F., Tegenfeldt, J. O., Bakajin, O., Chan, S. S., Cox, E. C., Darnton, N., Duke, T., Austin, R. H., *Biophysical Journal* 2002, *83*, 2170-2179.

[36] Jones, P. V., DeMichele, A. F., Kemp, L., Hayes, M. A., *Analytical and Bioanalytical Chemistry* 2014, *406*, 183-192.

[37] Lapizco-Encinas, B. H., Davalos, R. V., Simmons, B. A., Cummings, E. B., Fintschenko, Y., *Journal of Microbiological Methods* 2005, *62*, 317-326.

[38] Braff, W. A., Willner, D., Hugenholtz, P., Rabaey, K., Buie, C. R., *PloS one* 2013, *8*, e76751.

[39] Mehrishi, J. N., Bauer, J., *Electrophoresis* 2002, *23*, 1984-1994.

[40] Wagner, C., Hensel, M., in: Linke, D., Goldman, A. (Eds.), *Bacterial Adhesion: Chemistry, Biology and Physics*, Springer Netherlands, Dordrecht 2011, pp. 17-34.

[41] Mozes, N., Léonard, A., Rouxhet, P. G., *Biochimica et Biophysica Acta (BBA) - Biomembranes* 1988, *945*, 324-334.

[42] Wang, X. B., Huang, Y., Wang, X. J., Becker, F. F., Gascoyne, P. R. C., *Biophysical Journal* 1997, *72*, 1887-1899.

[43] Prescott, L. M. H., J. P.Klein, D.A., *Microbiology*, Wm. C. Brown Publishers, Dubuque, IAA 1996.

[44] Moat, A. G., Foster, J. W., Spector, M. P., *Microbial Physiology*, Wiley-Liss, New, York 2002.

[45] Suehiro, J., Hamada, R., Noutomi, D., Shutou, M., Hara, M., *Journal of Electrostatics* 2003, *57*, 157-168.

[46] Burt, J. P. H., Pethig, R., Gascoyne, P. R. C., Becker, F. F., *Biochimica et Biophysica Acta (BBA) - General Subjects* 1990, *1034*, 93-101.

[47] Sonohara, R., Muramatsu, N., Ohshima, H., Kondo, T., *Biophysical Chemistry* 1995, *55*, 273-277.

[48] Buszewski, B., Szumski, M., Kłodzińska, E., Dahm, H., *Journal of Separation Science* 2003, *26*, 1045-1049.

[49] Torimura, M., Ito, S., Kano, K., Ikeda, T., Esaka, Y., Ueda, T., *Journal of chromatography. B, Biomedical sciences and applications* 1999, *721*, 31-37.

[50] Kłodzińska, E., Szumski, M., Dziubakiewicz, E., Hrynkiewicz, K., Skwarek, E., Janusz, W., Buszewski, B., *Electrophoresis* 2010, *31*, 1590-1596.

[51] Crowther, C. V., Hayes, M. A., *Analyst* 2017, *142*, 1608-1618.

[52] Pohl, H. A., Crane, J. S., *Biophysical Journal* 1971, *11*, 711-727.

[53] Pohl, H. A., *Dielectrophoresis : the behavior of neutral matter in nonuniform electric fields*, Cambridge University Press, Cambridge; New York 1978.

[54] Srivastava, S., Gencoglu, A., Minerick, A., *Analytical and Bioanalytical Chemistry* 2011, *399*, 301-321.

[55] Irimajiri, A., Hanai, T., Inouye, A., *Journal of Theoretical Biology* 1979, *78*, 251-269.

[56] Bai, W., Zhao, K., Asami, K., *Colloids and Surfaces B: Biointerfaces* 2007, *58*, 105-115.

[57] Huang Ji-Ping and Yu Kin-Wah and Lei Jun and Sun, H., *Communications in Theoretical Physics* 2002, *38*, 113.

[58] Huang, J. P., Yu, K. W., Gu, G. Q., Karttunen, M., *Physical Review E* 2003, *67*, 051405.

[59] Jones, T. B., *Electromechanics of Particles*, Cambridge University Press 1995.

[60] Clarke, R. W., Piper, J. D., Ying, L., Klenerman, D., *Physical Review Letters* 2007, *98*, 198102.

[61] Castellarnau, M., Errachid, A., Madrid, C., Juárez, A., Samitier, J., *Biophysical Journal* 2006, *91*, 3937-3945.

[62] Crowther, C. V., Hilton, S. H., Kemp, L., Hayes, M. A., *Analytica Chimica Acta* 2018, In Submission.

[63] Pysher, M. D., Hayes, M. A., *Analytical Chemistry* 2007, *79*, 4552-4557.

[64] Staton, S. J. R., Chen, K. P., Taylor, J. P., Pacheco, J. R., Hayes, M. A., *Electrophoresis* **2010**, *31*, 3634-3641.

[65] Staton, S. J. R., Jones, P. V., Ku, G., Gilman, D. S., Kheterpal, I., Hayes, M. A., *Analyst* 2012, *137*, 3227-3229.

[66] Siegmund, L., Wostemeyer, J., *Understanding bacterial uptake by protozoa: A versatile technique for surface modification of bacteria*, 2016.

[67] Siegmund, L., Schweikert, M., Fischer Martin, S., Wöstemeyer, J., *Journal of Eukaryotic Microbiology* 2018, *0*.

[68] Majorek, K. A., Porebski, P. J., Dayal, A., Zimmerman, M. D., Jablonska, K., Stewart, A. J., Chruszcz, M., Minor, W., *Molecular Immunology* 2012, *52*, 174-182.

[69] Pédelacq, J.-D., Cabantous, S., Tran, T., Terwilliger, T. C., Waldo, G. S., *Nature Biotechnology* 2005, *24*, 79.

[70] Lapizco-Encinas, B. H., Simmons, B. A., Cummings, E. B., Fintschenko, Y., *Electrophoresis* 2004, *25*, 1695-1704.

CHAPTER 5

[1] Jones, P. V., Staton, S. J. R., Hayes, M. A., *Analytical and Bioanalytical Chemistry* 2011, *401*, 2103-2111.

[2] Luo, J., Abdallah, B. G., Wolken, G. G., Arriaga, E. A., Ros, A., *Biomicrofluidics* 2014, *8*, 021801.

[3] Staton, S. J. R., Jones, P. V., Ku, G., Gilman, S. D., Kheterpal, I., Hayes, M. A., *Analyst* 2012, *137*, 3227-3229.

[4] Nakano, A., Camacho-Alanis, F., Ros, A., *Analyst* 2015, *140*, 860-868.

[5] Washizu, M., Kurosawa, O., *Industry Applications, IEEE Transactions on* 1990, *26*, 1165-1172.

[6] Chou, C.-F., Tegenfeldt, J. O., Bakajin, O., Chan, S. S., Cox, E. C., Darnton, N., Duke, T., Austin, R. H., *Biophysical Journal* 2002, *83*, 2170-2179.

[7] Martinez-Duarte, R., Camacho-Alanis, F., Renaud, P., Ros, A., *Electrophoresis* 2013, *34*, 1113-1122.

[8] Jones, P. V., DeMichele, A. F., Kemp, L., Hayes, M. A., *Analytical and Bioanalytical Chemistry* 2014, *406*, 183-192.

[9] Lapizco-Encinas, B. H., Simmons, B. A., Cummings, E. B., Fintschenko, Y., *Analytical Chemistry* 2004, *76*, 1571-1579.

[10] Lapizco-Encinas, B. H., Simmons, B. A., Cummings, E. B., Fintschenko, Y., *Electrophoresis* 2004, *25*, 1695-1704.

[11] Jones, P. V., Hilton, S. H., Davis, P. E., Yanashima, R., McLemore, R., McLaren, A., Hayes, M. A., *Analyst* 2015, *140*, 5152-5161.

[12] Jones, P. V., Hayes, M. A., *Electrophoresis* 2015, *36*, 1098-1106.

[13] Abdallah, B. G., Chao, T.-C., Kupitz, C., Fromme, P., Ros, A., *ACS Nano* 2013, *7*, 9129-9137.

[14] Srivastava, S. K., Baylon-Cardiel, J. L., Lapizco-Encinas, B. H., Minerick, A. R., *Journal of Chromatography A* 2011, *1218*, 1780-1789.

[15] Hughes, M. P., Morgan, H., Rixon, F. J., Burt, J. P. H., Pethig, R., *Biochimica et Biophysica Acta (BBA) - General Subjects* 1998, *1425*, 119-126.

[16] Crane, J. S., Pohl, H. A., *Journal of The Electrochemical Society* 1968, *115*, 584-586.

[17] Pohl, H. A., Crane, J. S., *Biophysical Journal* 1971, *11*, 711-727.

[18] Hoettges, K. F., Hughes, M. P., Cotton, A., Hopkins, N. A. E., McDonnell, M. B., *Engineering in Medicine and Biology Magazine, IEEE* 2003, *22*, 68-74.

[19] Johari, J., Hübner, Y., Hull, J. C., Dale, J. W., Hughes, M. P., *Physics in Medicine and Biology* 2003, *48*, N193.

[20] Morgan, H., Hughes, M. P., Green, N. G., *Biophysical Journal*, *77*, 516-525.

[21] Hughes, M. P., Morgan, H., *Analytical Chemistry* 1999, *71*, 3441-3445.

[22] Hughes, M. P., *Electrophoresis* 2002, *23*, 2569-2582.

[23] Chen, K. P., Pacheco, J. R., Hayes, M. A., Staton, S. J. R., *Electrophoresis* 2009, *30*, 1441-1448.

[24] Chaurey, V., Polanco, C., Chou, C.-F., Swami, N. S., *Biomicrofluidics* 2012, *6*, 012806.

[25] Swami, N., Chou, C.-F., Ramamurthy, V., Chaurey, V., *Lab on a Chip* 2009, *9*, 3212-3220.

[26] Su, Y.-H., Tsegaye, M., Varhue, W., Liao, K.-T., Abebe, L. S., Smith, J. A., Guerrant, R. L., Swami, N. S., *Analyst* 2014, *139*, 66-73.

[27] Gencoglu, A., Camacho-Alanis, F., Nguyen, V. T., Nakano, A., Ros, A., Minerick, A. R., *Electrophoresis* 2011, *32*, 2436-2447.

[28] Cummings, E. B., Singh, A. K., *Analytical Chemistry* 2003, *75*, 4724-4731.

[29] Srivastava, S., Gencoglu, A., Minerick, A., *Analytical and Bioanalytical Chemistry* 2011, *399*, 301-321.

[30] Keshavamurthy, S. S., Leonard, K. M., Burgess, S. C., Minerick, A. R., *NSTI-Nanotech, Boston, MA* 2008, 401-404.

[31] Kang, Y., Li, D., Kalams, S., Eid, J., *Biomedical Microdevices* 2008, *10*, 243-249.

[32] Barbulovic-Nad, I., Xuan, X., Lee, J. S. H., Li, D., *Lab on a Chip* 2006, *6*, 274-279.

[33] Thwar, P. K., Linderman, J. J., Burns, M. A., *Electrophoresis* 2007, *28*, 4572-4581.

[34] Lapizco-Encinas, B. H., Davalos, R. V., Simmons, B. A., Cummings, E. B., Fintschenko, Y., *Journal of Microbiological Methods* 2005, *62*, 317-326.

[35] Sabounchi, P., Morales, A., Ponce, P., Lee, L., Simmons, B., Davalos, R., *Biomedical Microdevices* 2008, *10*, 661-670.

[36] Regtmeier, J., Duong, T. T., Eichhorn, R., Anselmetti, D., Ros, A., *Analytical Chemistry* 2007, *79*, 3925-3932.

[37] Braff, W. A., Pignier, A., Buie, C. R., *Lab on a Chip* 2012, *12*, 1327-1331.

[38] Braff, W. A., Willner, D., Hugenholtz, P., Rabaey, K., Buie, C. R., *PloS one* 2013, *8*, e76751.

[39] Barrett, L. M., Skulan, A. J., Singh, A. K., Cummings, E. B., Fiechtner, G. J., *Analytical Chemistry* 2005, *77*, 6798-6804.

[40] Zellner, P., Shake, T., Hosseini, Y., Nakidde, D., Riquelme, M. V., Sahari, A., Pruden, A., Behkam, B., Agah, M., *Electrophoresis* 2015, *36*, 277-283.

[41] Kang, K. H., Kang, Y., Xuan, X., Li, D., *Electrophoresis* 2006, *27*, 694-702.

[42] Staton, S. J. R., Chen, K. P., Taylor, T. J., Pacheco, J. R., Hayes, M. A., *Electrophoresis* 2010, *31*, 3634-3641.

[43] Pysher, M. D., Hayes, M. A., *Analytical Chemistry* 2007, *79*, 4552-4557.

[44] Gallo-Villanueva, R. C., Rodríguez-López, C. E., Díaz-de-la-Garza, R. I., Reyes-Betanzo, C., Lapizco-Encinas, B. H., *Electrophoresis* 2009, *30*, 4195-4205.

[45] LaLonde, A., Gencoglu, A., Romero-Creel, M. F., Koppula, K. S., Lapizco-Encinas, B. H., *Journal of Chromatography A* 2014, *1344*, 99-108.

[46] Cummings, E. B., *Engineering in Medicine and Biology Magazine, IEEE* 2003, *22*, 75-84.

[47] Srivastava, S. K., Artemiou, A., Minerick, A. R., *Electrophoresis* 2011, *32*, 2530-2540.

[48] Abdallah, B. G., Roy-Chowdhury, S., Coe, J., Fromme, P., Ros, A., *Analytical Chemistry* 2015, *87*, 4159-4167.

[49] Gallo-Villanueva, R. C., Sano, M. B., Lapizco-Encinas, B. H., Davalos, R. V., *Electrophoresis* 2014, *35*, 352-361.

[50] Saucedo-Espinosa, M. A., Lapizco-Encinas, B. H., *Electrophoresis* 2015, *36*, 1086-1097.

[51] Giddings, J. C., *Unified Separation Science*, John Wiley & Sons, Inc., New York 1991.

[52] Morton, K. J., Loutherback, K., Inglis, D. W., Tsui, O. K., Sturm, J. C., Chou, S. Y., Austin, R. H., *Proceedings of the National Academy of Sciences* 2008, *105*, 7434-7438.

[53] Huang, L. R., Cox, E. C., Austin, R. H., Sturm, J. C., *Science* 2004, *304*, 987-990.

[54] Streek, M., Schmid, F., Duong, T. T., Ros, A., *Journal of Biotechnology* 2004, *112*, 79-89.

[55] Ros, A., Hellmich, W., Regtmeier, J., Duong, T. T., Anselmetti, D., *Electrophoresis* 2006, *27*, 2651-2658.

[56] Ozuna-Chacón, S., Lapizco-Encinas, B. H., Rito-Palomares, M., Martínez-Chapa, S. O., Reyes-Betanzo, C., *Electrophoresis* 2008, *29*, 3115-3122.

[57] Pesch, G. R., Kiewidt, L., Du, F., Baune, M., Thöming*, J., *Electrophoresis* 2016, *37*, 291-301.

[58] Saucedo-Espinosa, M. A., Lapizco-Encinas, B. H., *Journal of Chromatography A* 2015, *1422*, 325-333.

[59] Weiss, N. G., Jones, P. V., Mahanti, P., Chen, K. P., Taylor, T. J., Hayes, M. A., *Electrophoresis* 2011, *32*, 2292-2297.

[60] Humble, P. H., Kelly, R. T., Woolley, A. T., Tolley, H. D., Lee, M. L., *Analytical Chemistry* 2004, *76*, 5641-5648.

[61] Allen, D. J., Accolla, R. P., Williams, S. J., *Electrophoresis* 2017, *38*, 1441-1449.

[62] Pohl, H. A., *Dielectrophoresis : the behavior of neutral matter in nonuniform electric fields*, Cambridge University Press, Cambridge; New York 1978.

[63] Pethig, R., *Biomicrofluidics* 2010, *4*, 022811.

[64] Probstein, R. F., *Physicochemical Hydrodynamics: An Introduction*, John Wiley & Sons, Inc. 1994, pp. 1-8.

[65] Jones, T. B., *Electromechanics of Particles*, Cambridge University Press 1995.

[66] Kwon, J.-S., Maeng, J.-S., Chun, M.-S., Song, S., *Microfluidics and Nanofluidics* 2008, *5*, 23-31.

[67] Baylon-Cardiel, J. L., Lapizco-Encinas, B. H., Reyes-Betanzo, C., Chavez-Santoscoy, A. V., Martinez-Chapa, S. O., *Lab on a Chip* 2009, *9*, 2896-2901.

[68] Dingley, J., in: Photo-Tools, J. (Ed.), JD Photo-Tools 2014, pp. 1-89.

[69] AZ Electronic Materials: AZ® 3300 Series Crossover Photoresists 2005.

[70] Bhardwaj, J., Ashraf, H., McQuarrie, A., *Proc. Symp. Microstructures and Microfabricated Systems, ECS* 1997.

[71] Shalliker, R. A., Broyles, B. S., Guiochon, G., *Journal of Chromatography A* 2000, *888*, 1-12.

[72] Staton, S. J. R., Chen, K. P., Taylor, J. P., Pacheco, J. R., Hayes, M. A., *Electrophoresis* **2010**, *31*, 3634-3641.

CHAPTER 6

[1] Nalepa, C. A., *Ecological Entomology* 2015, *40*, 323-335.

[2] Cleveland, L. R., *The Biological Bulletin* 1925, *48*, 309-[326]-301.

[3] Ware, J. L., Grimaldi, D. A., Engel, M. S., *Arthropod Structure & Development* 2010, *39*, 204-219.

[4] Bourguignon, T., Lo, N., Cameron, S. L., Šobotník, J., Hayashi, Y., Shigenobu, S., Watanabe, D., Roisin, Y., Miura, T., Evans, T. A., *Molecular Biology and Evolution* 2015, *32*, 406-421.

[5] Noda, S., Mantini, C., Meloni, D., Inoue, J.-I., Kitade, O., Viscogliosi, E., Ohkuma, M., *PLOS ONE* 2012, *7*, e29938.

[6] Kitade, O., *Microbes and Environments* 2004, *19*, 215-220.

[7] Noda, S., Kitade, O., Inoue, T., Kawai, M., Kanuka, M., Hiroshima, K., Hongoh, Y., Constantino, R., Uys, V., Zhong, J., Kudo, T., Ohkuma, M., *Molecular Ecology* 2007, *16*, 1257-1266.

[8] Yamin, M. A., *Sociobiology* 1979, 4:3-117.

[9] Inward, D., Beccaloni, G., Eggleton, P., *Biology Letters* 2007, *3*, 331-335.

[10] Gile, G. H., Slamovits, C. H., *Protist* 2012, *163*, 274-283.

[11] Light, S., Sanford, M., *University of California Publications in Zoology* 1928, *31*, 269-274.

[12] Gerbod, D., Edgcomb, V. P., Noël, C., Delgado-Viscogliosi, P., Viscogliosi, E., *International microbiology : the official journal of the Spanish Society for Microbiology* 2000, *3*, 165-172.

[13] Saldarriaga, J. F., Gile, G. H., James, E. R., HorÁK, A., Scheffrahn, R. H., Keeling, P. J., *Journal of Eukaryotic Microbiology* 2011, *58*, 487-496.

[14] Jones, P. V., DeMichele, A. F., Kemp, L., Hayes, M. A., *Analytical and Bioanalytical Chemistry* 2014, *406*, 183-192.

[15] Crowther, C. V., Hilton, S. H., Kemp, L., Hayes, M. A., *Analytica Chimica Acta* 2018, In Submission.

[16] Crowther, C. V., Hayes, M. A., *Analyst* 2017, *142*, 1608-1618.

[17] Jones, P. V., Staton, S. J. R., Hayes, M. A., *Analytical and Bioanalytical Chemistry* 2011, *401*, 2103-2111.

[18] Jones, P. V., Hilton, S. H., Davis, P. E., Yanashima, R., McLemore, R., McLaren, A., Hayes, M. A., *Analyst* 2015, *140*, 5152-5161.

[19] Abdallah, B. G., Chao, T.-C., Kupitz, C., Fromme, P., Ros, A., *ACS Nano* 2013, *7*, 9129-9137.

[20] Luo, J., Abdallah, B. G., Wolken, G. G., Arriaga, E. A., Ros, A., *Biomicrofluidics* 2014, *8*, 021801.

[21] Nakano, A., Camacho-Alanis, F., Ros, A., *Analyst* 2015, *140*, 860-868.

[22] LaLonde, A., Gencoglu, A., Romero-Creel, M. F., Koppula, K. S., Lapizco-Encinas, B. H., *Journal of Chromatography A* 2014, *1344*, 99-108.

[23] Lapizco-Encinas, B. H., Simmons, B. A., Cummings, E. B., Fintschenko, Y., *Electrophoresis* 2004, *25*, 1695-1704.

[24] Saucedo-Espinosa, M. A., Lapizco-Encinas, B. H., *Electrophoresis* 2015, *36*, 1086-1097.

[25] Saucedo-Espinosa, M. A., LaLonde, A., Gencoglu, A., Romero-Creel, M. F., Dolas, J. R., Lapizco-Encinas, B. H., *Electrophoresis* 2016, *37*, 282-290.

[26] Ding, J., Woolley, C., Hayes, M. A., *Analytical and Bioanalytical Chemistry* 2017, *409*, 6405-6414.

[27] Leester-Schadel, M., Lorenz, T., Jurgens, F., Richter, C., in: Dietzel, A. (Ed.), *Microsystems for Pharmatechnology*, Springer 2016, pp. 23-57.

[28] Lorenz, H., Despont, M., Fahrni, N., LaBianca, N., Renaud, P., Vettiger, P., *Journal of Micromechanics and Microengineering* 1997, *7*, 121.

[29] Crump, S. S., Stratasys Inc 1992.

[30] Sochol, R. D., Sweet, E., Glick, C. C., Wu, S.-Y., Yang, C., Restaino, M., Lin, L., *Microelectronic Engineering* 2018, *189*, 52-68.

[31] Bhattacharjee, N., Urrios, A., Kang, S., Folch, A., *Lab on a Chip* 2016, *16*, 1720-1742.

[32] Lewis, J. A., *Advanced Functional Materials* 2006, *16*, 2193-2204.

[33] Gratson, G. M., Xu, M., Lewis, J. A., *Nature* 2004, *428*, 386.

[34] Macdonald, N. P., Cabot, J. M., Smejkal, P., Guijt, R. M., Paull, B., Breadmore, M. C., *Analytical Chemistry* 2017, *89*, 3858-3866.

[35] Au, A. K., Huynh, W., Horowitz, L. F., Folch, A., *Angewandte Chemie International Edition* 2016, *55*, 3862-3881.

[36] Walczak, R., Adamski, K., *Journal of Micromechanics and Microengineering* 2015, *25*, 085013.

[37] Waldbaur, A., Rapp, H., Länge, K., Rapp, B. E., *Analytical Methods* 2011, *3*, 2681-2716.

[38] Fang, N., Sun, C., Zhang, X., *Applied Physics A* 2004, *79*, 1839-1842.

[39] Mishra, S., Yadava, V., *Optics and Lasers in Engineering* 2015, *73*, 89-122.

[40] Phillips, K. C., Gandhi, H. H., Mazur, E., Sundaram, S. K., *Advances in Optics and Photonics* 2015, *7*, 684-712.

[41] Nisar, S., Li, L., Sheikh, M., *Laser Glass Cutting Techniques - A Review*, 2013.

[42] da Costa, E. T., Santos, M. F. S., Jiao, H., do Lago, C. L., Gutz, I. G. R., Garcia, C. D., *Electrophoresis* 2016, *37*, 1691-1695.

[43] Fiorini, G. S., Chiu, D. T., *BioTechniques* 2005, *38*, 429-446.

[44] Fogarty, B. A., Heppert, K. E., Cory, T. J., Hulbutta, K. R., Martin, R. S., Lunte, S. M., *Analyst* 2005, *130*, 924-930.

[45] Hong, T.-F., Ju, W.-J., Wu, M.-C., Tai, C.-H., Tsai, C.-H., Fu, L.-M., *Microfluidics and Nanofluidics* 2010, *9*, 1125-1133.

[46] Gabriel, E. F. M., Coltro, W. K. T., Garcia, C. D., *Electrophoresis* 2014, *35*.

[47] Mazher, I. M. a. M. N. H. Z. A. a. A. K. a. I. G., *Journal of Micromechanics and Microengineering* 2017, *27*, 015021.

[48] Jensen, M. F., Noerholm, M., Christensen, L. H., Geschke, O., *Lab on a Chip* 2003, *3*, 302-307.

[49] Snakenborg, D., Klank, H., Kutter, J., *Journal of Micromechanics and Microengineering* 2004, *14*, 182.

[50] Evans, E., Gabriel, E. F. M., Benavidez, T. E., Coltro, W. K. T., Garcia, C. D., *The Analyst* 2014, *139*, 5560-5567.

[51] Evans, E., Gabriel, E. F. M., Coltro, W. K. T., Garcia, C. D., *The Analyst* 2014, *139*, 2127-2132.

[52] Ding, J., Lawrence, R. M., Jones, P. V., Hogue, B. G., Hayes, M. A., *Analyst* 2016, *141*, 1997-2008.

APPENDIX A

SUPPLEMENTAL MATERIAL FOR CHAPTER 5

The geometries were changed based on altering the shape of the base insulator, adding smaller length scale insulating features to the tops of the base insulators, altering the shapes of the small features, and altering the alignment of the insulators relative to each other (Figure S1 and S2).

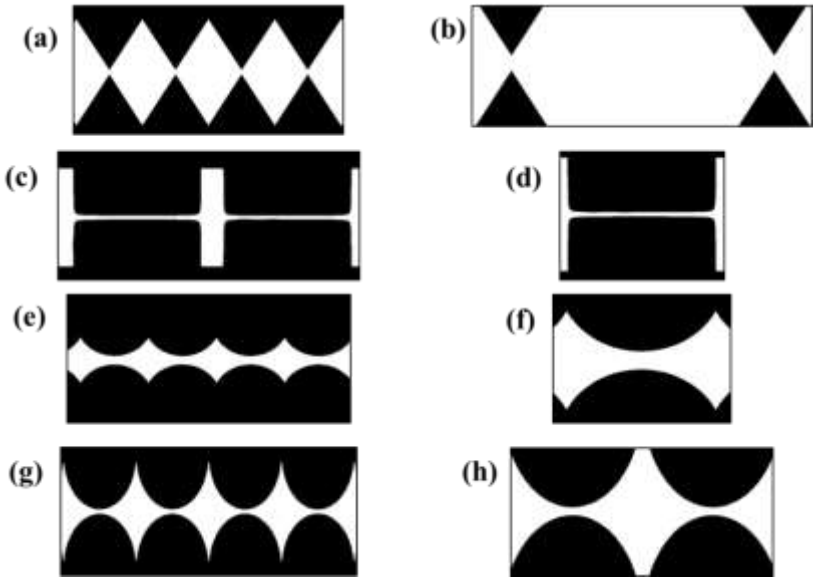

Figure S1 Examples of different base insulators modeled. (a,c,e,g) represent a view of several insulators (b,d,f,h) represent a zoom in of the points of constriction in the microchannel. (a&b) triangle/diamond (c&d) *Inverse 20× Curve* (e&f) circle (g&h) ellipse

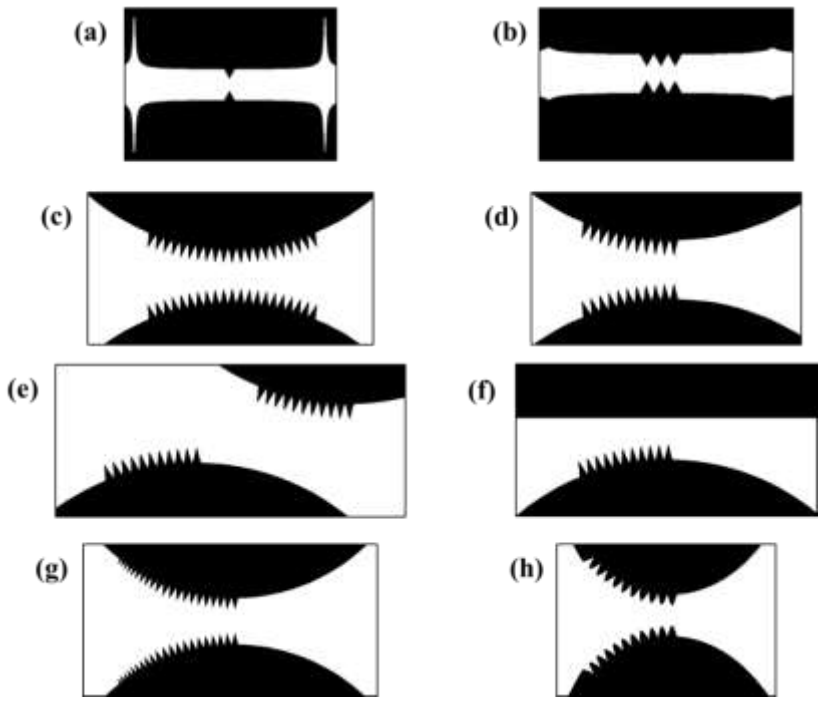

Figure S2 Examples of various insulators tested where all of the small insulators are 20 μm tall at the point of greatest constriction. (a) *Inverse 20× Curve* base insulator with 1 small triangle insulator (b) *Inverse 20× Curve* base insulator with 3 small triangular insulators (c) Circle base insulator with ellipse small insulators across the whole top of the insulator (d) Circle base insulator with ellipse small insulators across half the top, were the last small insulator is the point of greatest constriction. (e) Circle base insulator with ellipse small insulators such that the last small insulators on both side of the microchannel are offs set by 200 μm (f) Circle base insulator with ellipse small insulators where the wall of the microchannel is the other side of the constriction. (g) Circle base insulator with small ellipse insulators that diminish in size the further from the point of greatest constriction. (h) Ellipse based insulator with small elliptical insulators that are inset into the base insulator.

The mathematical derivation of the trapping equation is included below. All equations and variables are as defined in the Chapter 5.

Defined knowns:

$$\vec{v}_{EK} = \mu_{EK}\vec{E}$$

$$\vec{v}_{DEP} = -\mu_{DEP}\nabla \left| \vec{E} \right|^2$$

$$\vec{j} \approx C(\vec{v}_{EK} + \vec{v}_{DEP})$$

$$\vec{j} \cdot \vec{E} = 0$$

Therefore combining these equations the following can be stated as a trapping condition:

$$C[\mu_{EK}\vec{E} - \mu_{DEP}\nabla \left| \vec{E} \right|^2] \cdot \vec{E} \leq 0$$

$$\frac{\mu_{DEP}\ \nabla\left|\vec{E}\right|^2}{\mu_{EK}\ E^2} \cdot \vec{E} \geq 1$$

$$\frac{\nabla\left|\vec{E}\right|^2}{E^2} \cdot \vec{E} \geq \frac{\mu_{EK}}{\mu_{DEP}}$$

Design	$\nabla\|\vec{E}\|^2$ (V^2/m^3)[1]	Streaming[2]	Partial Trapping[3]	Disadvantageous Advantageous Lateral Heterogeneity[4]
Rectangle	6.3×10^{14}	Low/Medium	Medium	Low/Medium
Inverse 20× Curve	4.5×10^{14}	High	Lowest	Low
Circle	8.8×10^{14}	Medium	Low/Medium	Low/Medium
Ellipse	1.9×10^{15}	Medium	Low/Medium	Low/Medium
Triangle	3.2×10^{16}	Low	High	High
Multi-length Scale	1.7×10^{15}	High	Low	Low

Table S1 The designs compared in this table were limited to those presented in Figure 3 of the text. The effect of various traits is denoted as advantageous (dark maroon) to disadvantageous (white/pink). A global applied voltage of 500 V was used for all comparisons. **1** The value of $\nabla\left|\vec{E}\right|^2$ on the centerline at the first 34.10 μm gate was used. The highest gradient allows for the greatest dielectrophoretic force with the lowest applied global potential and/or the trapping of particles with lesser dielectrophoretic mobilities. **2** Streaming of particles towards the centerline results in a more homogeneous lateral trapping environment in the main trapping zone. This process is imperative to ensure all like-particles experience similar forces regardless of the specific pathline travelled. Designs rated 'high' indicates that particles are forced into a limited lateral zone close to the centerline. 'Medium' rated designs either allowed for limited streaming or indicated a relatively large area of interaction at the trapping area. Designs rated 'low' had limited or no streaming for some pathlines and a large area of interaction in the trapping zone. **3** Images of field lines and $\nabla\left|\vec{E}\right|^2$ values were inspected for lines crossing the gradient at acute angles, consistent with trapping. Advantageous designs rated 'high' had electric field lines no matter where in device that the streamlined particles are present they will either all pass a given zone or will experience their trapping ratio and be isolated. Those rated 'medium' indicate designs where the majority will experience trapping zones simultaneously, however small regions exist where analytes present close to the walls of the microchannel will experience trapping before those along the centerline. For the designs rated 'low' particles will experience larger regions close to the walls where a trapping ratio will occur, however analytes along the centerline will not experience this same phenomenon. Variations in the applied potential, constriction size, and trapping ratio will change the presence/amount of partial trapping at a given constriction making analytical comparison impractical. **4** Within the zone of capture, there will be an unavoidable range of values for the capture ratios. For each design, an assessment of the variation of the $\nabla\left|\vec{E}\right|^2$ values in the vertical dimension, as show in Figure 3, was performed based on the accessible area to the analytes. The most advantageous designs are rated 'low' and have limited variance across this zone. 'Medium' and 'high" ratings indicated higher variability across this dimension. The increased variability generally resulted from the particles being able to access areas near the insulators where the gradients are necessarily highest.

APPENDIX B

FINITE ELEMENT MULTI-PHYSICS MODELING

To assess the distribution of the electric field in the insulator-based microchannels presented in this dissertation finite element modeling software (COMSOL Multiphysics) was utilized. These models were utilized to understand the effects of the application of potential both globally, across the entire microchannel, and at localized regions within the microchannel. Models of the V1 microchannel were utilized in Chapters 3 and 4 to approximate the mobilities of the analytes assessed within the chapters. Chapter 5 details in depth the use of modeling to develop a novel insulator shape. Chapter 6 utilized modeling to probe the distribution of the electric field in a larger microchannel and determine the effect of incorporating side channels to the device.

All modelled microchannels were first built as accurately scaled 2D geometries using AutoCAD and exported as DXF files, specifically from the 2007 version. For all geometries, which include sharp features, like the V1 channels used in Chapters 3 and 4, the triangles were slightly rounded more similarly model the real-world shape of the PDMS microchannels. 2D geometries were utilized as it decreases the required computational time and the height of the microchannel is considered negligible to the overall distribution of the electric field.

The *AC/DC module* was used to predict the $\vec{E}$, $\nabla\left|\vec{E}\right|^2$, and $\frac{\nabla\left|\vec{E}\right|^2}{E^2}\cdot\vec{E}$. This module uses the Laplace equation, which assumes the electric potential is continuous in the microchannel, to model the distribution of the electric field. The specific boundary conditions used are laid out in Chapter 5. This means that the boundaries of the microchannel were set as boundaries, which assumes that no current flow across the boundaries. The user then defines the materials of the system, either using built-in materials or user defined materials. For the work done in this dissertation the boundaries

were defined as silica glass and the fluid in the microchannel was defined as water. In some cases the approximate conductivity and permittivity of the aqueous media utilized were used to better approximate the properties of the aqueous buffer used in experimentation. The inlet reservoir was defined as the ground, and the outlet reservoir was assigned a potential between -50 to -3000 V, depending upon the desired approximation.

COMSOL utilizes a mesh of the geometry at hand to assess the underlying physics and therefore the distribution of the electric field. The mesh can be manipulated to be coarse or fine depending on the needs of the assessment and available computational power. The optimal mesh will minimize error and noise, but limit computation time. Finer meshes approximate the physics at more locations throughout the geometry but is more computationally intensive and therefore more time consuming. Whereas courser meshes are potentially less accurate but require less computational time. For the work done in this dissertation a free triangular mesh was used, starting from the preset for fine resolution. Adjustments were made to the mesh to achieve the maximum mesh density at the gates in the microchannel, to get the most accurate representation of the electric field in the narrow regions of the channel.

The distribution of the electric field was computed for a stationary, rather than time-dependent, study. Various representations, including 2D plots, line graphs, and contour plots, were utilized to interpret the $\vec{E}$, $\nabla\left|\vec{E}\right|^2$, and $\frac{\nabla|\vec{E}|^2}{E^2}\cdot\vec{E}$ both along the centerline and near the gates of interest. Furthermore, as described throughout this dissertation the trapping condition of a given analyte $\left(\frac{\mu_{EK}}{\mu_{DEP}}\right)$ can be correlated to the

channel effects ($\frac{\nabla|\vec{E}|^2}{E^2} \cdot \vec{E}$). Using independently measured μ_{EK}values, the onset potential of trapping, an approximation of $\mu_{DEP}$is possible.

APPENDIX C

PUBLISHED PORTIONS

Portions of this dissertation have been previously published, submitted for publication, or will be submitted for publication in following journals. The published materials were included with permission from all co-authors.

Chapter 3

Crowther, C. V., Hilton, S. H., Kemp, L., Hayes, M. A., *Analytica Chimica Acta*, 2018, In Review.

Chapter 4

Crowther, C.V. Sanderlin, V., Gile, G. H., Hayes, M. A., 2018, In Preparation.

Chapter 5

Crowther, C. V., Hayes, M. A., Analyst, 2017, *142*, 1608-1618.

190